

In-situ Measurement and Formability Improvement in
Stamping of High Strength Steel and Titanium Alloy Sheets

January 2014

DOCTOR OF ENGINEERING

ZAMZURI BIN HAMEDON

TOYOHASHI UNIVERSITY OF TECHNOLOGY

Abstract

The information and visualization of deformation behaviour of the high strength steel sheet during the stamping process are useful for designing tools and processes in metal forming industry. However, it is not easy to measure the deformation behaviour during stamping processes because a deforming sheet is generally surrounded with complicated tools during a stamping operation, and thus, application of sensors for the in-situ measurement has been still limited. Borescopes consisting of a small camera and a flexible cable have possibility of application to forming processes as an imaging sensor and the installation of the borescopes inside tools enables the in-situ measurement. The three-dimensional deformation behaviour of the sheet and tools were successfully measured using borescope.

The use of the ultra-high strength steel sheets for automobile body-in-white parts is increasing, whereas it is not easy to form the the ultra-high strength steel sheets. A gradually contacting punch was developed to reduce a tensile stress during the forming process with controlling a stress state around sheared edges undergoing plastic deformation. However, the punch stroke increased for stretch flanging, i.e. increases in production time and cost. In order to reduce the punch stroke, a 2-stage process using a recessed punch was developed for stretch flanging.

In order to increase the safety of cars, the structure of body members was optimized. Front rail hollow sections act as an energy absorber during collision, and are permanently deformed in order to absorb the kinetic energy during the crash. These hollow sections typically joined by resistance spot welding have insufficient energy absorption, because the

joint are not continuous. In order to overcome this problem, the hollow section is joined by hemming. Since the hollow section having hemmed joints is overlapped, the strength is increased in comparison with resistance spot welded joints.

Although titanium alloy sheets are widely used for airplane parts due to its properties of high strength at high temperatures, low density and high corrosion resistance, ductility of the titanium alloy sheets is very low, and thus it is difficult to form the titanium alloy sheets at room temperature. The sheets are generally formed at elevated temperatures. Hot hat-shaped bending of the Ti-6Al-4V titanium sheet using the resistance heating was carried out. The titanium alloy sheet was successfully formed at the elevated temperatures, the bending load was reduced and the springback and oxidation are prevented.

Table of contents

	Page
Abstract	i
Table of Contents	iii
Chapter 1 Introduction	1
1.1 An overview	1
1.1.1 In-situ measurement using borescope	1
1.1.2 Formability improvement of high strength steel sheets in flanging process	7
1.1.3 Joining of ultra-high strength steel sheet by hemming for improvement of joint strength	11
1.1.4 Improvement of formability using hot stamping	13
1.2 Research objectives	14
1.2.1 In-situ measurement of deformation behaviour of sheet and tools during stamping process.	14
1.2.2 Formability improvement of high strength steel and titanium alloy sheets	14
1.3 Outline of dissertation	15
Chapter 2 In-situ measurement of deforming shapes of sheet and tools during stamping using borescope	17
2.1 Introduction	17
2.2 Procedure of in-situ measurement using borescope	18
2.3 In-situ measurement of deformation behavior of sheet	22
2.4 In-situ measurement of deflection of punch	26

2.5 Conclusions	29
Chapter 3 In-situ measurement of 3-dimensional deformation during flanging of sheet metal using 2 borescopes	29
3.1 Introduction	29
3.2 Measuring method of edge of deforming sheet	30
3.2.1 Measuring using 2 borescopes	30
3.2.2 Tools of shrink flanging	33
3.2.3 Accuracy of measurement using 2 borescopes	34
3.2.4 Bending of inclined sheet	35
3.3 Measurement of 3-dimensional deformation of sheet in shrink flanging	36
3.4 Conclusions	39
Chapter 4 Improvement of formability of ultra-high strength steel sheets in flanging	40
4.1 Introduction	40
4.2 Shrink flanging	42
4.2.1 Procedure of shrink flanging	42
4.2.2 Optimization of projection angle of punch	44
4.2.3 Results for punch having gradual contact	47
4.3 Stretch flanging of the high strength steel sheets	51
4.3.1 Procedure of stretch flanging of 2-stage stretch flanging by using a flat punch and punch with recessed.	54
4.3.2 Calculation conditions and results	56
4.3.3 Width of punch groove on the flange height	60
4.3.4 Delayed fracture for 2-stage stretch flanging method	63

4.4 Conclusions	65
Chapter 5 Joining of high strength steel sheets by hemming and improvement of joint strengths	67
5.1 Introduction	67
5.2 Hemming process of high strength steel sheets	69
5.3 Results in crash test of high strength steel hollow sections	74
5.3.1 Result of crash test for short hollow section	74
5.3.2 Optimization of flange length in hemming	79
5.3.3 Crash test for long high strength steel hollow sections	80
5.4 Conclusions	83
Chapter 6 Improvement of formability of titanium alloy sheet using hot bending by resistance heating	85
6.1 Introduction	85
6.2 Procedure of hot bending of titanium alloy sheet	86
6.2.1 Experimental procedure	86
6.2.2 Heating behaviour of sheet	89
6.3 Results of hot bending of titanium alloy sheet using resistance heating	91
6.3.1 Bent sheets	91
6.3.2 Bending load and springback	93
6.3.3 Microstructure and hardness of bent sheet	96
6.4 Resistance heating of curve sheet	98
6.5 Conclusions	100
Chapter 7 Concluding remarks	102

7.1 Summary	
7.1.1 In-situ measurement of deformation behaviour of sheet and tools during stamping using borescopes	102
7.1.2 Formability improvement in flanging of high strength steel sheets	103
7.1.3 Joining of ultra-high strength steel sheets by hemming and improvement of joint strengths	104
7.1.4 Improvement of formability of titanium alloy sheet using hot bending by resistance heating	106
7.2 Future perspectives	106
References	111
List of publications	119
List of conferences	120
Acknowledgements	122
Resume	124

Chapter 1

Introduction

1.1 An overview

1.1.1. In-situ measurement using borescope

The transformation of the cars toward the lower CO₂ emission and higher safety of the cars is associated with considerable changes in the stamping processes, requiring new solutions for the inherent conflict in design between weight and strength [1]. Future requirements of stamping process will be characterised by trends in measurement system and development of a sensor technology. The scientific and technical challenges do not lie entirely in the capability to produce stamped parts with greater precision, but also mass produced the parts at reasonable production costs. One fundamental initiative to find a solution in the area of process development is the application of the sensors technology for early detection of the defect in the stamping process. This must be accomplished by increasing the flexibility of the sensors for applications during the stamping process. Although many such sensors were employed for the applications of the measurement during the stamping process, the results obtained are very limited for specific purpose. Figure 1.1 shows an example of the application of the piezo sensors in the stamping process to measure a punch pressure.

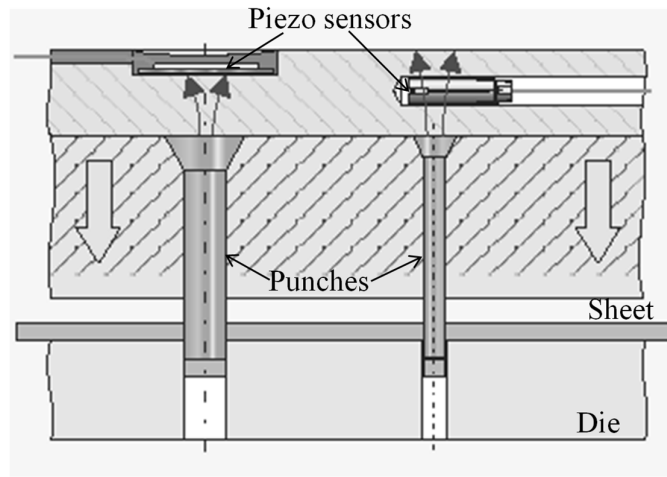
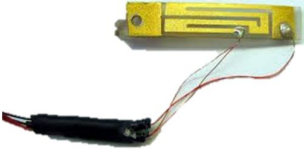


Fig. 1.1. Application of piezo sensors in stamping tool to measure punch pressure.

In order to obtain the deformation behaviour of the sheet during the stamping process, finite element simulation is established as a developmental method for such situations, and today it constitutes the key element in designing stamping tools. However, calculated results by the finite element simulation are reaching the limit of the accuracy, because the simulation includes some approximations and assumptions. It is not easy to accurately measure material constants used in the simulation such as the flow stress curve or the coefficient of friction. When elastic deformation of tools and press machines is taken into consideration in the simulation, the computing time becomes extremely long due to huge number of elements. Even constitutive equations used in the finite element simulation are not highly accurate for large strain and anisotropy. Not only the finite element simulation, but also in-situ measuring methods are required to design stamping processes at present. The finite element simulation has been remarkably developed with the advancement of computer and is an attractive tool of designing stamping processes.

Table 1.1 Several types of sensors used for in-situ measurement.

Sensors	Images	Minimum size	Measuring range
LVDT		Ø5 x 15 mm	0.01 - 5 mm
Dial gauge		Ø3 x 25 mm	0.01 – 5 mm
Acoustic emission		Ø3 x 8 mm	300 – 800 kHz
Laser displacement		15 x 20 x 5 mm	0.01 - 5 mm
Stain gauge		30 x 0.3 x 0.1 mm	0 – 0.03 mm
CCD camera		15 x 25 x 10 mm	5 - 25 mm

Although a deformation of the sheets and deflection of the tools is useful information of designing forming processes, it is not easy to measure the deformation and deflection during forming due to small space of the tool cavity. The current inspection practices and monitoring technologies in stamping industry are still based on contact and non-contact measurement [2]. The equipment such as the coordinate measuring machine (CMM), laser displacement devices and CCD camera were among general equipment used for this purpose. Since these devices are too large to be installed inside the tools in general stamping processes, the applications were limited for measuring the parts after the stamping processes. A deforming sheet is generally surrounded with complicated tools during a stamping operation thus; the in-situ measurement is not easy. Table 1.1 shows several types of sensors used for in-situ measurement for the stamping process.

Sensors used for the application of in-situ measurement of deformation behaviour of the sheet and tools during the stamping operations are shown in Figure 1.2. A laser type sensor and dial gauges were used to measure the displacement of a die during deep drawing. Although laser displacement sensors and dial gauges are accurate in measuring the displacement, many sensors are necessary to measure three-dimensional deformation behaviour. Pin type sensors embedded with the strain gauges were used to measure contact pressure and movement of the sheet [3-5]. Conical cantilever sensors having strain gauges were used to measure three-dimensional contact pressure in rolling [6]. However, for the strain gauges, the measuring range is limited to local and small strain. A piezoelectric load sensor was used to measure a blank holder force and performed a closed-loop control of a stamping process [7]. The acoustic emission sensor

was used to detect friction sources during deep drawing [8]. However, for these measurements, fine machining with tools is required for the installation and the obtained results are local.

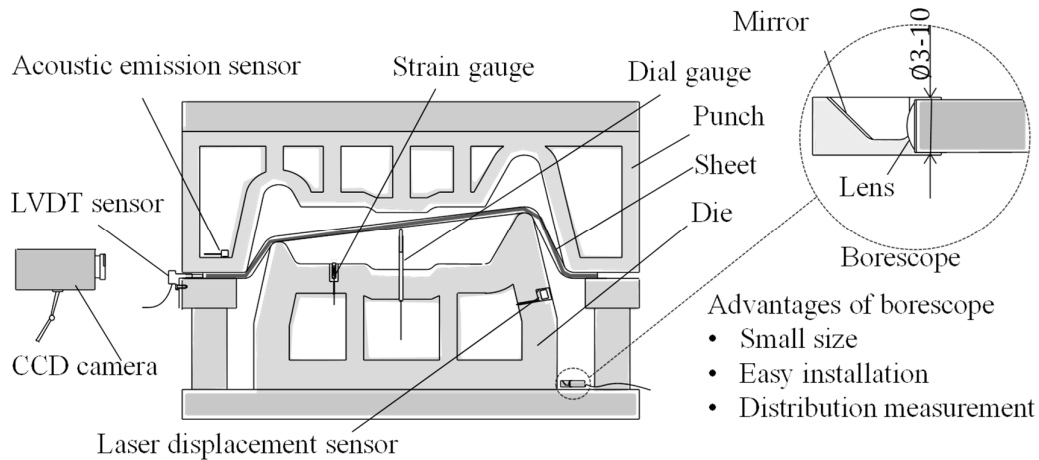


Fig. 1.2. Sensors used for in-situ measurement of deformation behaviour of sheet and tools in stamping operations.

In order to obtain the three-dimensional pictorial data, CCD camera is used. The CCD cameras are attractive in three-dimensional in-situ measurement in metal forming. The CCD is found to be used in obtaining the data of the deformation behaviour of the sheet and tools during the forming process [9-15]. Although the conventional CCD camera is successful in measuring the deformation behaviour during the stamping processes, it is too large to be installed inside the dies. On the other hand, the borescope having a small camera connected with a flexible thin cable can be installed in a small space surrounded with dies without machining. Various types of the borescopes are shown in Figure 1.3. The small camera is set inside the dies, and the cable is taken outside through small gaps between the dies.



Fig 1.3. Various types of borescopes.

Borescopes and endoscopes having a small CCD camera and thin cable are generally used in the medical field, and the application of the borescope has been recently extended to engineering fields. Applications of borescope in different engineering fields are shown in Figure 1.4. The borescopes have been used to inspect wear and damage of components in a turbine engine without dismantling the engine [16], measure the surface profile of a turning tool [17] and obtain the surface roughening behaviour of a hole machined by water jet [18]. The borescope is applicable as a sensor for in-situ measurement in stamping because of the small size.



Fig 1.4. Applications of borescope in engineering field.

1.1.2. Formability improvement of high strength steel sheets in flanging process

To improve the fuel consumption of automobiles, the development of lightweight automobiles is in global competition. The two approaches for the weight reduction are structure optimisation and lightweight materials. The body structure is optimised so as to reduce the weight under a desired strength. The uses of hollow parts are effective in reducing the weight, and tube hydroforming is increasingly employed. On the other hand, aluminium and titanium alloy sheets are attractive lightweight materials for automobiles [19-21]. Although the application of these sheets to the automobile parts offers a high potential for the reduction of the automobile weight, high cost and small formability are crucial problems [22,23]. In stamping of the aluminium alloy sheets, large springback is the main problem, whereas a small formability and high cost for titanium alloy sheet are also problematic, thus the industry still has a great interest in steel sheets.

The application of the high strength steel sheets to the structural body parts which need higher strength is thought of as a measure for reducing the weight of automobiles. The areas of the body structures which are considered for applying the high strength steel sheets are shown in Figure 1.5. By applying high strength steel sheets replacing the mild steel sheets, the reinforcement parts are eliminated and the sheet thickness is decreased, thus the body mass is reduced. However, for the high strength steel sheets, dimensional accuracy of formed products deteriorates due to large springback and die deflection, and the formability is small [24,25]. The design of stamping processes of high strength steel sheets becomes difficult. Studies for improving the formability of the high strength are carried out by several researchers. For example, a gradually contacting

punch is used in order to improve formability of the high strength sheets during the flanging process of the ultra-high strength steel sheets [26]. A conical punch is used to improve the expansion of a hole of a punched ultra-high strength steel sheet by smoothing fracture surface of the sheared edge [27], thus minimized the occurrence of the crack.

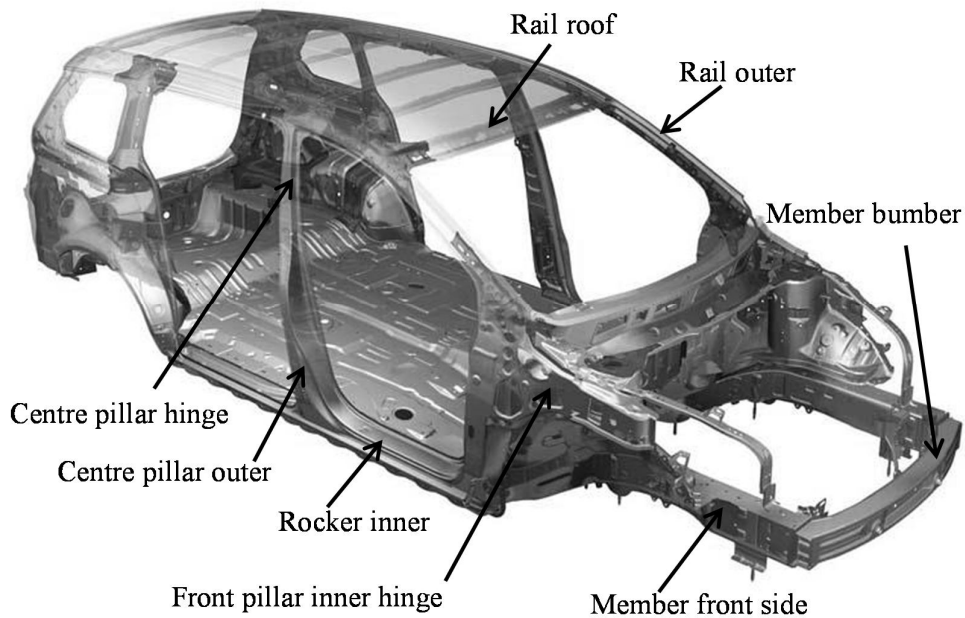
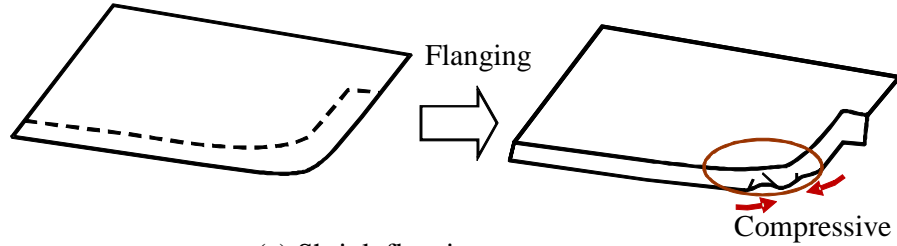


Fig. 1.5. Application of high strength steel sheets to automobile parts [28].

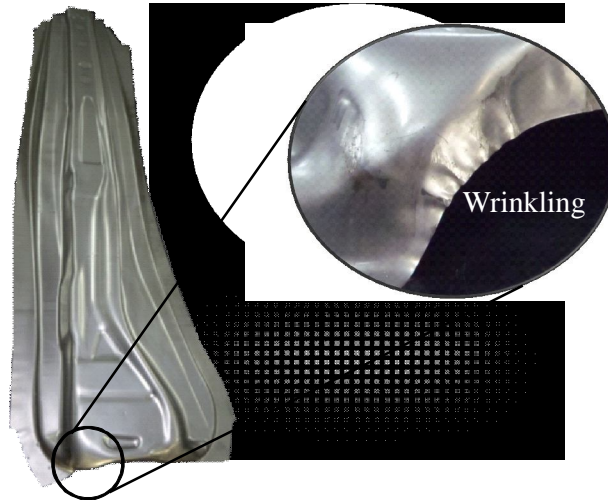
Although the function of the car is to provide comfort to the driver while driving, the safety of the car is important and need to be improved. The application of the high strength steel sheets in the car has improved the safety of the vehicles since the strength of the parts is increased. The high-tensile strength steel sheets 440-980 MPa classes are mainly used in present car body parts. For the outside body panel, 440 MPa class is used, for structures such as door beams and member bumpers, materials in class of

590-780 MPa are used [29]. However, for the centre pillars and member front rails, it requires ultra-high strength tensile strength of 980 MPa class for good crash protection reasons. The problems of using the ultra-high strength steel sheets are the large springback and low formability due to high strength and low ductility of the ultra-high strength steel sheets [30,31].

A flange bending is common forming for the high-tensile steel sheets in car body parts. Instead of bending the flange in a straight line, the parts are bent in convex (shrink) shape which caused the product to wrinkle due to the compressive stress as shown in Figure 1.6. The shrinkage flange of the ultra-high strength steel sheets not only defects the product by the occurrence of the wrinkling, but also causes the seizure and wear of the dies and shorten the life of dies [32]. Since the formed part with wrinkling defect requires to be trimmed at later stage using the trim dies, it will also shorten the life of the trim dies. Although using the thin high strength steel sheet gives advantages in manufacturing the lightweight car, it is less stiff and tendency to become wrinkle is high. To prevent the wrinkling in the shrinkage flanging of the high-strength steel sheets, the punch having gradual contact shape was proposed. The sheet was gradually bent from the corner to reduce the compressive stress.



(a) Shrink flanging process



(b) Wrinkle in 980 MPa class steel shrink flanged sheet

Fig. 1.6. Shrink flanging for ultra-high strength steel sheets.

The stretch flanging is shown in Figure 1.7. The high strength steel sheet is bent in concave (stretch) shape and the tensile stress at the edge of the sheet increased due to the low ductility of the sheets crack that occurred once exceeded the tensile strength limits. The shears conditions of the edge of the sheet with low ductility property are the main factors that contribute to the occurrence of the crack [33]. To prevent the occurrences of the crack and improve the formability of the flange, the gradual contact punch was used [26]. However, the punch strokes for the stretch flanging of the dies

using the punch having gradual contact is larger compared to the flat punch, thus increases the production time, the size of the die and the cost of the die.

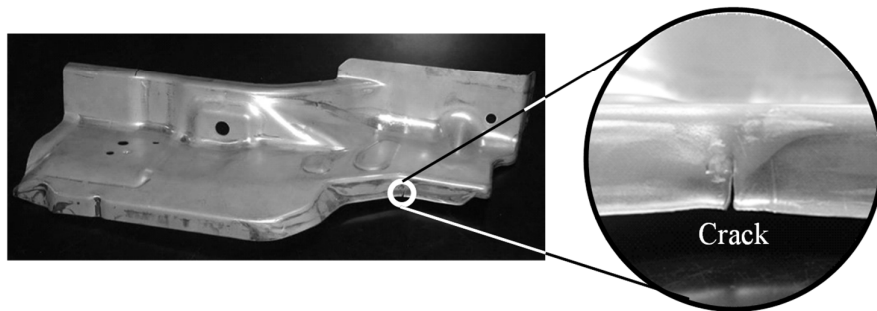
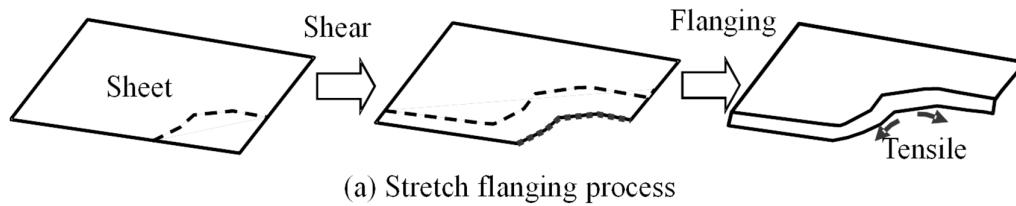


Fig. 1.7. Stretch flanging of high strength steel sheet.

In order to reduce the punch strokes of the stretch flanging using gradual contact punch, a 2-stage flanging was developed using the flat punch with recessed at the centre as a first punch and gradual contact punch as a second punch.

1.1.3 Joining of ultra-high strength steel sheet by hemming for improvement of joint strength

In order to improve the passenger safety of the automobile, the structures of the automobile needs to improve and become stronger. Two approaches are applied for the improvement, the use of stronger materials and the optimization of structure of body members. The high strength steel sheet is used to make the hollow sections for the body

structure of the automobiles [34] and the shape of the structures of the hollow sections are optimized to increase crashworthiness of the vehicles for human safety. A front rail hollow section during crash situations is shown in Figure 1.8. In the crash situation, a kinetic energy is absorbed by the hollow section. The hollow sections typically joined by resistance spot welding have insufficient energy absorption because the joints are not continuous. Although laser welding is a better approach to overcome this problem, high heating temperatures reduce the quality, accuracy and reliability of joined parts [35].

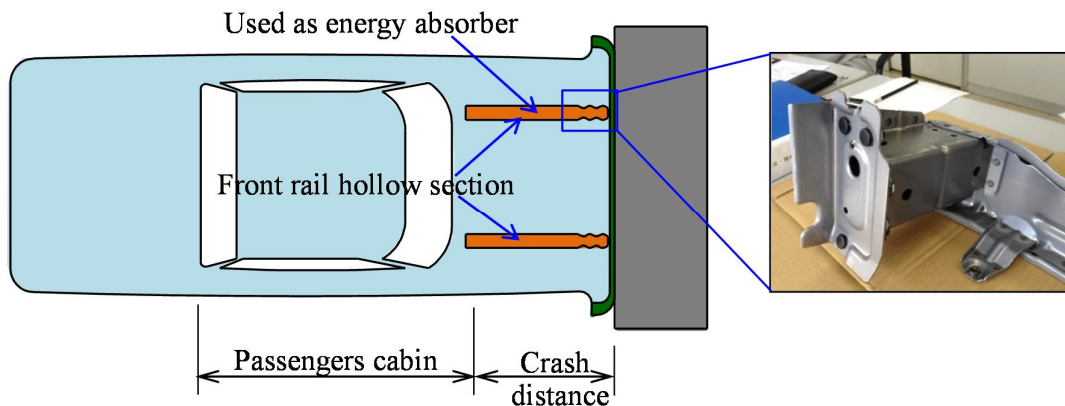


Fig. 1.8. Front rail hollow section.

In order to improve the joint strengths, both edges of hollow sections are joined by hemming. Therefore it produces a continuous joining without external heat supply. Since the hollow section having hemmed joints is overlapped, the strength is increased as compared to the resistance of spot welding joints. Thus, hemming is effective for increasing energy absorption during the crash test.

The usage of titanium alloy sheets for airplane parts increases due to the high strength at high temperatures, low density and high corrosion resistance. In Figure 1.9, it shows an aircraft engine and an example of a structure component made of titanium alloy sheet. Since the cold formability of the titanium alloy sheets is low, the sheets are generally formed at elevated temperatures. Although the conventional hot stamping process using a furnace indicates the effectiveness for reducing the stamping load [36, 37] and improving the formability of the sheets, additional apparatus preheating and cooling systems, low productivity, and oxidation for the heating [38] become problems, thus resistance heating is preferable.

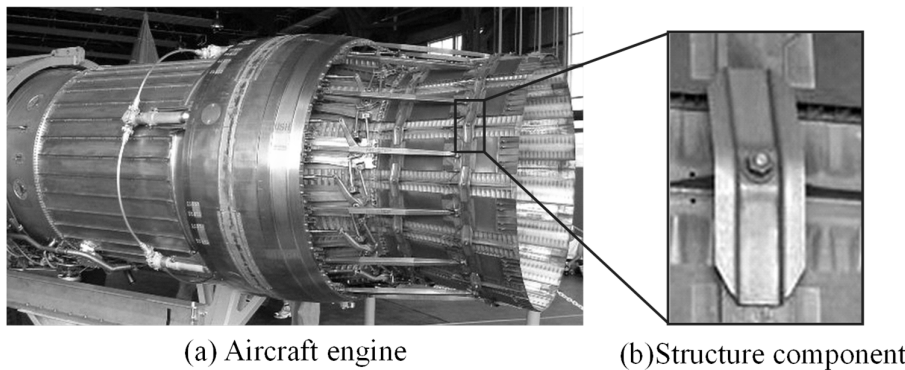


Fig. 1.9. Structure component made of titanium alloy sheet for aircraft engine [39].

The rapid resistance heating was effective in the hot stamping, only a short time is required for heating the sheet up to 900°C [40]. The resistance heating is generally employed for the preheating of forging billets. The warm and hot stamping using resistance heating are used in the tailor die-quenching for producing ultra-high strength steel formed parts having a strength distribution and to the spline forming of ultra-high

strength steel gear drums [41-43], respectively. The local resistance heating of a shearing zone is used in a punching process of the ultra-high strength steel sheets [44]. The hot stamping using the resistance heating is also applied to the titanium alloy sheets, however forming results were hardly shown [45].

1.2. Research objectives

1.2.1. In-situ measurement of deformation behaviour of sheet and tools during stamping process.

The aim of this dissertation is to develop an in-situ measurement of deformation behaviour of the sheet and tools during stamping process. The borescopes having a small CCD camera and thin cable are used and placed inside the tools. The three-dimensional deformation behaviour of the sheet and tools is measured.

1.2.2. Formability improvement of high strength steel and titanium alloy sheets

Although the applications of high strength steel and titanium alloy sheets to the automobile and airplane parts respectively, offer a high potential for the reduction of the weight, the dimensional accuracy of formed products deteriorates due to large springback and small formability are crucial problems. In order to improve the formability of the sheets and reduce the defects of the products, new types of the punches are proposed for the flanging and hemming of the high strength steel sheets. In addition, the hot forming using resistance heating is applied to form the titanium alloy sheet.

1.3. Outline of dissertation

This dissertation discusses about the in-situ measurement of deformation behaviour of the sheet during stamping process using the borescopes, followed by the prevention of the occurrence of the wrinkle and cracks during the shrink and stretch flanging respectively. The improvement of the formability of the titanium alloy sheet using hot bending is discussed in following chapter. Finally, the improvement of the joints strength and the absorbed energy in crash test of the high strength steel sheets by the joined by the hemming method are presented.

This dissertation consists of seven chapters:

Chapter 1 presents the general introduction for the overall contents of the thesis.

Chapter 2 presents the new method of in-situ measurement for the stamping process. The borescope with a tiny camera and a small cable is installed in a small space surrounded with tools to measure a deforming sheet and punch during shrink flanging. The variation of the distance between the sheet and die during the process is measured and compared with the result obtained from the laser displacement equipment. The distribution measurement is obtained using borescope.

Chapter 3 presents the in-situ measuring method using two borescopes to measure the three-dimensional deformation behaviour during a flanging process of sheets. The small size borescopes with a flexible cable is placed inside the tool to measure three-dimensional deforming edge of the sheet. The distribution of the springback is increased and more data were obtained when measuring using the two borescopes. The height of wrinkling for different strokes is also measured using the borescope.

Chapter 4 presents the prevention of the occurrence of the wrinkle and cracks during the shrink and stretch flanging respectively. A shape of a punch having gradual contact was used in order to prevent the wrinkling in shrinkage flanging of ultra-high strength steel sheets. The sheet was gradually bent from the corner of the sheet to reduce the compressive stress. For the stretch flanging, the operation is divided into 2 stages, peripheral bending and corner bending in order to reduce the punch stroke of the press and the tensile stress around the corner edge. In the 1st stage, the periphery of the corner is bent with the punch having a recessed in the middle and in the 2nd stage, the residual portion is bent with the flat bottom punch, and the tensile stress around the corner edge is reduced by restraint of the bent periphery.

Chapter 5 presents the joining of ultra-high strength steel sheets by hemming and improvement of joint strength. The high strength steel sheets are joined by hemming method to form a hollow section. The punch with a stopper is used to prevent the crack during the hemming process. The crashing behaviour of the high strength steel hollow sections joined by hemming is examined through an experiment by crushing the hollow section at a high speed stroke in a press machine. The absorbed energy obtained from the crash test is compared between hollow section joined by hemming and spot welding.

Chapter 6 presents the hot bending process of a titanium alloy sheet using resistance heating. Besides to increase the formability and to reduce the forming load, the hot bending process using the resistance heating method is also used to prevent the occurrence of the oxidation to the titanium sheet. The springback and hardness of the hot bent sheet were also measured.

Finally, the concluding remarks and future perspective are given in Chapter 7.

Chapter 2

In-situ measurement of deforming shapes of sheet and tools during stamping using borescope

2.1. Introduction

Deformation of sheets and deflection of tools are useful information of designing forming processes, however it is not easy to measure the deformation and deflection during forming due to small space of the tool cavity. A strain gauge is used by several researchers for in-situ measurement in the stamping process. Yoneyama and Tozawa [3] measured histories of contact pressure and temperature in die forging with a pin sensor having strain gauges and thermocouples embedded in a die. Jeswiet and Nyahumwa [6] used some conical cantilever sensors having strain gauges embedded in a roller to measure three-dimensional contact pressure in rolling. Siegert et al. [7] performed closed-loop control of a stamping process by blank holder force measured with piezoelectric load sensors. The installation of strain gages for measuring deflection of tools becomes complex, and it is not easy to measure a distribution of deflection.

CCD cameras are attractive in three-dimensional in-situ measurement in metal forming. Azushima [10] developed a microscope video system with a CCD camera to observe contact behaviour at the interface between a transparent glass die and workpiece during drawing. Bech et al. [11] used a similar approach to observe trapping behaviour of lubricant in extrusion. Mori et al. [2] measured two-dimensional

springback behaviour in V-shaped bending of ultra-high strength steel sheets with a CCD camera outside tools. Jäger et al. [12] measured depth and length of the bulge profiles of a tube during electromagnetic forming using a CCD camera. The conventional CCD cameras are too large to be installed inside tools.

Hamedon et al. [46] have used a borescope with a tiny camera and a small cable for in-situ measurement of deformation behavior of a sheet during shrink flanging. Since the size of the borescope is small, it is comparatively easy to install the borescope in a small space surrounded with tools. In this study, deforming shapes of high strength steel sheets and a punch during shrink flanging were measured by means of a borescope having higher resolution.

2.2. Procedure of in-situ measurement using borescope

A borescope consisting of a CCD camera with flexible cable having specifications as shown in table 1 was used to measure a deforming sheet and punch during shrink flanging. Since the sizes of the camera and cable are small, the borescope is installed in a small gap surrounded with tools.

Table 2.1 Specifications of borescope.

Size	Ø8 x 40 mm
Resolution	640 x 480 pixels
Display speed	30 fps
Focusing	Auto-focusing (20 – 80 mm)
Cable size	Ø3 x 2,000 mm (extendable)

The variations of the measuring error and measuring length of the image with the distance from the object are shown in Fig. 2.1, where the error is obtained from the difference between lengths of 1 and 5 mm indicated with a micrometer, and the measuring length l is the distance between both edges of the image. As the distance from the object increases, the measuring length increases, whereas the measuring error becomes large. The error of the borescope with 1.3 MP in resolution is improved from that for the borescope with 0.3 MP in resolution. The measuring data were corrected by this error.

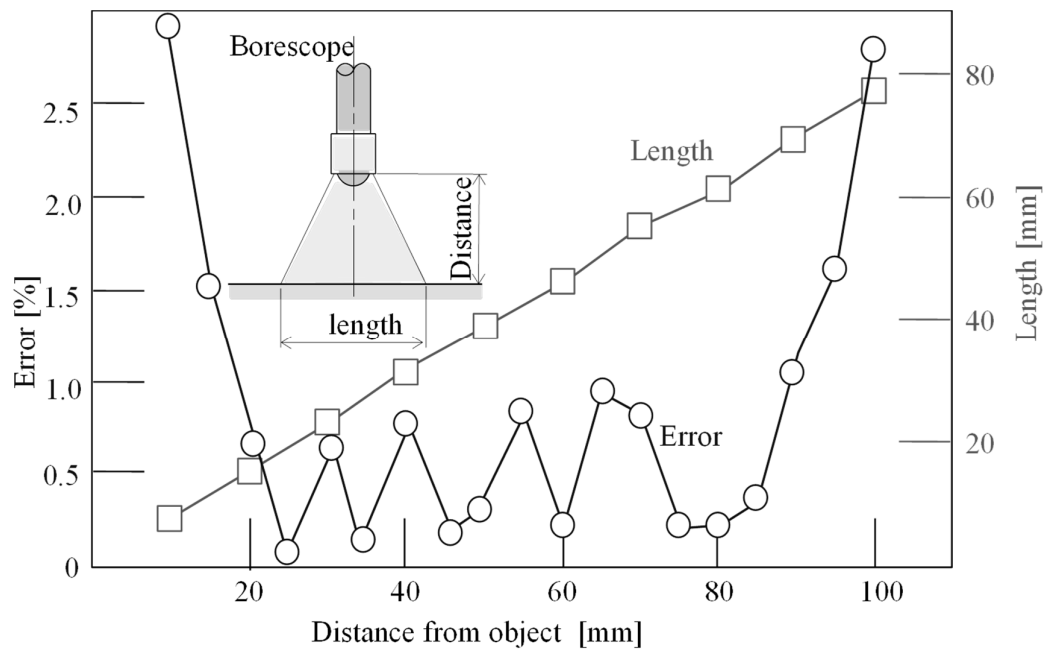


Fig. 2.1 Variations of measuring error and measuring length of image with distance from object

The in-situ measurement of the deforming behavior of the sheet and tools during

the shrink flange shown in Fig. 2.2 was performed, where W is the distance between the edges of the sheet and die. The borescope was placed in the small space between the tools and attached with a 90° deflection mirror. High strength steel sheets with 140 mm in length, 190 mm in width and 1.2 mm in thickness were used for an experiment of shrink flanging. A servo press with a maximum load capacity of 800 kN was used for the shrink flanging. The experimental conditions are given in Table 2.1.

Table 2.2 Experimental conditions of in-situ measurement using borescope.

Ratio of clearance to thickness c	0.9-1.2
Distance from object h /mm	5-25
Distance from center d /mm	0-25

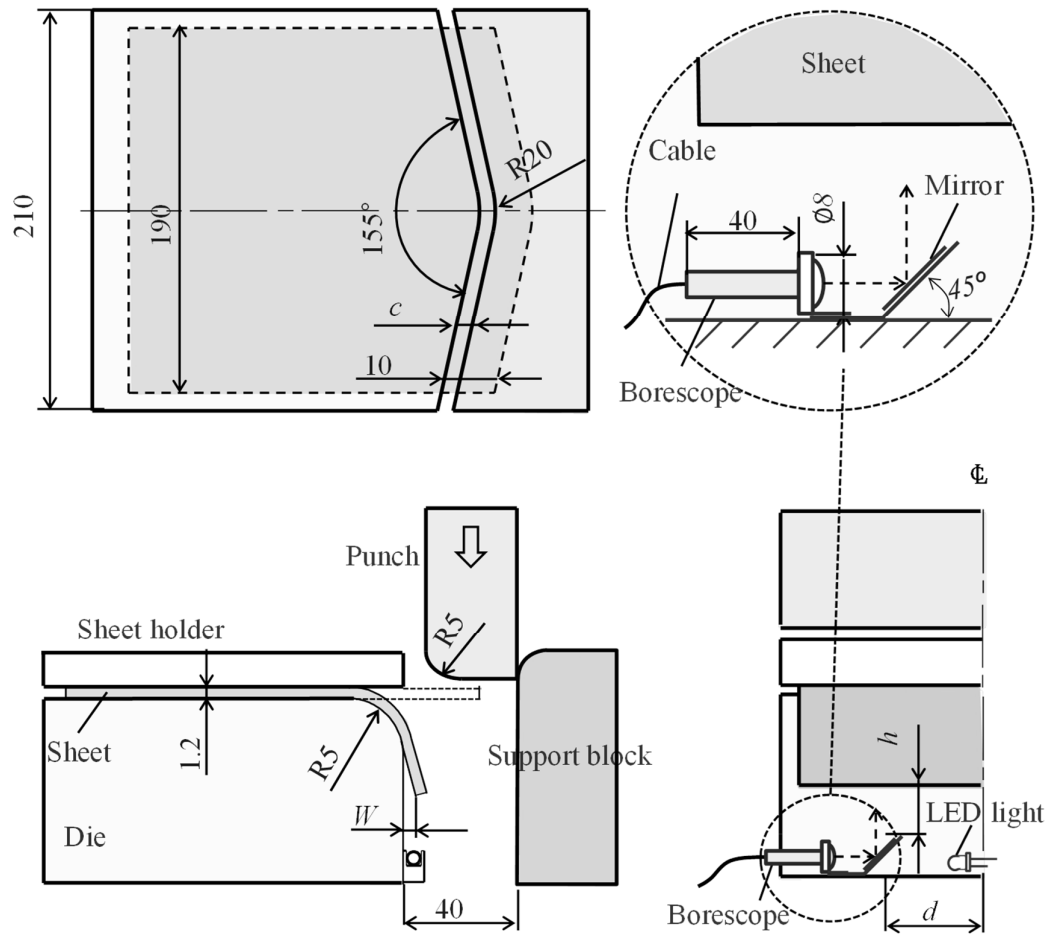
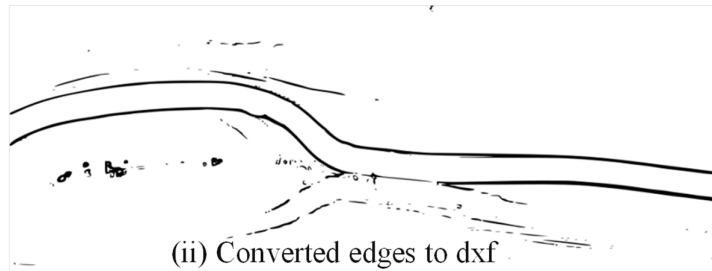


Fig. 2.2 In-situ measurement of deforming shape of sheet and tool during shrink flanging.

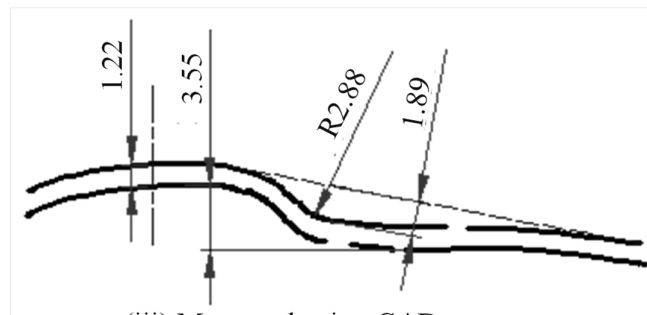
An image captured using borescope is processed by converting the picture into a monochrome format. In order to obtain clear edge identifications when changing the format to monochrome, the edge of the sheet is painted to white color. The outline of the picture is then trace by using commercial software Inscap and converted into dxf format. The dxf file format is opened using CAD and automatics measurement is carried out. A procedure of the image processing is shown Fig. 2.3.



(i) Image from borescope



(ii) Converted edges to dxf



(iii) Measured using CAD

Fig. 2.3 Procedure of image processing.

2.3. In-situ measurement of deformation behavior of sheet

The image around the corner of the die measured by the borescope at different punch strokes is shown in Fig. 2.4. At the punch stroke $s=5$ mm, the wrinkle appears in the corner of the die, whereas the wrinkle is almost eliminated at $s=20$ mm.

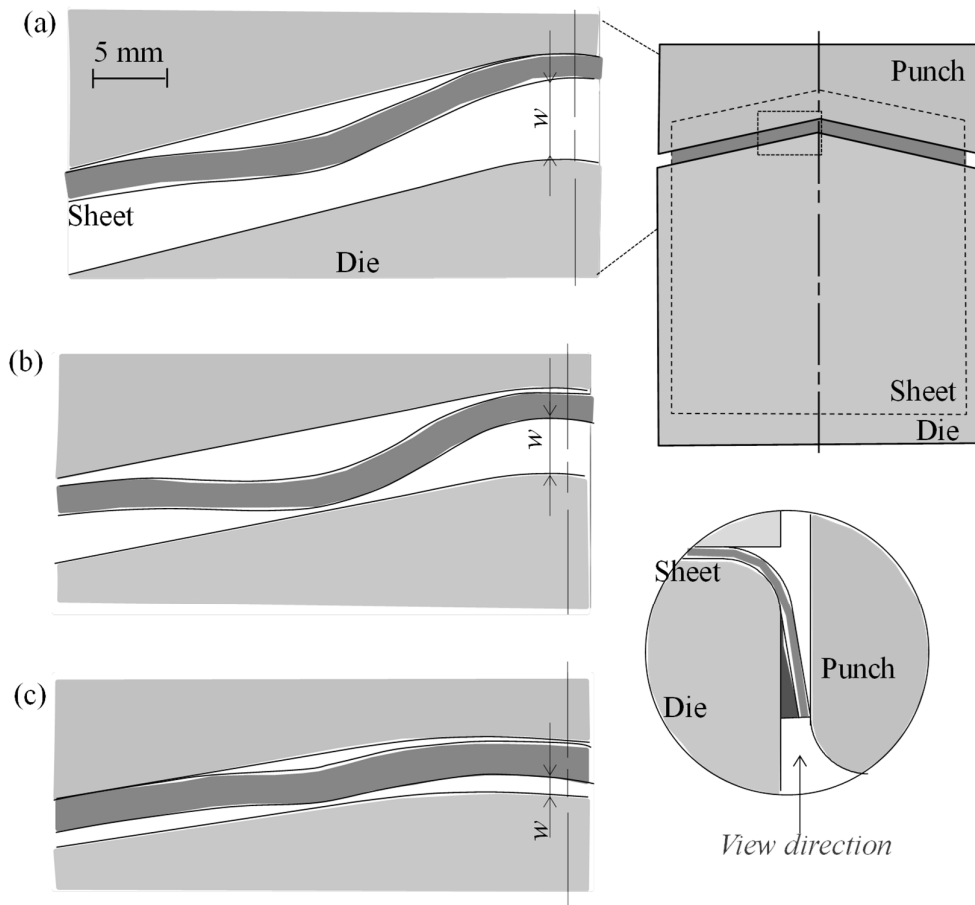


Fig. 2.4. Image around die corner measured by borescope at different punch stroke for $c=1.2$.

The variation of the distance between the sheet and die with the punch stroke for $c=1.1$ is given in Fig. 2.5. When the punch moves down, the distance between the sheet and die at the center of the corner, $d=0$ mm, is larger than that at $d=10$ mm due to higher pressure. The distributed distance can be measured by the borescope. The distance is the lowest at the bottom dead center, and then the springback occurs.

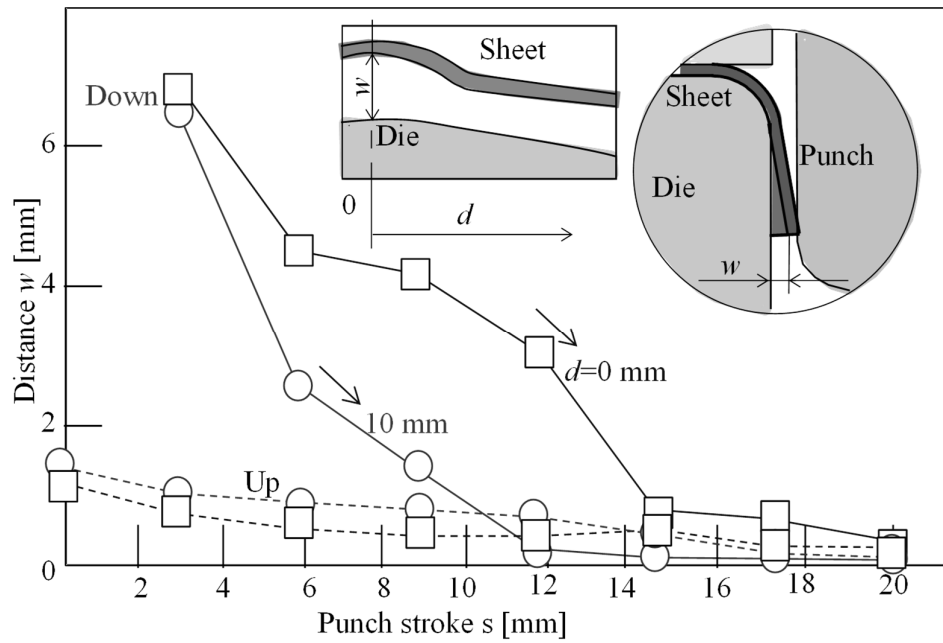


Fig. 2.5. Variation of distance between sheet and die with punch stroke for $c=1.1$.

The distance between the sheet and die after the unloading measured by the borescope is compared with that measured by the laser displacement sensor for $d=0$ and 10 mm and $c=1.1$ in Fig. 2.6. The measuring error of the borescope is very small, about 1.2%. All of the measurement is corrected by this value. Since the measuring error is too small, the measurement obtained from pictorial data using borescope is considered reliable.

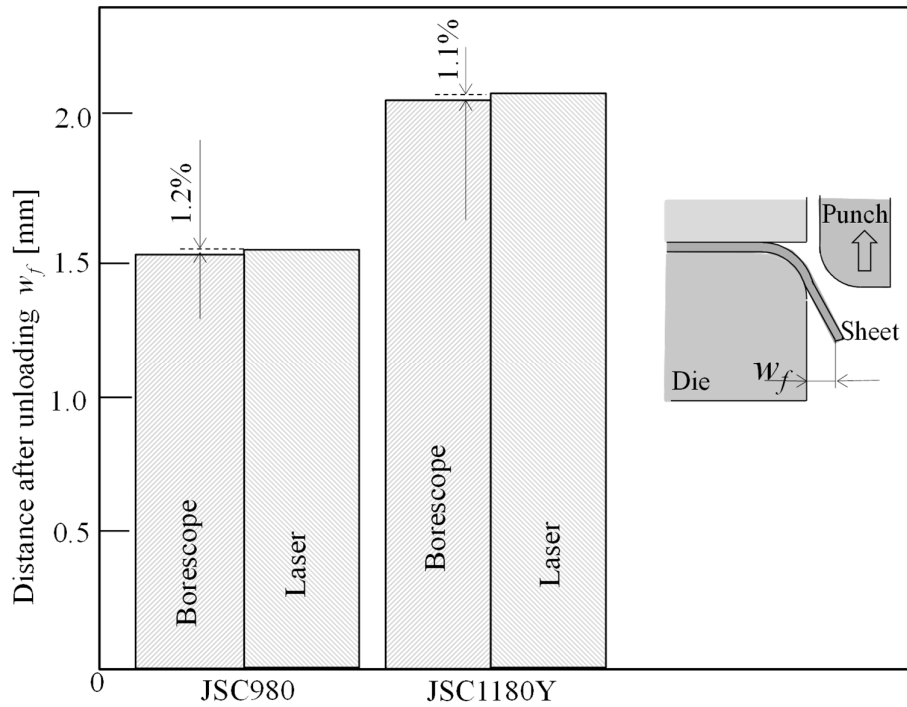


Fig. 2.6. Comparison between distances between sheet and die after unloading measured by borescope and laser displacement sensor for $c=1.1$ and $d=0$.

The relationship between the real springback distance and the ratio of clearance to the thickness for $d=20$ mm is given in Fig. 2.7. Since the bent angle just before the unloading is not 90° , the real springback distance was obtained from the difference of the distance between the sheet and die just before the unloading and after unloading. Since the in-situ measurement is possible for the borescope, the real springback was obtained. The real springback distance is lower than that from 90° for the conventional measurement. As the ratio of clearance to the thickness increases, the real springback distance slightly increases.

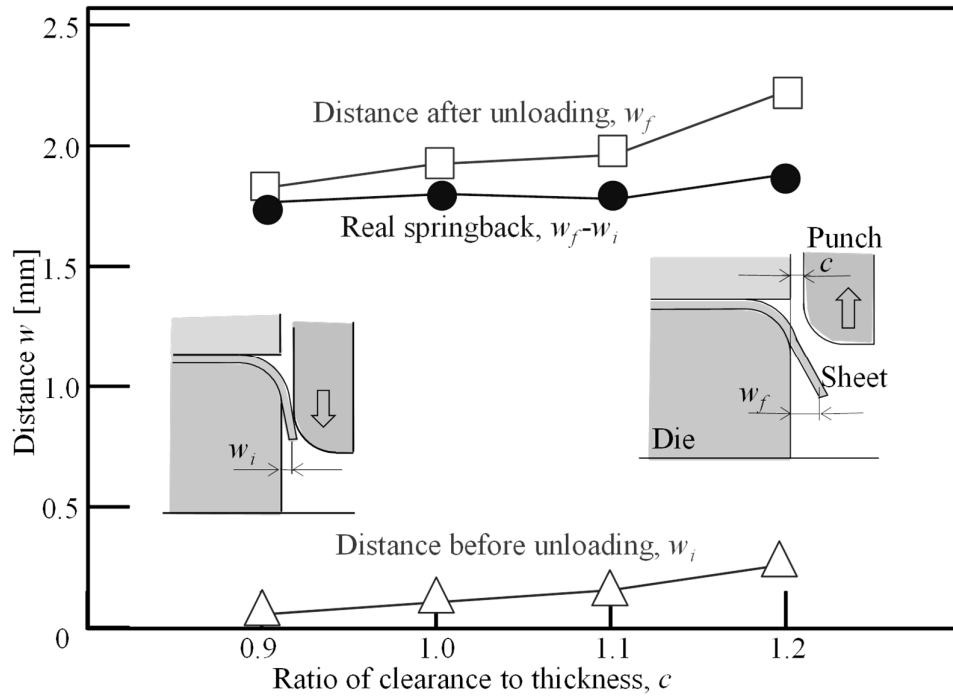


Fig. 2.7. Relationship between distances of sheet to the die, real springback and ratio of clearance to thickness for JSC1180Y, $d=20$ mm.

2.4. In-situ measurement of deflection of punch

The deflection of the punch was also monitored using the borescope. The variation of the punch deflection with the punch stroke for $c=1.1$ is given in Fig. 2.8. The punch deflection has a peak at $s=10$ mm for all 3 sheets due the maximum flanging load. The deflection of the punch is reduced by the support block.

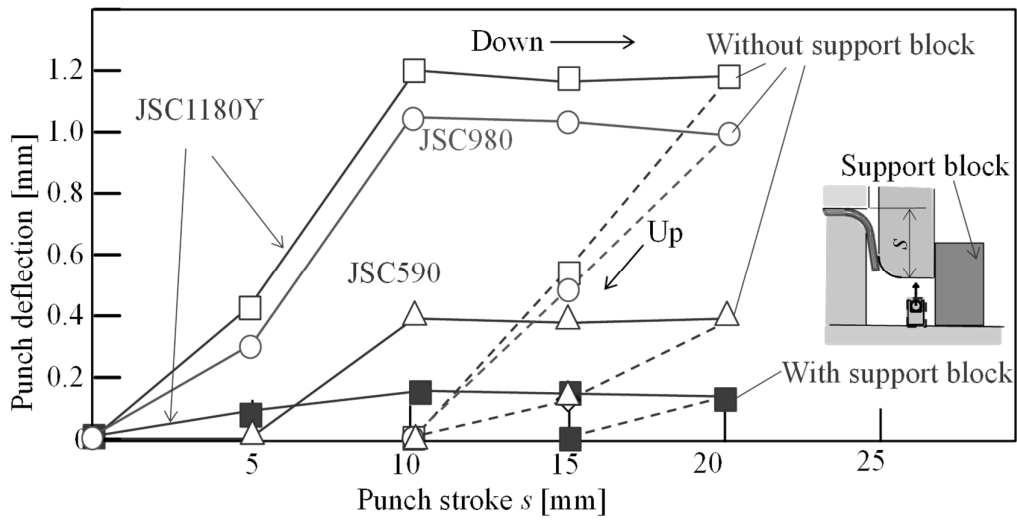


Fig. 2.8. Variation of punch deflection with punch stroke for $c=1.1$.

The relationship between the punch deflection and the ratio of clearance to the thickness is shown in Fig. 2.9. The error of the borescope is within 7 % in comparison with the dial gage. As the clearance increases, the punch deflection decreases due to the decrease in flanging load.

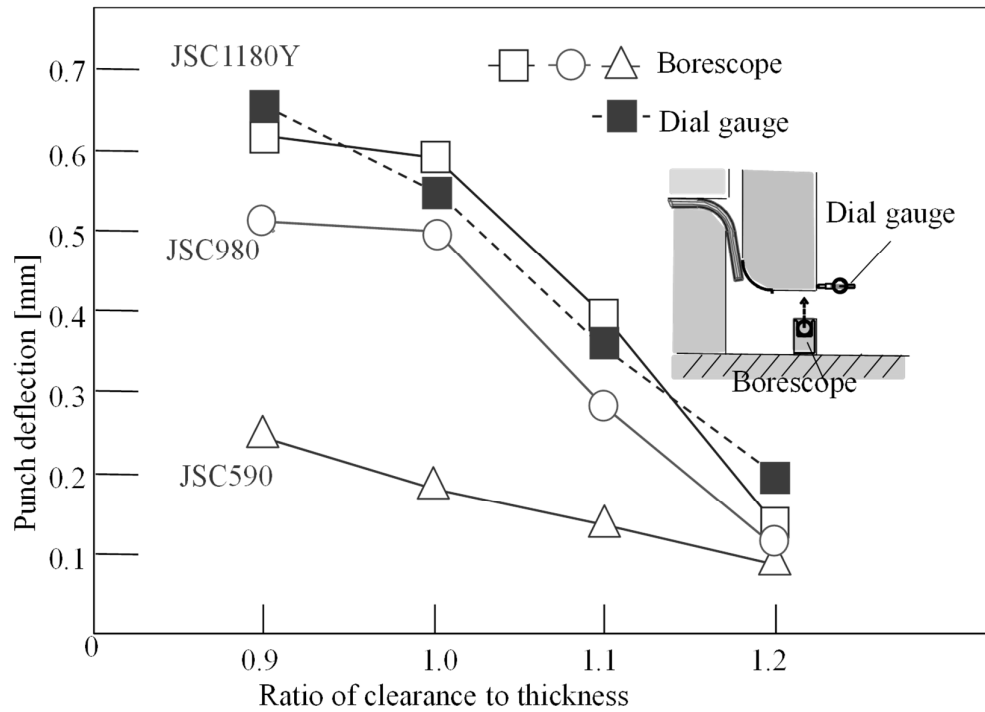


Fig. 2.9. Relationship between deflection of punch and ratio of clearances to thickness.

2.5. Conclusions

The in-situ measurement of deforming shapes of the sheet and punch deflection using the borescope during the shrink flanging process was successfully carried out. The image of the formation and elimination of the wrinkling during the shrink flanging was obtained using the borescope. The real springback distance was measured from the distances just before the unloading and after the unloading. The borescope was also used to measure the deflection of the punch during the flanging.

Chapter 3

In-situ measurement of 3-dimensional deformation during flanging of sheet metal using 2 borescopes

3.1. Introduction

Although the information about a deformation behavior useful for design of tools, it is not easy to measure during stamping processes. Since a deforming sheet is generally surrounded with complicated tools during a stamping operation, application of sensors for the in-situ measurement become limited. Several methods were used to obtain the measurement of the deformation behaviour during the stamping process. Yang et al. [8] used acoustic emission sensors to detect friction sources during deep drawing. Lupoi and Osman [5] located the pin sensors for measuring contact pressure in extrusion beneath the die surface to avoid interference with material flow by the sensors. Roizard et al. [4] used LVDT sensors to measure movement of a sheet and die during deep drawing. Kim et al. [9] measured the displacement of a die during deep drawing using a laser sensor. For these measurements, fine machining with tools is required for the installation and the obtained results are local, i.e. spatial data cannot be easily provided.

CCD cameras were also found to be used in order to obtain data of the deformation behaviour of the sheets during the stamping process. Mori et al. [2] measured two-dimensional springback behaviour in V-shaped bending of ultra-high strength steel sheets with a CCD camera outside tools. Hofman et al. [13] observed a melt pool with a

CCD camera to adjust laser power in laser cladding. Kuwabara and Sugawara [14] measured surface strains and curvature of a tube in hydraulic bulging with two CCD cameras. Kaupper and Merklein [15] detected the initiation, growth and distribution of surface failures in bending of a high strength steel sheet using a CCD camera. Hamedon et al. [46,47] have used a borescope with a tiny camera and a small cable for an in-situ measurement of 2-dimensional deformation behavior of a sheet and deflection of a punch during shrink flanging of a high strength steel sheet. Although CCD cameras are attractive in three-dimensional in-situ measurement in metal forming, the cameras are not enough small to be installed in a small gap surrounded with tools in general stamping processes. However, the measurement of 3-dimensional deformation during bending is difficult to get due to absents of the suitable equipment and methods.

In this study, an in-situ measuring method using 2 borescopes was developed to measure the 3-dimensional deformation behavior during a flanging process of sheets. The small size borescope with a flexible cable is placed inside the tool to measure 3-dimensional deformation behavior of the sheets during shrink flanging.

3.2. Measuring method of edge of deforming sheet

3.2.1 Measuring using 2 borescopes

The two borescopes having a CCD camera of 8 mm in diameter, 1.3 MP (megapixels) in image resolution, 30 fps in frame rate were used to measure the deforming edge of the sheet. Since the size of the borescope is small, the borescopes are installed in a small gap surrounded with tools. A measuring error of an image for the different height and distance from the center is carried out and the obtained error was

less than 2.5%. Table 3.1 shown the specifications of the borescopes used for the measurements.

Table 3.1 Specifications of borescopes.

Size	Ø8 x 40 mm
Resolution	640 x 480 pixels
Display speed	30 fps
Focusing	Auto-focusing (20 – 80 mm)
Cable size	Ø3 x 2,000 mm (extendable)

The two borescopes are used to measure the shape of the sheet edge as shown in Fig 3.1. The length l , from the edge of the deforming sheet is calculated by

$$l = \frac{c}{\tan \alpha_1 + \tan \alpha_2} \quad (1)$$

where d is the distance between the two cameras and the angles α_1 and α_2 are determined by counting the number of pixels from the camera center in the taken image.

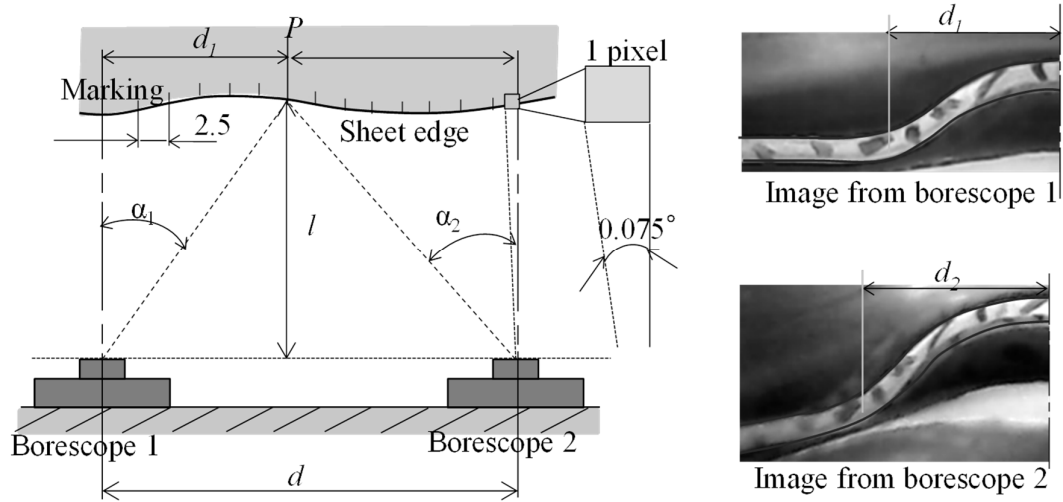


Fig. 3.1. Measuring method of distance from sheet edge using 2 borescopes.

In order to obtain the length from the sheet edge to the borescope, the angle per one pixel of the borescope is required. Fig. 3.2 shows the relationship between the angle per one pixel and the length between the borescope and sheet edge. The measurable angle of 48° is obtained, thus the angle per one pixel is 0.075° , and this value was used in the measurement.

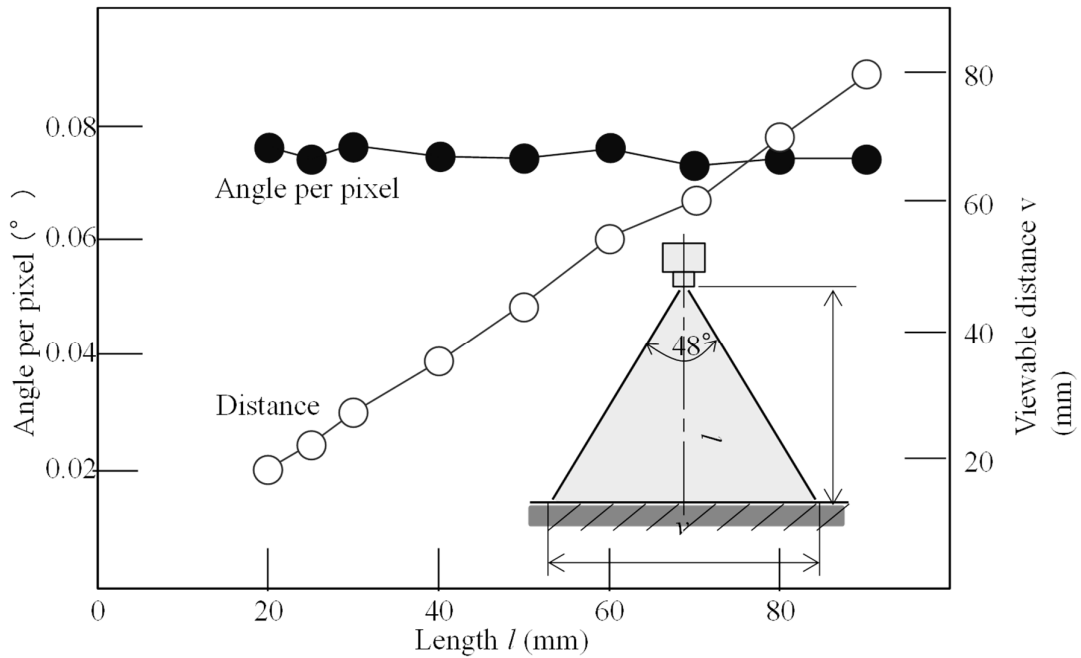


Fig. 3.2. Relationship between angle per one pixel and length between borescope and sheet edge.

3.2.2 Tools of shrink flanging

The tools of shrink flanging for the in-situ measurement of 3-dimensional deformation of a sheet were shown in Fig 3.3. The borescopes with a 90° reflection mirror were placed in the small space between the tools. The ultra-high strength steel sheet JSC1180 was used and the clearance ratio between the punch and die to the sheet thickness was 1.2.

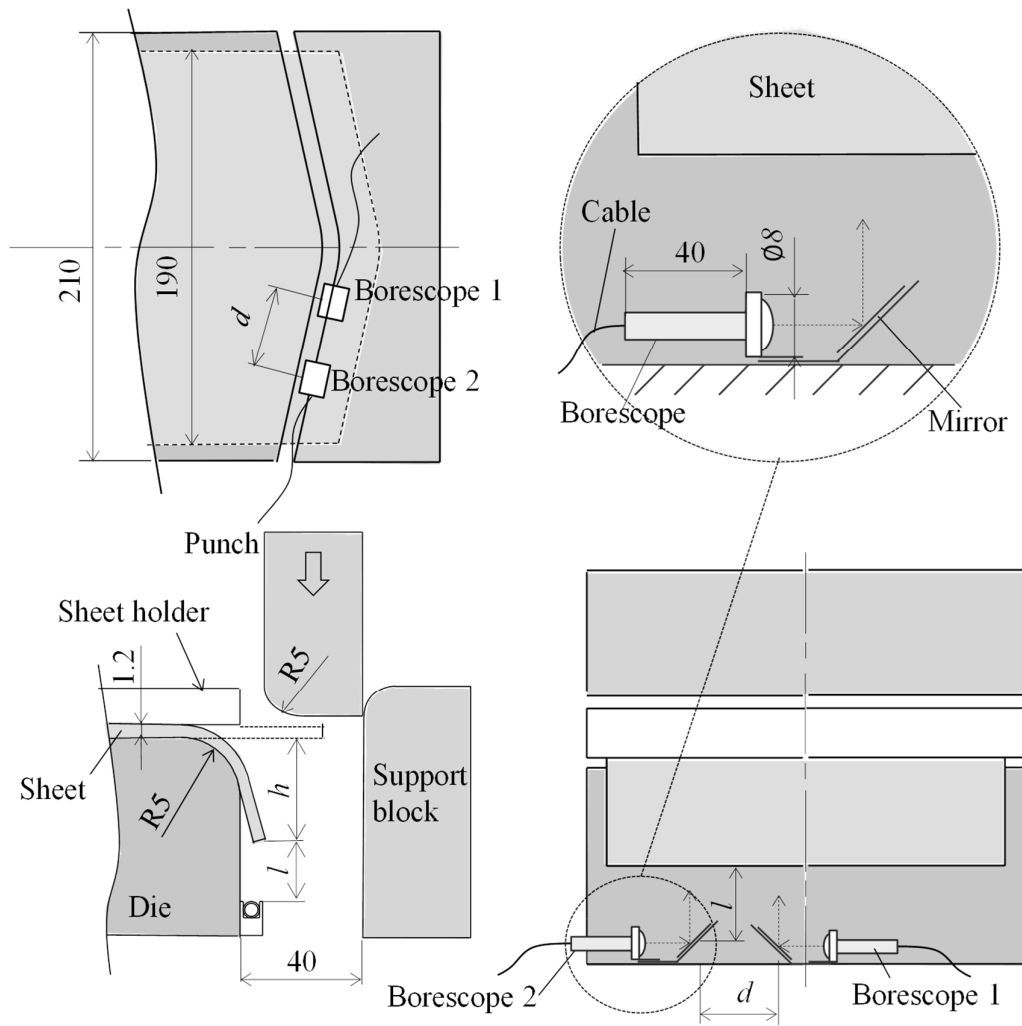


Fig. 3.3. Tools of in-situ measurement of 3-dimensional deformation of during shrink flanging using 2 borescopes.

3.2.3 Accuracy of measurement using 2 borescopes

The accuracy of the measuring method using 2 borescopes was examined from the scale placed on the flat surfaces, where the length from the borescope was $l=73$ mm and the distance between the two borescopes was $d=20$ mm. The images taken with the 2 borescopes are shown in Fig 3.4. The length from the two borescopes to the points A, B

and C on both of the images was measured and calculated using Eq. (1), and the errors were 0.3, 0.8 and 0.1%, respectively.

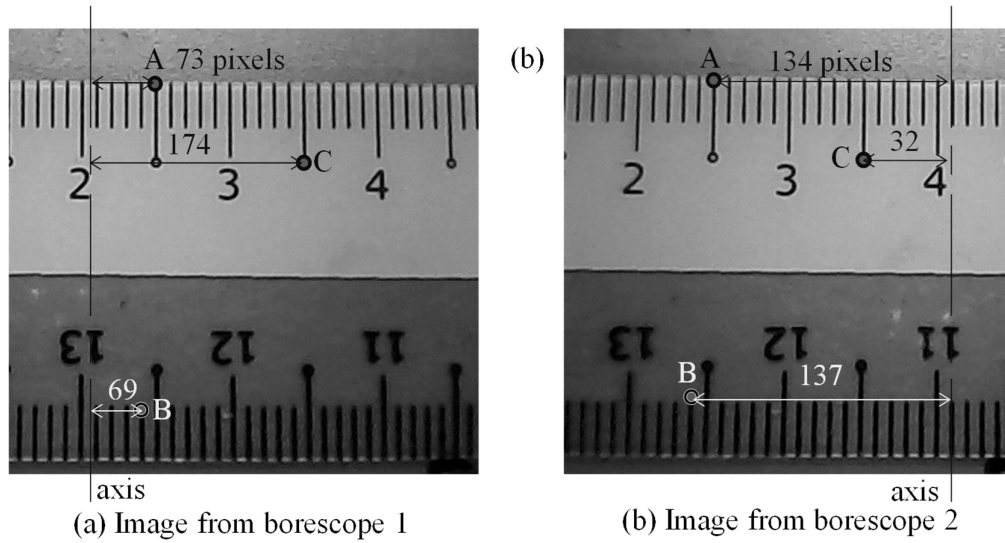


Fig. 3.4. Images of scale taken with 2 borescopes for $l=73$ mm and $d=20$ mm.

3.2.4 Bending of inclined sheet

The measured flange height h of the sheet and the springback for bending of the inclined sheet are shown in Fig. 3.5. In the comparison with the result obtained from AutoCAD, the maximum error was 3%. As the distance from the center increases, the springback becomes large.

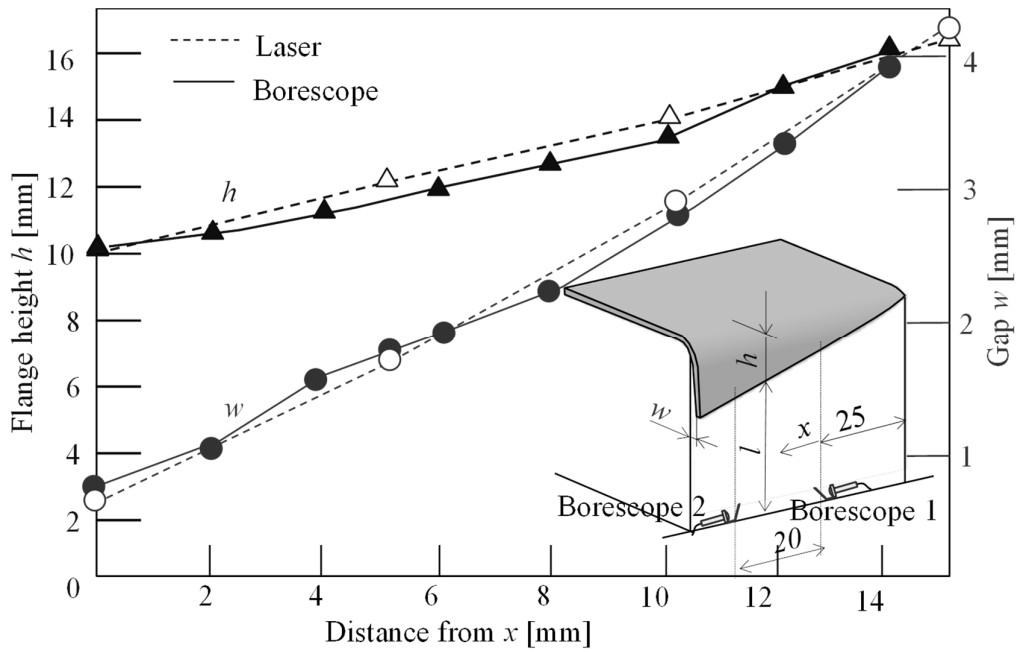


Fig. 3.5. Measured flange height of sheet and springback for bending of inclined sheet.

3.3 Measurement of 3-dimensional deformation of sheet in shrink flanging

The variation of the distribution of the flange height with the punch stroke is shown in Fig. 3.6. For the lower stroke, the flange height is almost constant, whereas for the higher stroke the flange length near the corner becomes larger due compression from the surrounding portions. The error of the flange height for the sheet after unloading was 5.2% from comparison with that measured from the laser sensor.

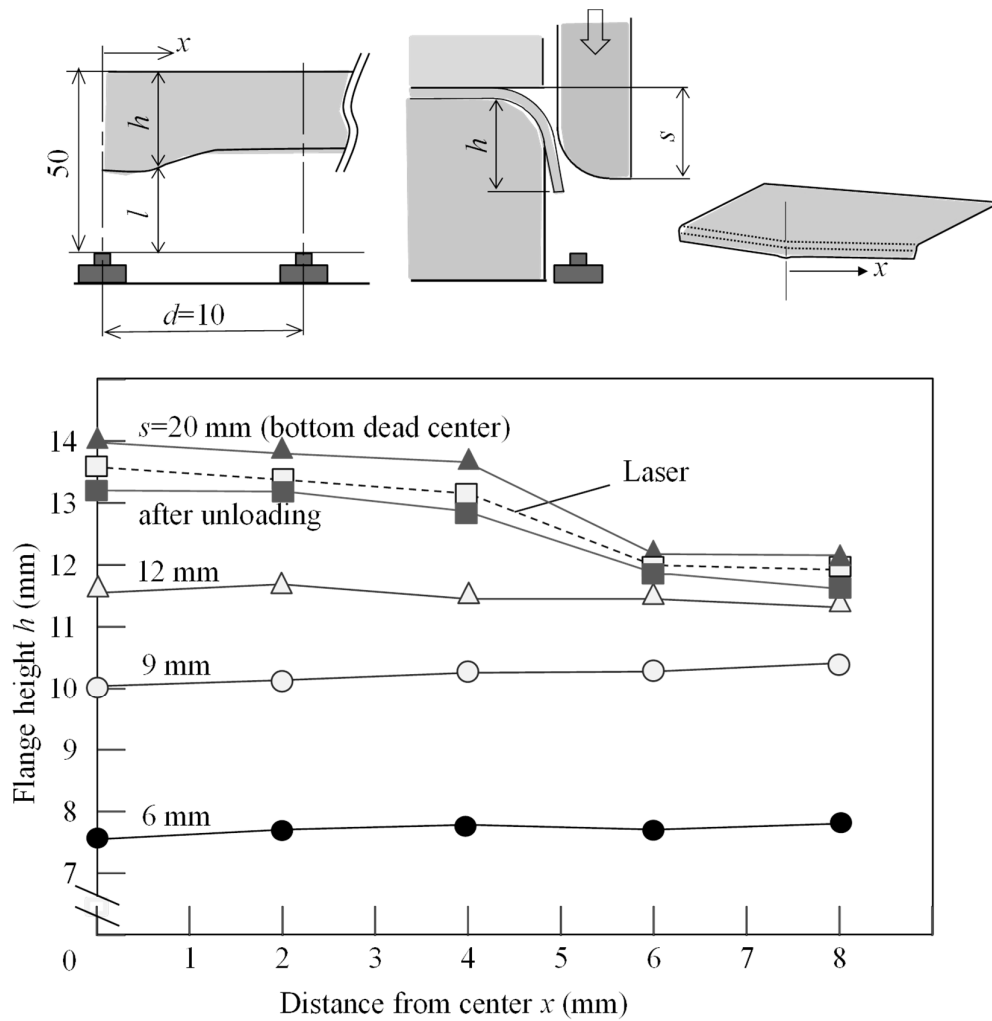


Fig. 3.6. Variation of distribution of flange height with punch stroke.

The distribution of the springback from the center measured with the two borescopes is shown in Fig. 3.7. The measuring length of the distribution of the springback is increased 2 times by the 2 borescopes. Since the bent angle at the bottom dead center is not 90° , the real springback was obtained from the difference between the gaps before and after unloading. The real springback is lower than that the nominal springback.

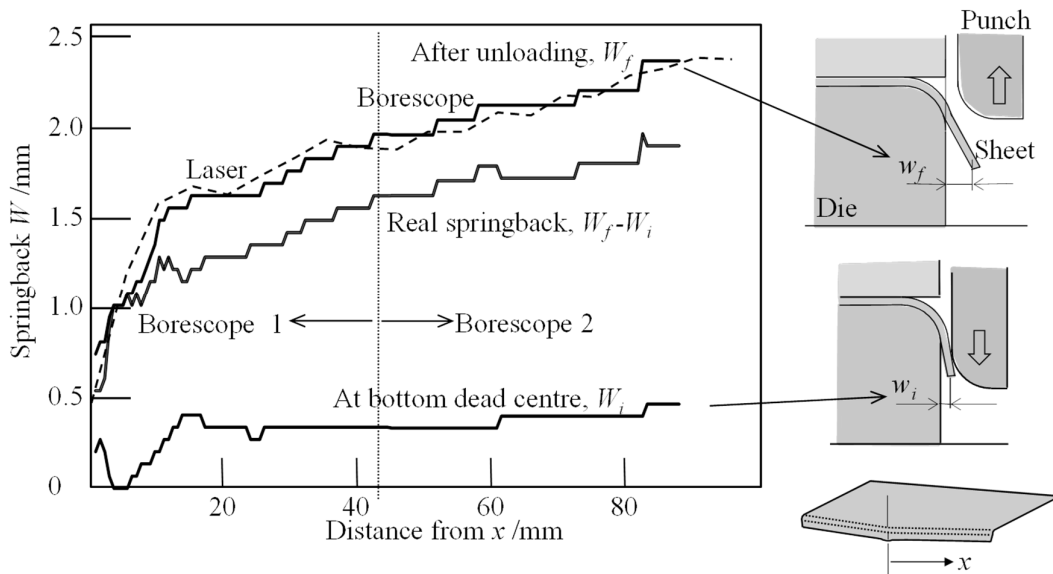


Fig. 3.7. Variation of distribution of springback with distance from center.

The variation of the distribution of the wrinkling height with the punch stroke is shown in Fig. 3.8. The wrinkling height is the largest near the corner due to the larger compressive stress, and is maximum for a punch stroke of 15 mm. The wrinkling height slightly increases after unloading.

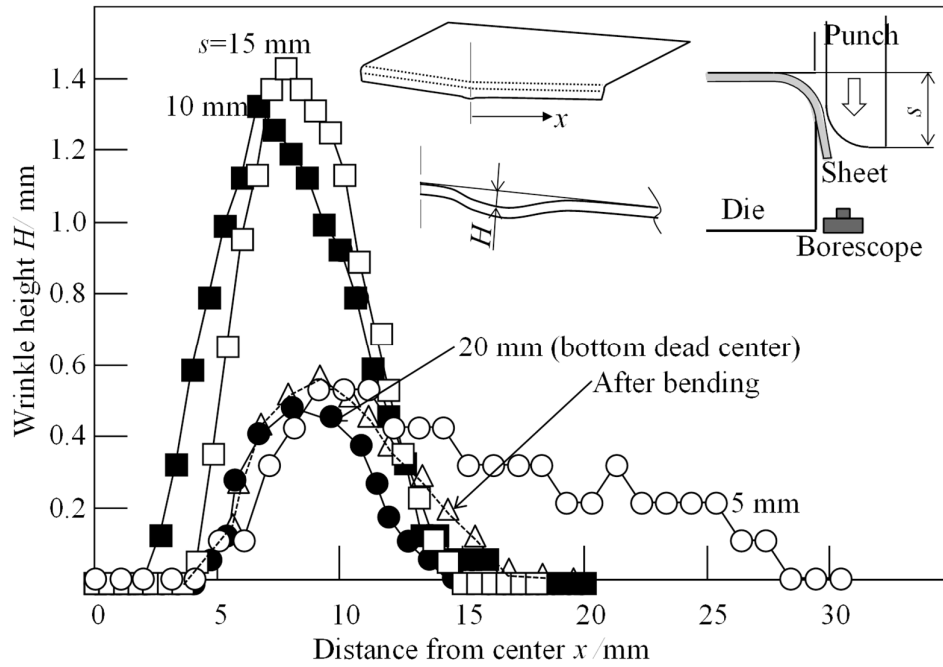


Fig. 3.8. Variation of distribution of wrinkling height with punch stroke.

3.4. Conclusions

The measuring method using the 2 borescopes is able to measure the flange length of the edge of the sheet from the borescope during the bending process. The distribution of the springback is increased and more data were obtained when measuring using the 2 borescopes. The height of the wrinkling for different strokes is also measured using the borescope.

Chapter 4

Improvement of formability of ultra-high strength steel sheets in flanging

4.1. Introduction

The reduction in weight of automobiles is effective in improving the fuel efficiency, and forming processes of lightweight materials have been actively developed [19]. Although the application of aluminium and titanium alloy sheets are attractive lightweight materials for reduction of the automobile weight [21], the high cost and small formability are crucial problems [22,23], thus the industry still has a great interest in steel sheets. By having the high specific strength and cost competitiveness, the high strength steel sheets are the most attractive for body-in-white parts. The strength of high tensile strength steel sheets remarkably increases and ultra-high tensile strength steel sheets more than 1 GPa have been developed. In stamping operations of high strength steel sheets, large springback, small formability, short tool life, etc. are problems, particularly ultra-high strength steel sheets having a tensile strength above 1 GPa [48].

Since most of the high strength steel sheets are made for body-in-white parts, the bending is a more preferable process for ultra-high strength steel sheets [2]. However, the bending becomes difficult due to the ultra-high strength steel sheets have large strength and small ductility. In addition, instead of a bending the flange in a straight line,

the parts are bend in convex (shrink) and concave (stretch) shape which caused the product to wrinkle due to the compressive stress and crack due to the excessive tensile stress, respectively [27]. Thus, the design of the stamping processes of the high strength steel sheets becomes difficult.

In the shrinkage flanging, the wrinkling tends to occur due to compressive stress [26]. The wrinkling becomes difficult to assemble parts, and severe wrinkling brings about rupture of parts [49]. The shrinkage flange of the ultra-high strength steel sheets not only defect the product by the occurrence of the wrinkling but also caused the seizure and wear of the dies and shorten the life of dies [32]. Since the formed part with wrinkling defect requires to be trimmed at later stage using the trim dies, it will also shorten the life of the trim dies. Although using the thin high strength steel sheet give advantages in manufacturing the lightweight car however it is less stiff and tendency to become wrinkle is high. For the stretch flanging of the high strength steel sheet, the sheet is bend in concave (stretch) shape, the tensile stress at edge of the sheet increased due to the low ductility of the sheets therefore, crack is occurred once exceed the tensile strength limits. The shears conditions of the edge of the sheet with low ductility property are main factors contribute to the occurrence of the crack [33].

In the present study, a shape of a punch having gradual contact was optimized in order to prevent the wrinkling in shrinkage flanging of ultra-high strength steel sheets. The sheet was gradually bent from the corner of the sheet to reduce the compressive stress. Although the occurrences of the crack was prevented and the formability of the high strength steel sheet was improve during the flange process [26] by the gradual contact punch, the punch strokes for the stretch flanging of the dies using the punch

having gradual contact is larger compared to the flat punch thus increased the production time, increased the size of the die and the cost of die. In order to reduce the punch strokes of the stretch flanging using gradual contact punch, a 2-stages flanging was developed using the flat punch with recessed at the center as a first punch and gradual contact punch as a second punch.

4.2. Shrink flanging

4.2.1. Procedure of shrink flanging

An ultra-high strength steel sheet JSC1180YN with a length, width and thickness of 140, 190 and 1.22 mm respectively was used. The mechanical properties of the sheet are given in the Table 4.1.

Table 4.1 Mechanical properties of JSC1180YN.

Thickness	1.22 mm
Tensile strength	1215 MPa
Elongation	10.8%
Flow stress	$\sigma = 1183\epsilon^{0.1}$ MPa

The dimensions of the tools used in the shrink flanging with a punch having gradual contact are shown in Fig. 4.1. The punch having gradual contact has a projection in the central region for gradually bending the sheet from the corner. The experimental conditions are given in Table 4.2, where α is the projection angle of the punch shown in Fig. 4.1 and C is the clearance ratio between the punch and die.

Table 4.2 Experimental conditions of shrink flanging with punch having gradual contact.

Projection angle of punch	$\alpha = 0 - 30^\circ$
Clearance ratio	$C = 100 - 120\%$
Flange length	$L = 7 - 12 \text{ mm}$
Punch velocity	80 mm/s

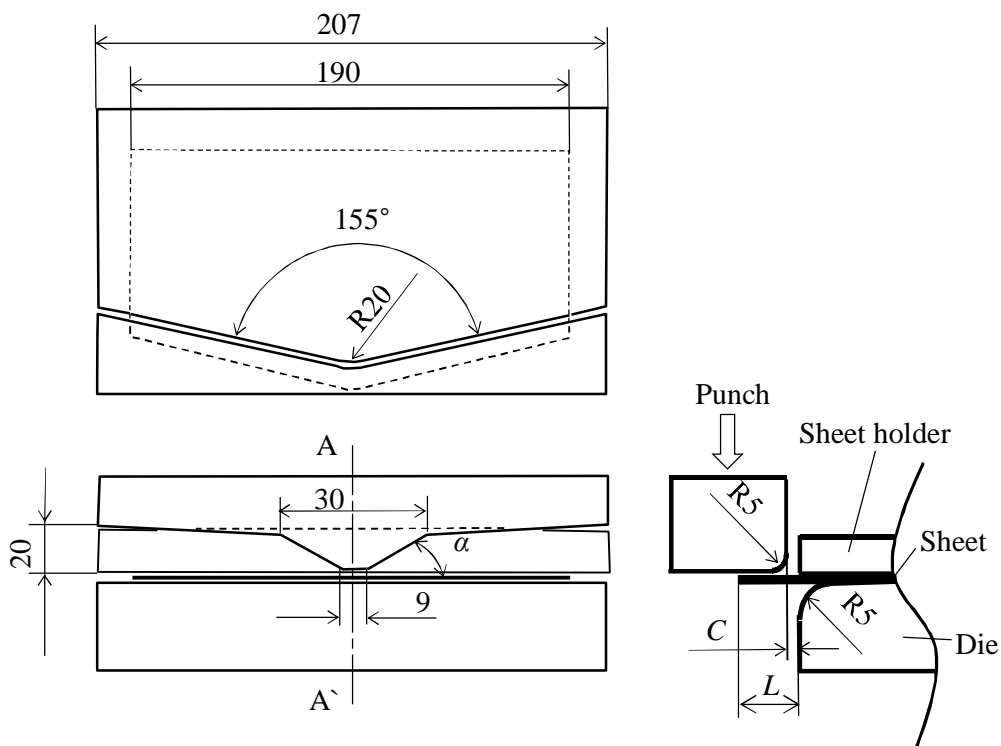


Fig. 4.1. Dimensions of tools used in shrink flanging with punch having gradual contact.

4.2.2. Optimization of projection angle of punch

To optimize the projection angle of the punch, the finite element simulation using the commercial software LS-DYNA was performed. In the calculation, the coefficient of friction between the punch and sheet was assumed to be 0.1.

The relationship between the calculated wrinkle height and punch stroke for the clearance ratio $C=110\%$ and the bent flange length $L=10$ mm is shown in Fig. 4.2. The wrinkling occurs in the vicinity of the corner of the sheet, and the wrinkle is very large for the flat punch of $\alpha=0^\circ$. When the wrinkle height is larger than 0.075 mm, the wrinkling becomes visible in the experiment, and thus the wrinkling was defined to occur.

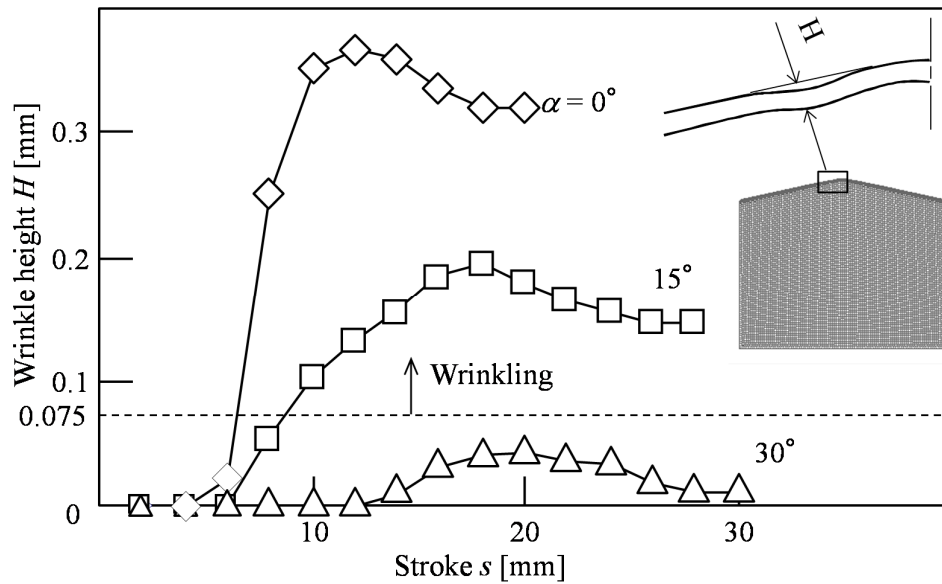


Fig. 4.2. Relationship between calculated wrinkle height and punch stroke for $C=110\%$ and $L=10$ mm.

The calculated distributions of the strain in the width direction for $C=110\%$ and $L=10$ mm are illustrated in Fig. 4.3. The strain in the width direction in the shrinkage flanging is compressive, and the strain has a peak in the vicinity of the corner of the sheet. When the strain in the width direction exceeds a critical value, the wrinkling occurs.

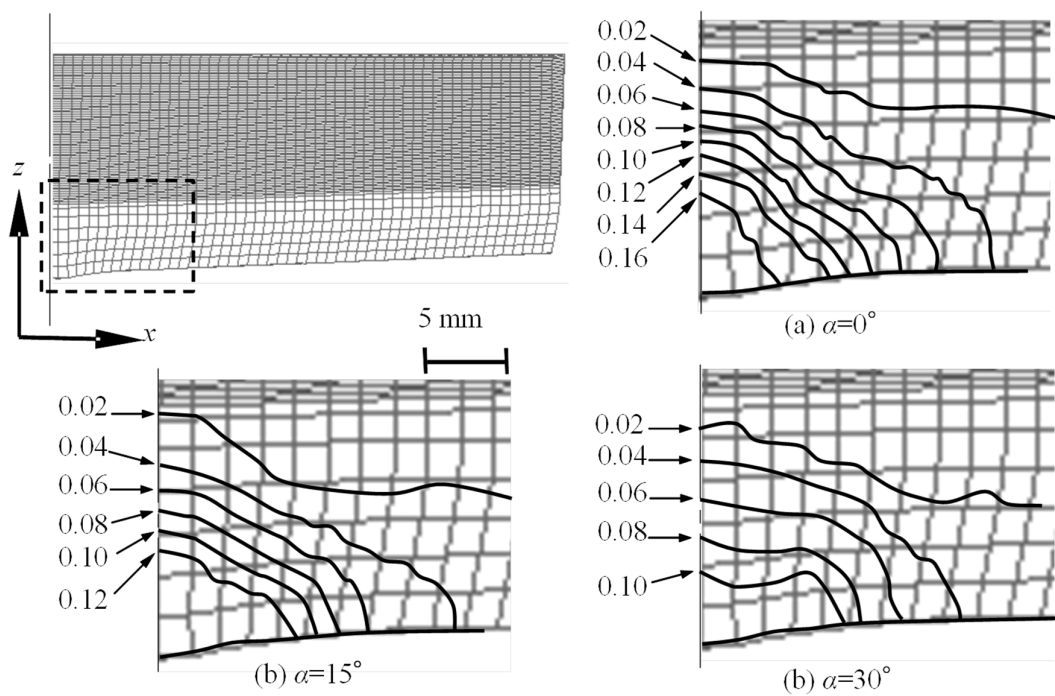


Fig. 4.3. Calculated distributions of strain in width direction for $C=110\%$ and $L=10$ mm.

The flanges in the bent sheet for $\alpha=0$ and 30° , $C=110\%$ and $L=10$ mm obtained from the experiment are shown in Fig. 4.4. For the shrink flanging using the flat punch of $\alpha=0^\circ$, the corner of the sheet wrinkles due to the excessive compressive stress. No wrinkling occurs for the punch having gradual contact of $\alpha=30^\circ$.

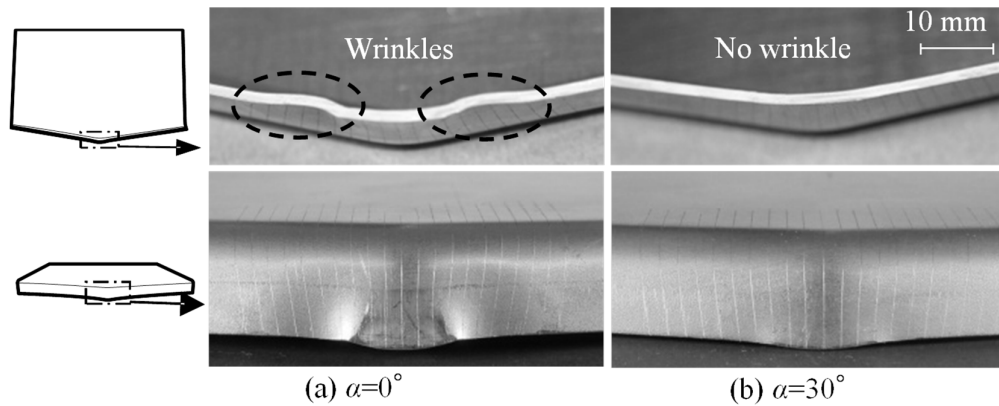


Fig. 4.4. Flanges in bent sheet for $\alpha=0$ and 30° , $C=110\%$ and $L=10$ mm obtained from experiment.

A comparison between the experimental and calculated wrinkling heights is illustrated in Fig. 4.5. As the projection angle of the punch increases, the wrinkle height decreases. The calculated wrinkle height is in good agreement with the experimental one.

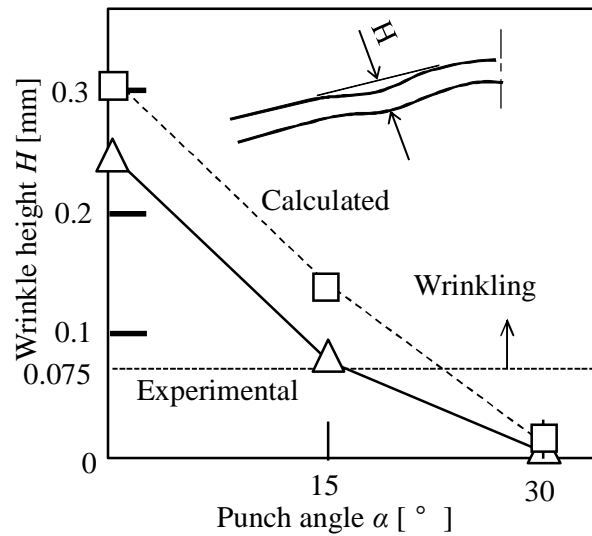


Fig. 4.5. Comparison between experimental and calculated wrinkle heights for $C=110\%$ and $L=10$ mm.

4.2.3. Results for punch having gradual contact

The distribution of the change in thickness obtained from the experiment for $C=110\%$ and $L=10$ mm is illustrated Fig. 4.6. The change in thickness is the highest in the vicinity of the corner of the sheet due to the compressive stress. As the indentation angle of the punch increase, the peak change in thickness decreases, i.e. the decrease in compressive stress. The change of thickness of the sheet for the punches with $\alpha=15^\circ$ and $\alpha=30^\circ$ are almost similar, whereas for punch with of $\alpha=30^\circ$ is larger.

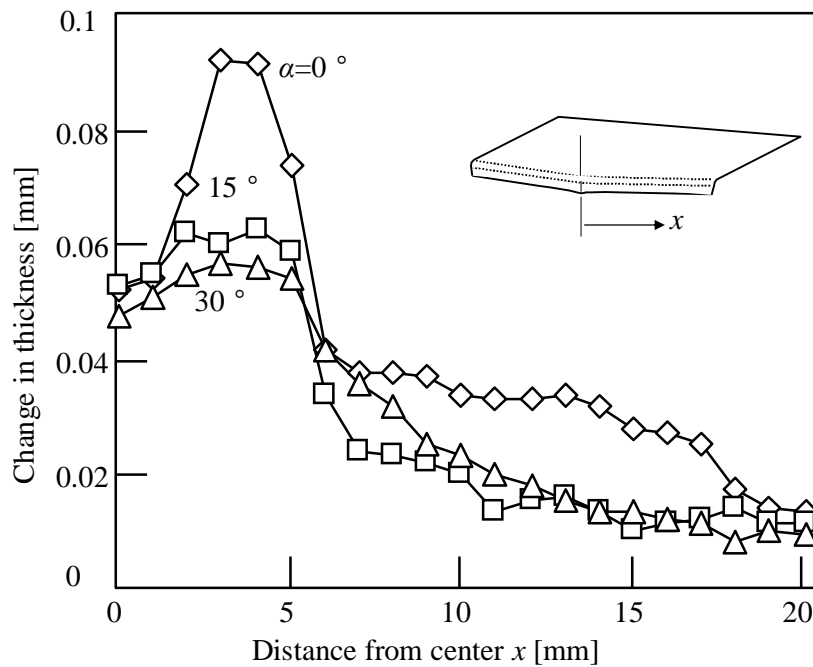


Fig. 4.6. Distribution of the change in thickness obtained from the experiment for $C=110\%$ and $L=10$ mm.

The relationship between the wrinkle height and flange length obtained from the experiment for $C=110\%$ is illustrated in Fig. 4.7. For $\alpha=30^\circ$, the limiting flange length is 11 mm, whereas those for $\alpha=0$ and 15° are 9 mm.

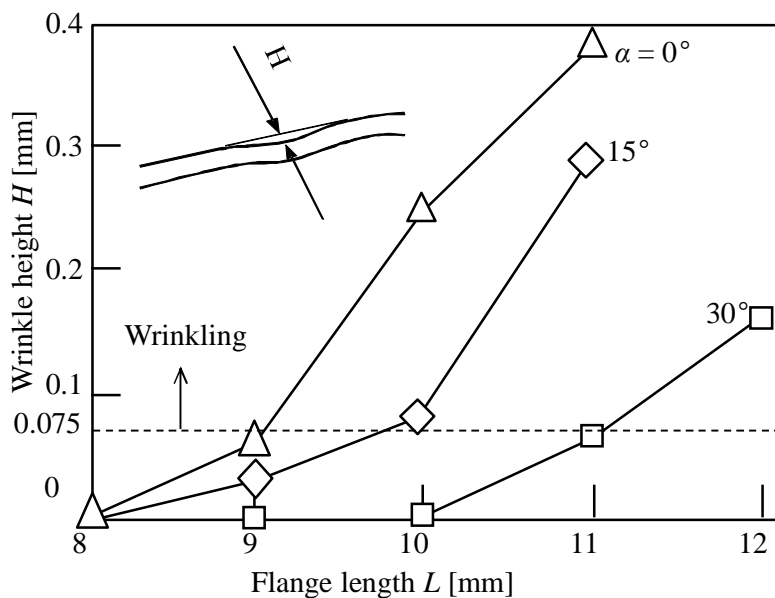


Fig. 4.7. Relationship between wrinkle height and flange length obtained from experiment for $C=110\%$.

The relationship between the wrinkle height and flange length obtained from the experiment and calculation for $\alpha=30^\circ$ is shown in Fig. 4.8. For $C=110\%$, the wrinkling is successfully prevented up to $L=11$ mm, whereas the limiting flange lengths for $C=100\%$ and 120% are 9 and 8 mm, respectively.

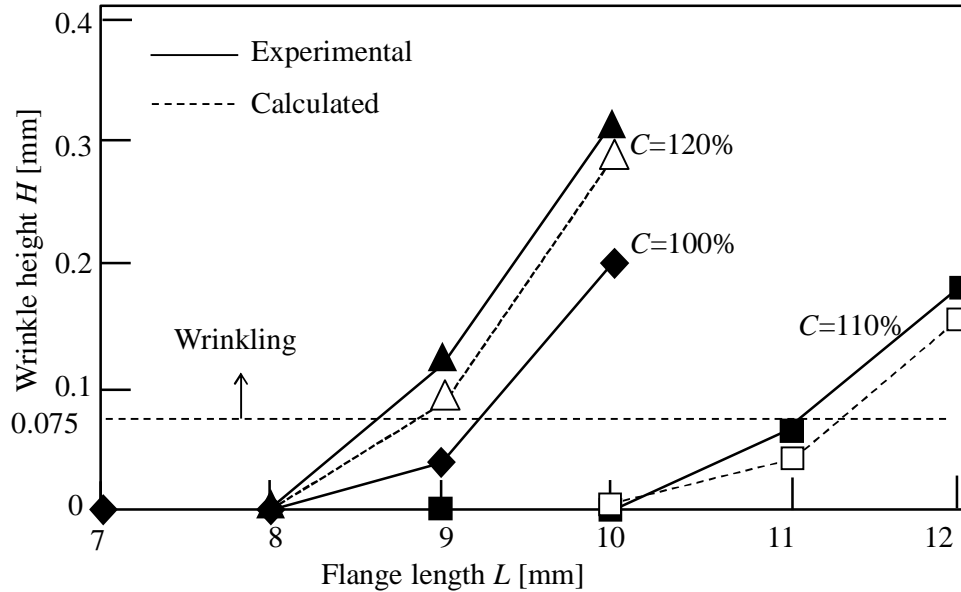


Fig. 4.8. Relationship between wrinkle height and flange length obtained from experiment and calculation for $\alpha = 30^\circ$.

The relationship between the bending load and stroke obtained from the experiment and calculation and the deformation behavior obtained from the experiment for $C=110\%$ and $L=10$ mm is shown in Fig. 4.9. As the projection angle decreases, the peak bending load decreases due to the gradual contact between the punch and sheet. The calculated bending load for $\alpha = 0$ and 30° are in good agreement with the experimental one.

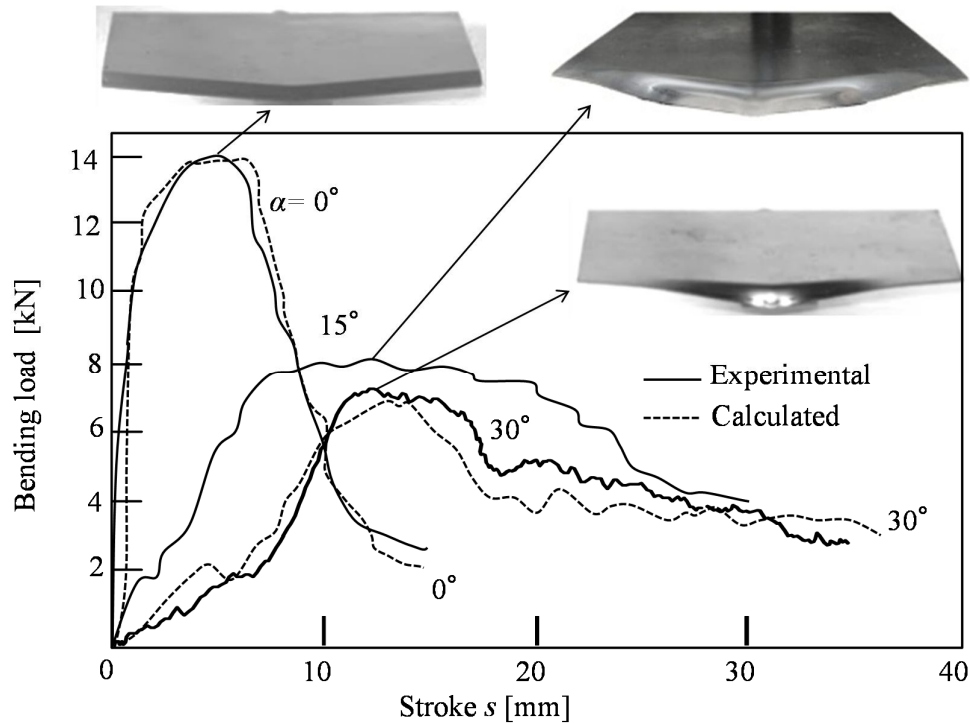


Fig. 4.9. Relationship between bending load and stroke obtained from experiment and calculation and deformation behavior obtained from experiment for $C=110\%$ and $L=10$ mm .

4.3. Stretch flanging of the high strength steel sheets

A stretch flanging using a flat punch and a punch with concave shape for gradual contact is shown in Fig. 4.10. In the stretch flanging using a flat punch the concentration of the tensile stress at the corners of the blank increased thus cracking is likely to occur. By using the gradual contact punch, the sheet is bent from outside of the sheet and reduced the tensile stress at the corner of the sheet. However the punch stroke increased by having the inclined portion of the punch.

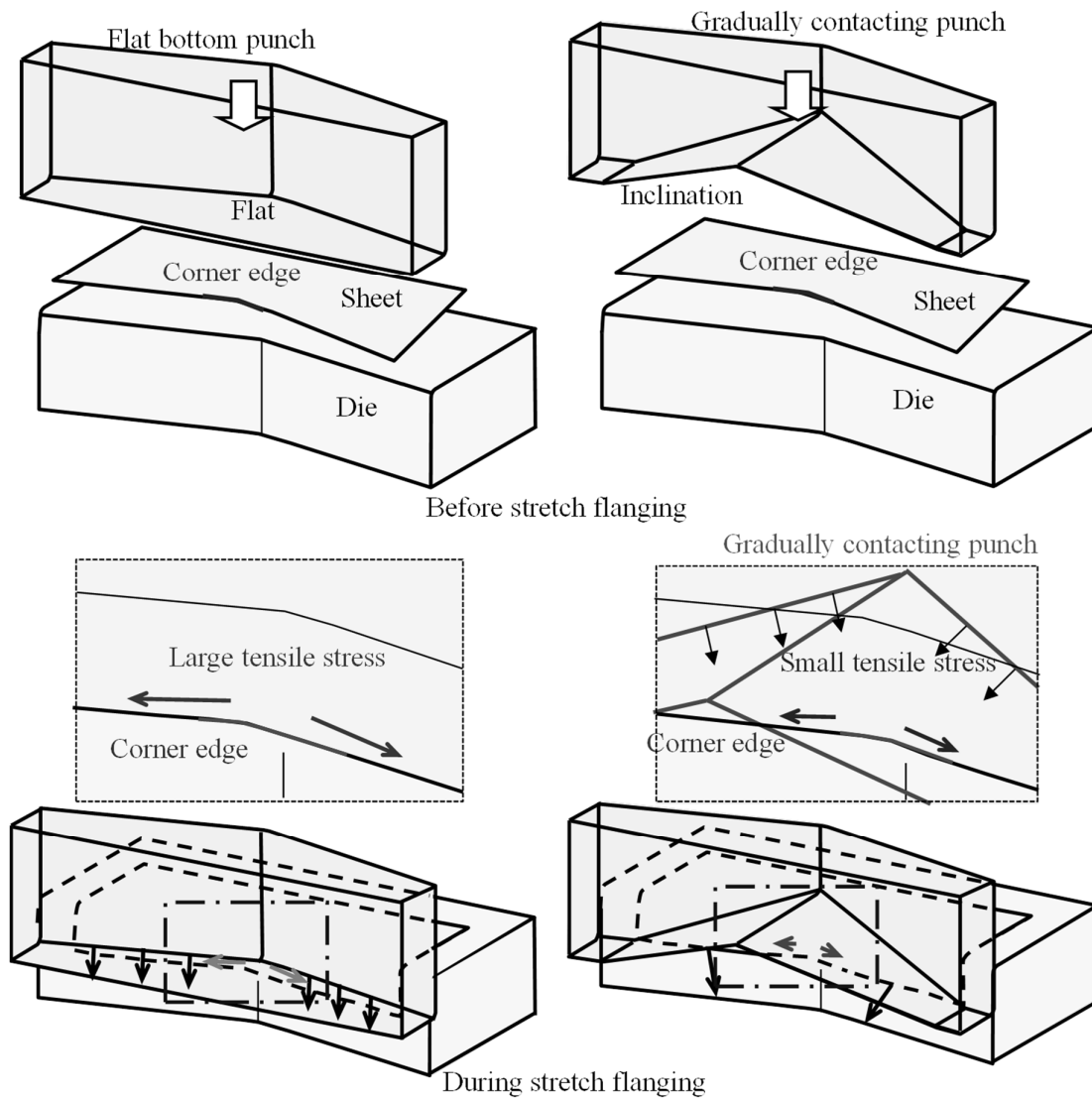


Fig. 4.10. Flat punch and gradual contact punch stretch flanging.

To reduce the punch stroke of the press, the flanging operation is divided into 2 stages, peripheral bending and corner bending, as shown in Fig. 4.11. In the 1st stage, the periphery of the corner is bent with the punch having a recessed in the middle and no contact with the corner of the sheet. In the 2nd stage, the residual portion is bent with

the flat bottom punch, and the tensile stress around the corner edge is reduced by restraint of the bent periphery.

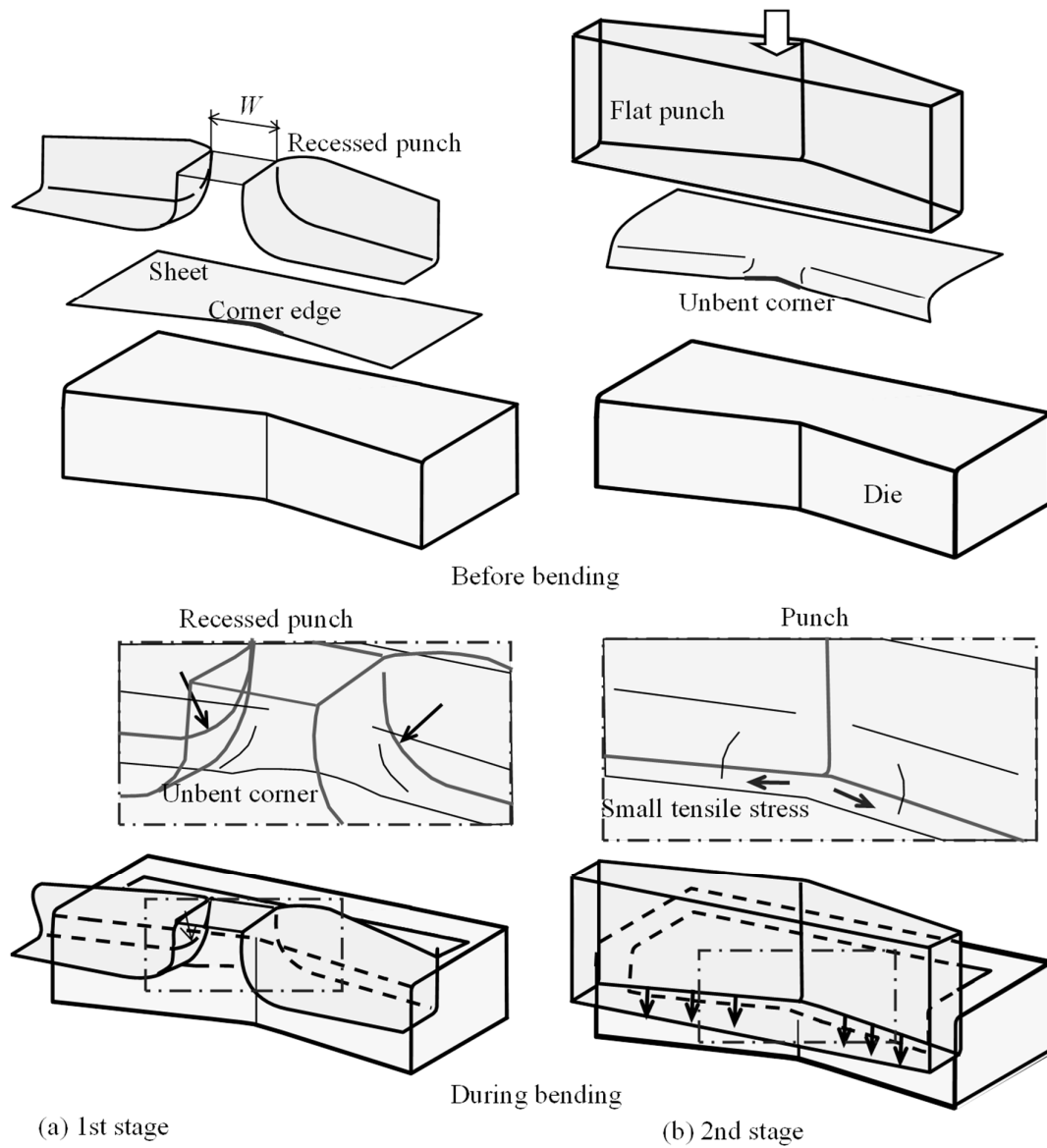


Fig. 4.11. 2-stage stretch flanging using recessed punch and flat punch.

4.3.1 Procedure of stretch flanging of 2-stage stretch flanging by using a flat punch and punch with recessed.

The sheets used in the experiment are high strength steel JSC980 with a thickness of 1.02 mm, 1.43 mm and ultra-high strength steel sheet JSC1180 with thickness of 1.22mm. The mechanical properties of the sheets are shown in Table 4.3.

Table 4.3: Mechanical properties of the steel.

Sheets	JSC980Y	JSC980Y	JSC1180Y
Thickness t [mm]	1.43	1.22	1.22
Tensile strength [MPa]	1014	1051	1250
Elongation [%]	16.4	13.0	8.2
n-value	0.15	0.10	0.09

The sheet that cut by the shearing process with the length L is formed. In the stretch flanging only the corner at the center sheet is having the tensile stress in the longitudinal direction while both sides of the corner are experienced normal L-bending phenomenon. The stretch flanging using the punch with recessed to bent the sheet at both sides of the corner is shown Fig. 4.12. The experimental conditions of 2-stage stretch flanging are shown in table 4.4. In the Fig. 4.12 shown, L is the bending length, W is the width of groove of the punch, s is the punch stroke and L is the flange length. The flange length limit is defined when the crack start to occur at the corner of the sheet in the 2nd

stage of the flanging. The punch stroke is defined when the punch passes the flange through completely.

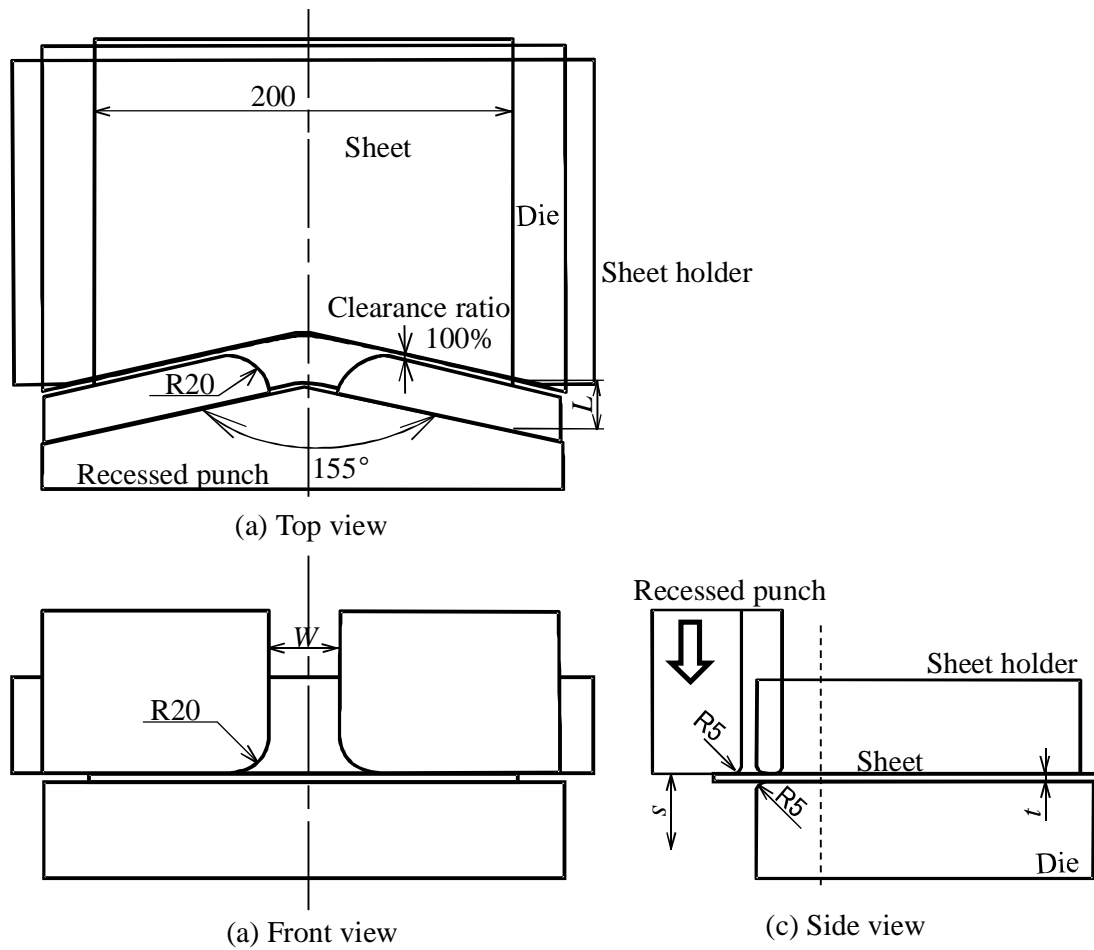


Fig. 4.12. Stretch flanging tool with recessed punch.

Table 4.4. Forming conditions of 2-stage stretch flanging.

Width of the recessed W [mm]	10 - 50
Flange length L [mm]	5 - 20
Punch stroke s [mm]	5 - 28
Punch speed [mm/s]	30

4.3.2. Calculation conditions and results

The model of the calculation is shown in Fig. 4.13. The calculation is using the dynamic explicit algorithm by commercial software LS-DYNA ver.9.7.1. The calculation conditions are shown in the table 4.5.

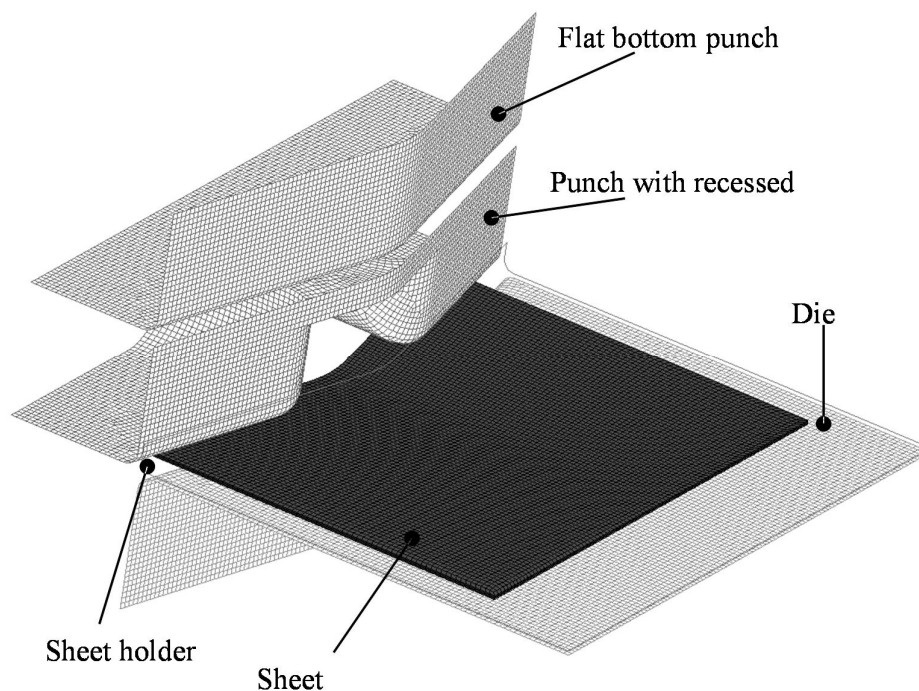


Fig. 4.13. Model of stretch flange.

The deformation behavior of the calculated high strength sheet for JSC980, $t = 1.4$ mm, $W = 40$ mm, $L = 15$ mm is shown in Fig. 4.14. In the first stage the sheet around the corner in the center is not formed.

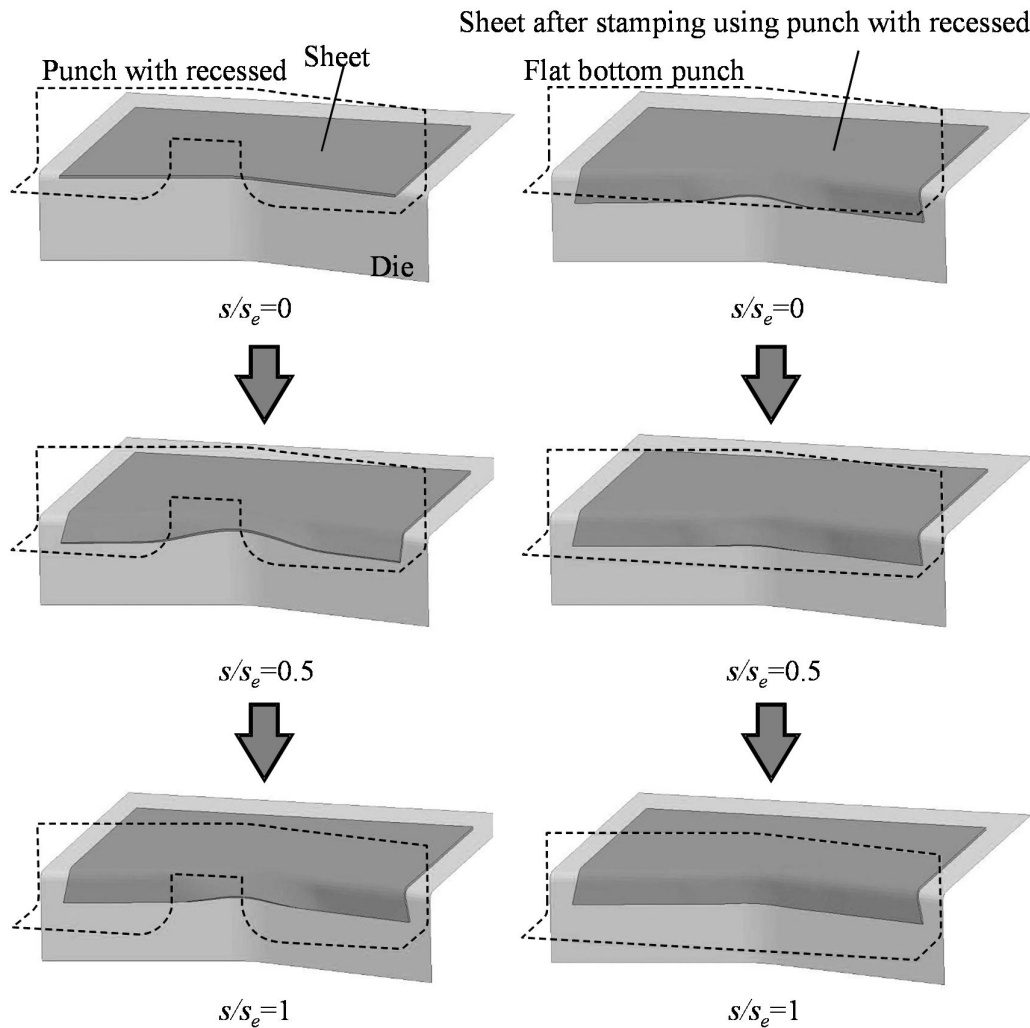


Fig. 4.14. Calculations of deformation behavior for JSC980Y, $t = 1.4$ mm, $L = 15$ mm and $W = 40$ mm.

The longitudinal strain of the sheet between 1-stage flanging using flat punch and the 2-stage flanging using the punch with recessed is calculated and compared for high strength steel sheet of JSC980Y, $t = 1.4$ mm, $L = 20$ mm, $W = 40$ mm. The calculated longitudinal stress distribution of the sheet is shown Fig. 4.15. Large longitudinal strain

occurred on the corner of the sheet in the 1 stage forming using flat punch. However, the strain is reduced in the 2-stage forming.

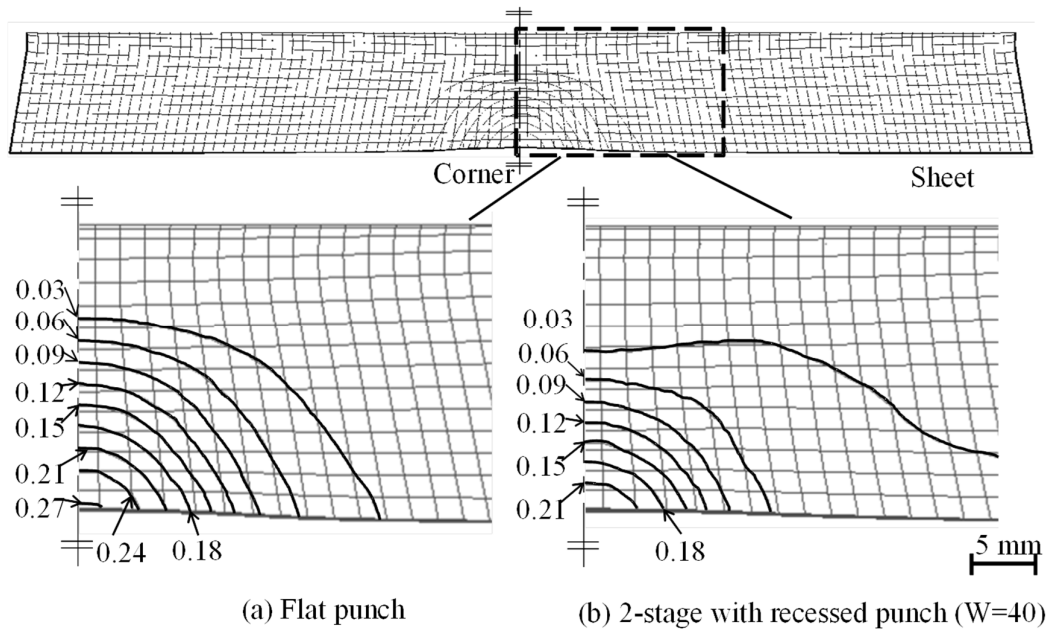


Fig. 4.15. Longitudinal stress distribution for JSC980Y, $t=1.4$ mm, $L=20$ mm and $W=40$ mm.

The relationship of the calculated maximum longitudinal strain of the sheet to the different widths of the punch groove for the JSC980, $t=1.4$ mm and $L=15$ mm is shown in Fig. 4.16.. In this calculations the $W=10$ mm gives smallest calculated longitudinal strain and 20% less than the flat punch thus the $W=10$ mm is considered as optimum conditions.

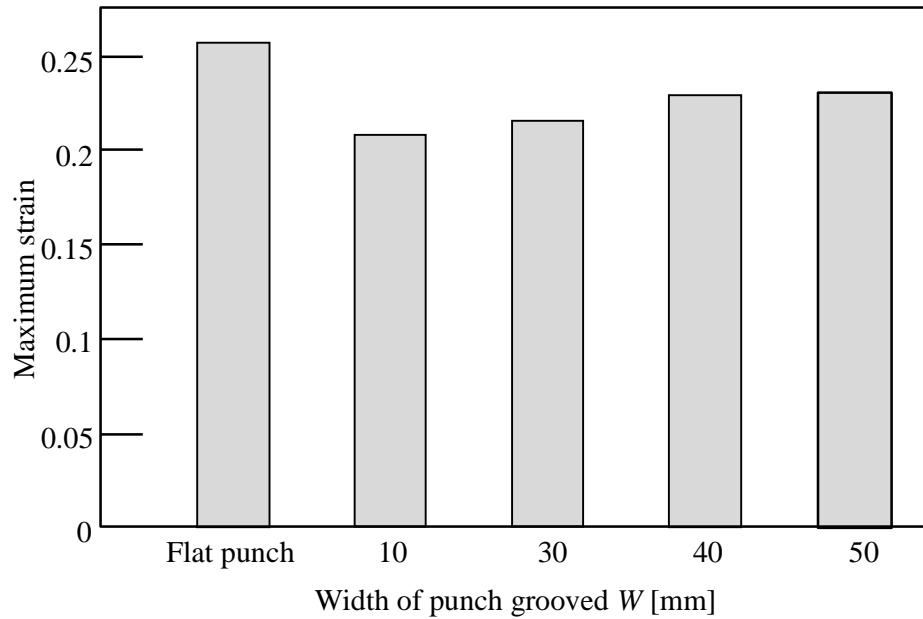


Fig. 4.16. Calculation of maximum strain for different width of groove of punch for JSC980Y, $t=1.4$ mm and $L=15$ mm.

4.3.3. Width of punch groove on the flange height

The ultra-high strength steel sheet JSC1180 are formed using the flat punch and 2-stage forming with the same length of bending $L=15.5$ mm. The picture of the formed part is shown in the Fig. 4.17. The sheet formed by 1 stage forming using flat punch is cracked, however for the 2-stage forming stage the sheet is successfully formed.

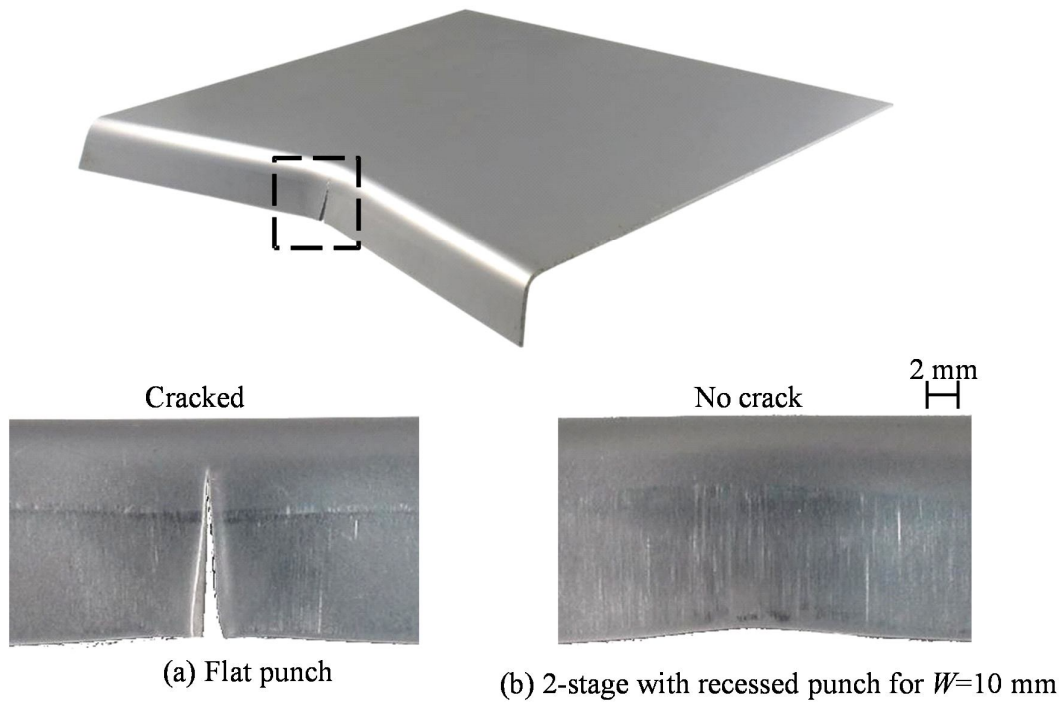


Fig. 4.17. Corner of formed flange sheets for $L=15.5$ mm $t=1.2$ mm and JSC1180Y.

The relationship of the load and punch stroke for 1-stage and 2-stage stretch flange is shown in figure 34. The high strength sheet JSC980 is formed using flat punch in 1-stage flanging and in 2-stage the recessed punch and flat punch is used. The load for the 2-stage forming is less than the load of using the flat punch in the 1-stage punch. The punch stroke and total punch load of the 2-stage forming is almost equal to the 1-stage forming using flat punch.

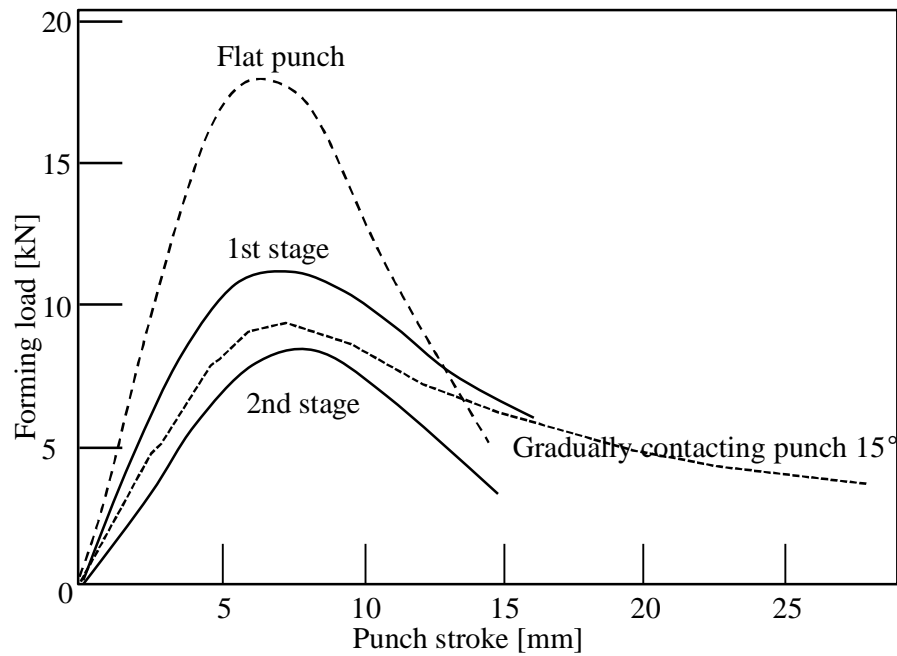


Fig. 4.18. Relationship of load and punch stroke for 1-stage and 2-stage stretch flange for JSC980Y, $W=40$ mm, $L=13.5$ mm and $L=1.4$ mm.

A maximum flange length of the part bend using flat punch, gradual contact punch and 2-stage using punch with recessed is shown in Fig. 4.19. The maximum flange length for the 2-stage bending improved by 28% compared to the flat punch for the JSC980 sheet with $t=1.4$ mm and for sheet with $t=1.2$ mm, the flange length improved by 31% for JSC1180 sheet and 32% for JSC980 sheet. Regardless of the strength of the sheet, the maximum flange height was improved by about 30% in stretch flanging using 2-stage bending method with recessed punch. In addition, the flange length is almost the same with the flanging using gradual contact punch.

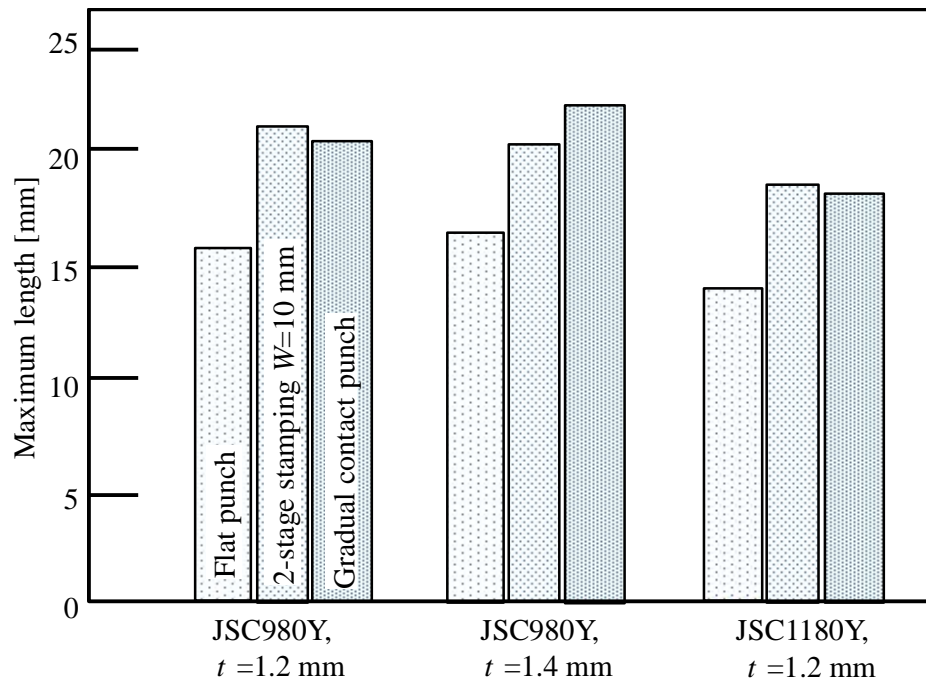
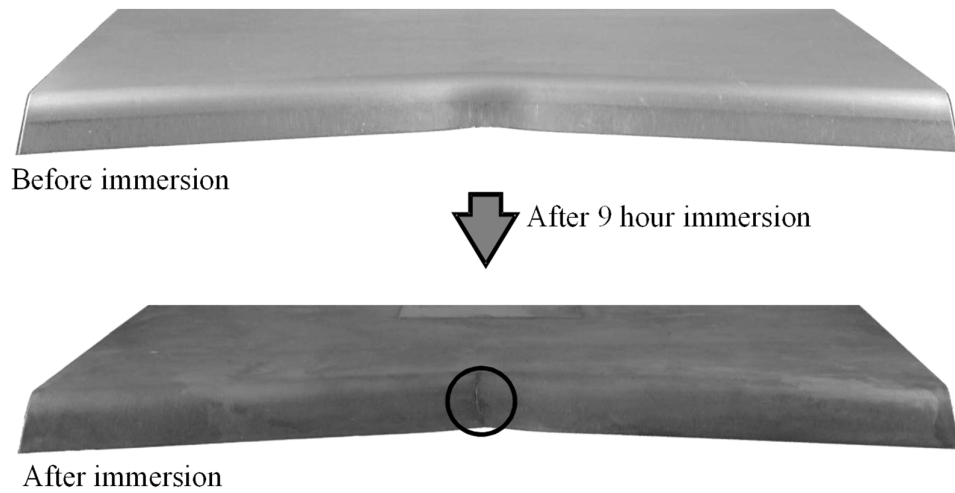


Fig. 4.19. Maximum flange length for different punches.

4.3.4. Delayed fracture for 2-stage stretch flanging method

Hydrochloric acid immersion tests were performed to the sheet from a 2-stage flanging method and flanging using the flat punch. The test was carried out at room temperature by dipping the flange part into a hydrochloric acid with a concentration of 35%. The image of the sheet flanged using flat punch before and after immersed into the hydrochloric acid is shown in Fig. 4.20. The crack is appeared in the corners blank after the outside layer of the sheet is eroded by hydrochloric acid.



(a) Bent sheets before and after immersion



(b) Crack due to delay fracture

Fig. 4.20. Crack from delayed fracture for JSC1180Y, $L=12.5$ mm and $t=1.2$ mm.

The time of occurrence of the delayed fracture during immersion experiment in hydrochloric acid shown in Fig. 4.21. The time of the occurrence crack to appear for the JSC1180 sheet is improved by 1.8 times for the 2-stage method compared to flat punch. The crack for the JSC980 sheet flanging using the flat punch occurred in 18 hours, whereas no crack is observed for the JSC1180 sheet flanging using 2-stage method after 24 hour immersed in the hydrochloric acid

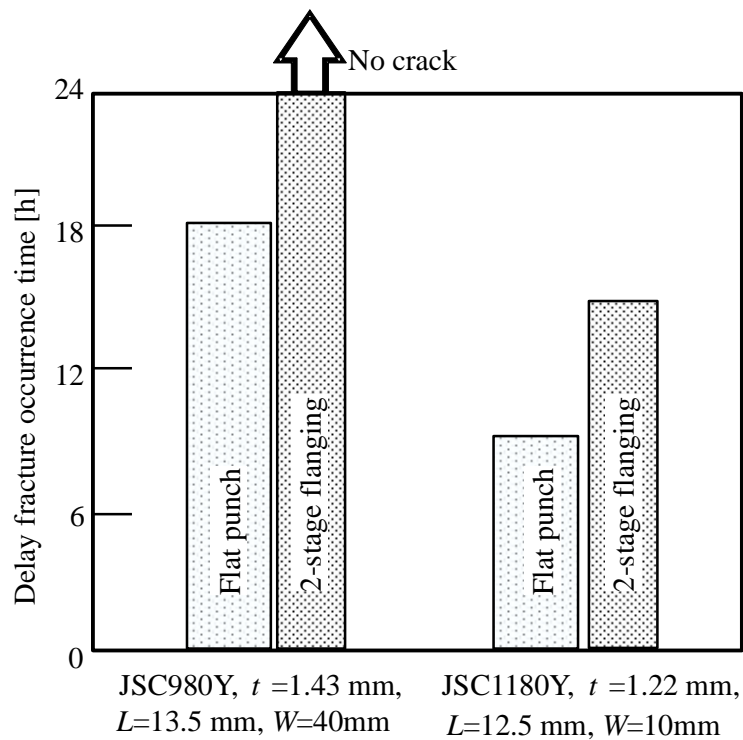


Fig. 4.21. Delay in hydrochloric acid immersion test failure occurred.

4.4. Conclusions

For the shrink flanging, compressive strain at the corner of the flange for JSC980 sheet was reduced by 20% during the shrinkage flanging using a punch with gradual contact. In the shrinkage flanging using the gradual contact punch, the flange height limit without wrinkling is improved by 27% compared to the flat punch for ultra-high strength sheet JSC980. For the shrinkage flanging using the gradual contact punch the height of the wrinkles can be reduced by reducing the apex angle of the punch. The maximum forming load for shrink flanging using gradual contact punch was decreased 43 percent compared to the flat punch.

In order to improve the formability of the high strength sheet in flanging process, the gradual contact punch is used in the shrink flanging and the 2-stage method using punch with recessed is used in stretch flanging. It was found that the punch having gradual contact and 2-stage method using punch with recessed are effective in preventing the occurrence of wrinkling in the shrinkage flanging and cracking in stretch flanging, respectively. The following findings were obtained for both of the methods.

In the stretch flanging, the maximum height of the flange using the 2-stage method by a recessed and a flat punch is improved by 28% and 32% for JSC980 and JSC1180 sheet, respectively as compared with the flanging using 1-stage method by the flat punch . The occurrence of the delayed fracture in the stretch flanging is eliminated by flanging using the 2-stage method.

Chapter 5

Joining of high strength steel sheets by hemming and improvement of joint strengths

5.1. Introduction

Since the number of vehicles is continuously increased over the last two decades, the number of accident and injuries are also increased. It is strongly desirable for the vehicles to improve passenger safety due to this reason. Continuous researches are carried out in optimizing the design of vehicle body structure to obtain efficient energy absorbent parts during the accident and able to protect the user of the vehicle. Hollow sections or tubes with different shape are used extensively as the energy absorbers in most of the vehicles [50]. The shape such as square or circular cross sections are most commonly used [51]. Tarlochan et al. calculated the deformation behaviour during crash in axial and oblique direction of different cross section of the tube using finite element simulation [52]. Olabi et al. carried out a study in improving the energy absorption of hollow structures due to direct axial impact [53]. These structures are used as a member frontal rail and the structures will permanently deform in order to absorb the kinetic energy during the crash. The studies were also carried out by inserting fillers inside the

hollow structure, and the results showed an increase of the energy absorption capability and also decreasing in crush length of the parts. [54-56].

Since it is too costly to manufacture prototypes for physical testing, a finite element simulation is a useful tool to understand the deformation behaviour and obtain the data of the hollow section as an energy absorber under the crash loads. A calculation using finite element simulation analysis is also found used by several researchers to understand the deformation behaviour of the hollow section during the crash [57,58]. The finite element simulation has been remarkably developed with advance of computer, thus it is an attractive tool in calculating the optimized shape of the hollow section during the crash. However, calculated results by the finite element simulation are reaching the limit of the accuracy, because the simulation includes some approximations and assumptions. It is not easy to accurately measure material constants used in the simulation such as the flow stress curve, the coefficient of friction, etc. In addition, constitutive equations used in the finite element simulation are not highly accurate for large strain and anisotropy.

In order to improve the crashworthiness of the vehicles without increasing the weight the vehicles, two approaches are applied for the improvement, the use of stronger materials and the optimization of structure of body members. High strength steel hollow sections are used for body structure of the automobiles for this purpose [34]. The structures of hollow sections are optimized to increase crashworthiness of vehicles for human safety. In the crash situation, a kinetic energy is absorbed by the hollow section. The hollow sections typically joined by resistance spot welding have insufficient energy absorption because joint are not continuous. Although laser welding is a better approach

to overcome this problem, high heating temperatures reduce the quality, accuracy and reliability of joined parts [11]. In order to overcome this problem, the hollow section is joined using the hemming method. However, designing the hemmed part is not easy and influenced by the mechanical properties of the bended part. Main problem for the automotive industry arise when bending high strength steel sheets. The high strength steel sheets are more difficult to hem due to its susceptibility to strain localization during the hemming process [59]. This will cause cracking on the hemmed edge .

In this study, the crashing behavior of high strength steel hollow sections joined by hemming was examined by an experiment by crushing the hollow section at a high speed stroke in a press machine.

5.2. Hemming process of high strength steel sheets

Both edges of hollow sections are joined by hemming to produce continuous joining without external heat supply. Fig. 5.1. shows the geometry of the hollow section having welded and hemmed joints. Since the hollow section having hemmed joints is overlapped, the strength is increased as compared to the resistance spot welding joints. Thus, hemming is effective for increasing energy absorption during the crash test.

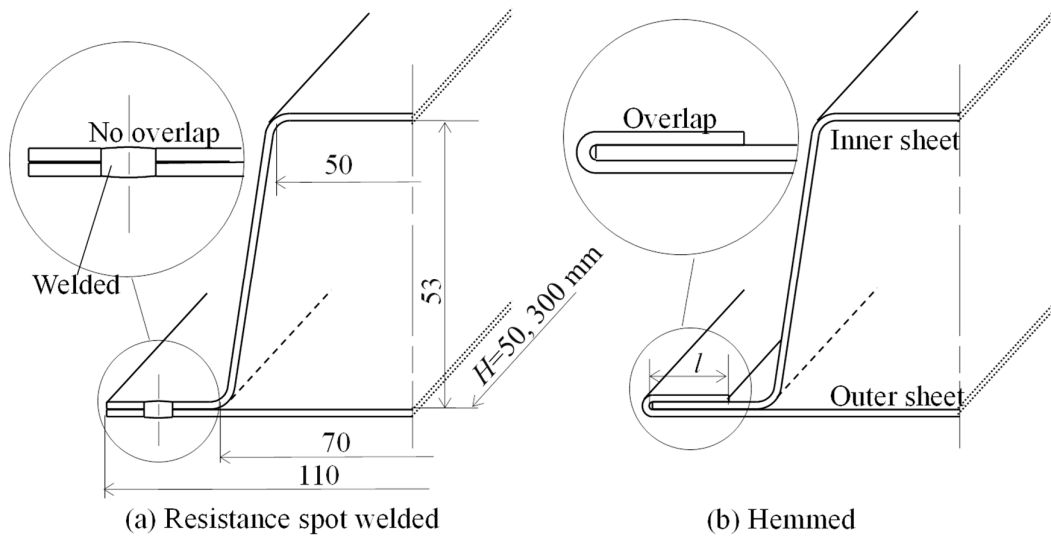


Fig. 5.1. Hollow section having welded and hemmed joints.

Fig. 5.2. shows the dimension and the cross section of the hollow section having welded. For welded of 2 and more, the distance between weld is fix to 40 mm each. The cross section of the welded showed that the complete fusion between upper sheet and lower sheet with the welded diameter of approximately 6.5 mm. The conditions for the resistance spot welding are shown in table 5.1.

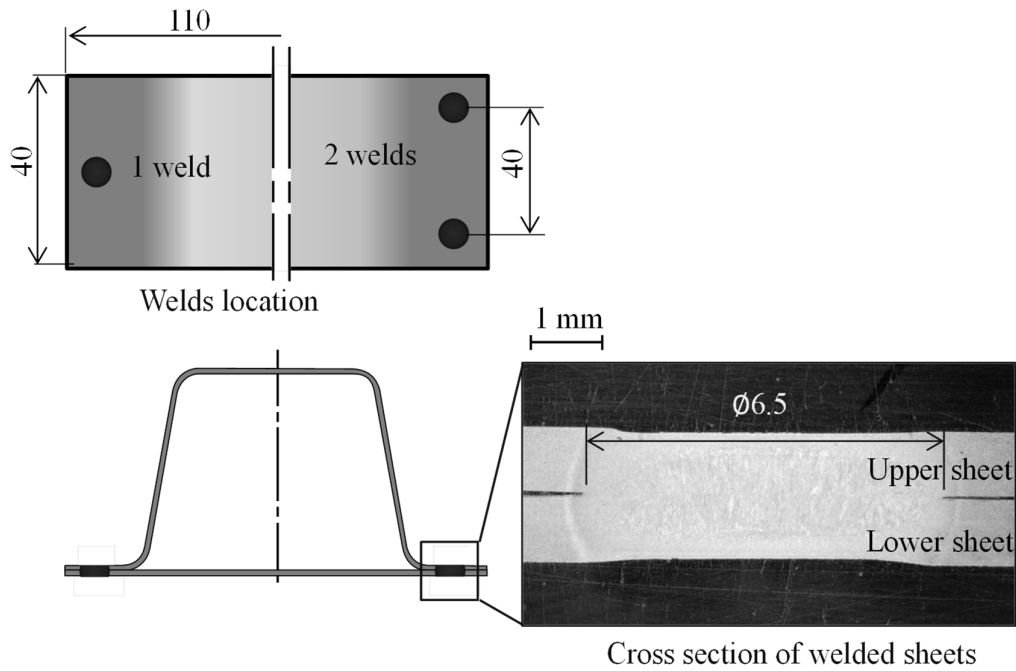


Fig. 5.2. Resistance spot welding.

Table 5.1. Conditions for resistance spot welding.

Electrode material	Copper
Electrode diameter /mm	5
Current /kA	7.5
Pressure /kN	3.5
Welding time /cycle	20
Dwell time /cycle	5

The high strength hat-shaped part and the flat sheet were joined by hemming to form a hollow section. The hollow section is then crashed to determine the absorbed energy. The mechanical properties of the sheets are given in table 5.2.

Table 5.2. Mechanical properties of hemmed sheets.

Sheets	JSC590YN	JSC780YN	JSC980YN
Thickness	1.22	1.22	1.23
Tensile strength /MPa	628	813	1026
Elongation /%	22.7	17.3	14.7
Reduction in area /%	63	56	53
<i>n</i> -value	0.11	0.10	0.07

In hemming of high strength sheets having low ductility, a crack tends to occur at the outer surface of the hemming due to the small radius produced. In order to prevent the occurrences of cracks, a punch with a stopper was employed in the 3rd step. The dimensions of the tools used in the hemming process are shown in Fig. 5.3. The sheet is bent in the 3 steps to join the sheets and form the hollow section by the hemming process, 90°, 135° and 180° bending. The clearance between the die and punch in the 1st step was fixed to 100% of the thickness. A servo press with a load capacity of 800kN and a maximum ram speed of 700 mm/s was used for the crash test. The range of the flange length for hemming was between 5 and 20 mm.

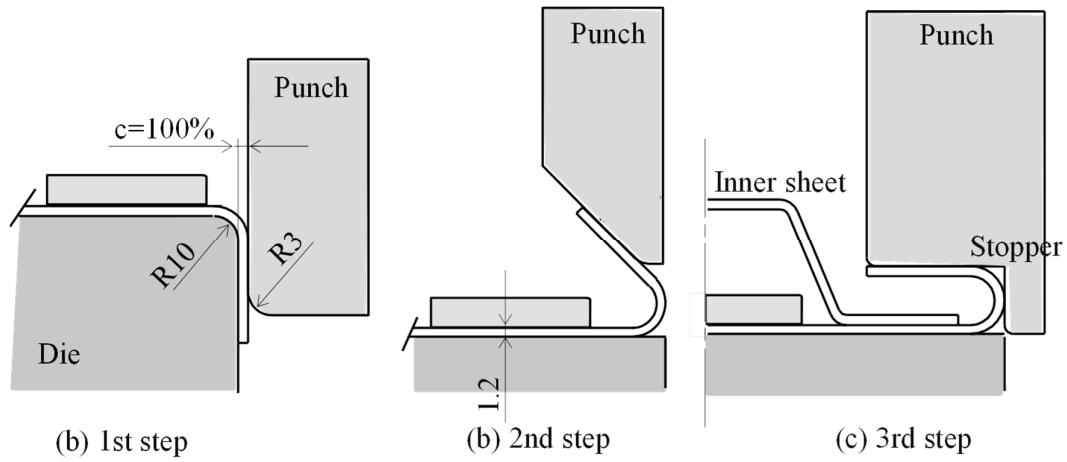


Fig. 5.3. Dimensions of tools used in hemming process.

The comparison between the hemmed sheets for the punches without and with the stopper for JSC980YN is shown in Fig. 5.4. Without the stopper, cracks occurred at the outer surface, whereas the occurrence of cracks was prevented with the stopper.

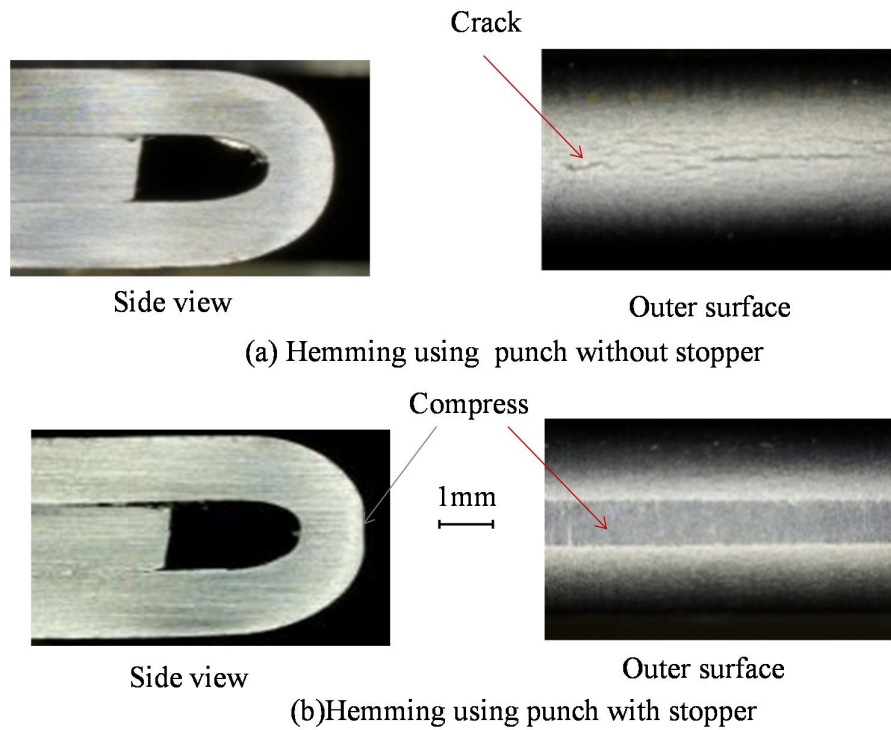


Fig.5.4. Comparison of hemming sheet between conventional punch and punch with stopper for JSC980YN.

5.3. Results in crash test of high strength steel hollow sections

5.3.1 Result of crash test for short hollow section

The hollow section having hemmed joints and resistance spot welded joints are crashed. The load-stroke curve for JSC980YN is shown in Fig. 5.5. The maximum load for the hollow section having hemmed joints is almost double as that for the welded joints.

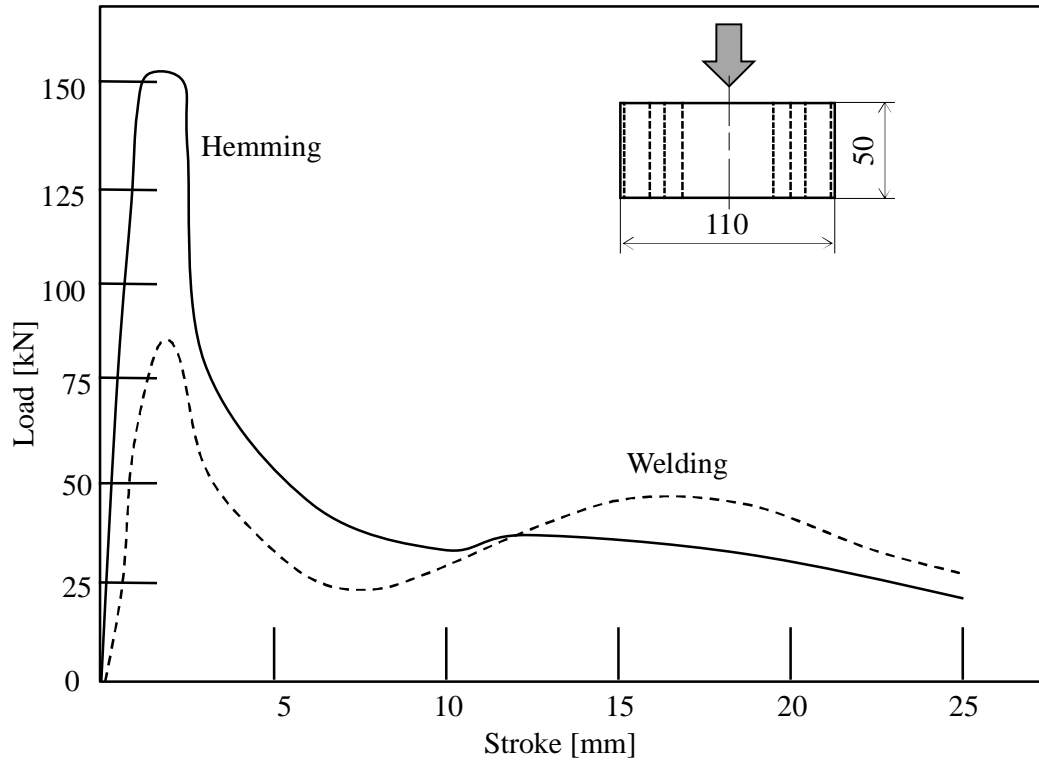


Fig. 5.5. Load-stroke curve for JSC980YN.

The relationship between the absorbed energy and stroke for JSC780YN and JSC980YN is shown in Fig. 5.6. The amount of the absorbed energy for the hollow section having hemmed joints is approximately 10% larger than that for the hollow section having welded joints.

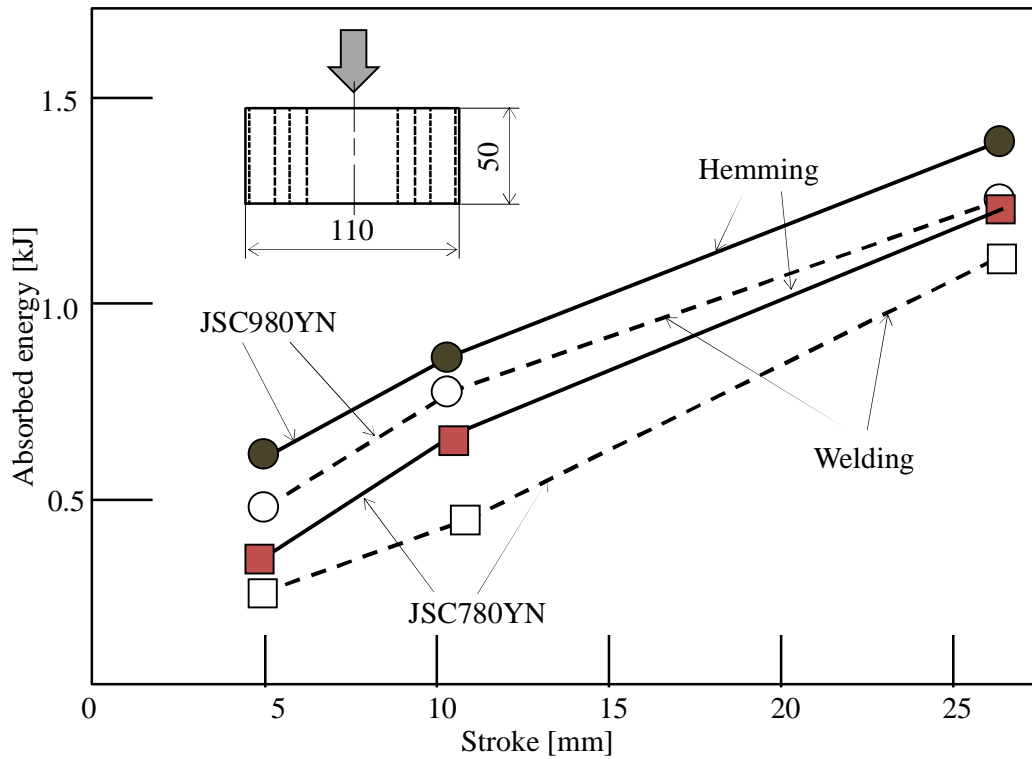


Fig.5.6. Relationship between absorbed energy and stroke for JS7980YN and JSC980YN.

The hollow sections after the crash test are shown in Fig. 5.7. After the crash, the inner sheet and the outer sheet for the 1 and 2 welded joints are not attached to each other whereas for the hemmed joints the sheets are remained sticking together.

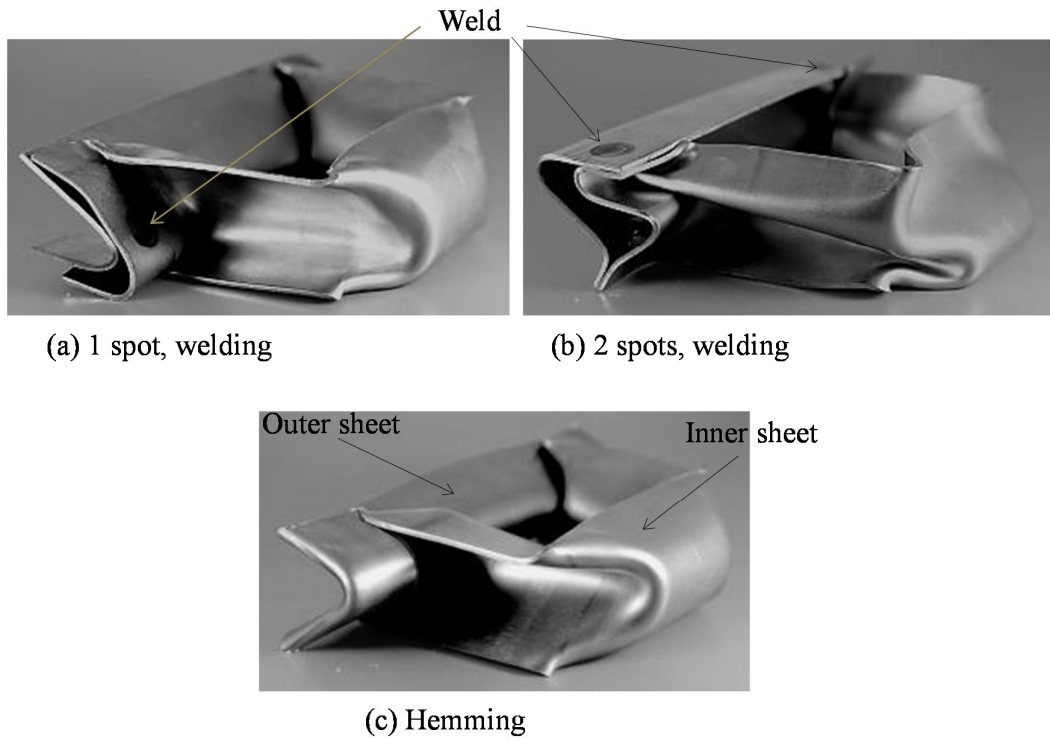


Fig. 5.7. Hollow sections after crash test for JCS590YN and $H=50$ mm.

The load-curve of the hollow section having 1 and 2 spots welded joints and hemmed joints for JSC590YN is shown in Fig.5.8. The maximum load for the hollow section having the hemmed joints is larger than those for the hollow section having 1 and 2 spots welding, 25% and 15%, respectively.

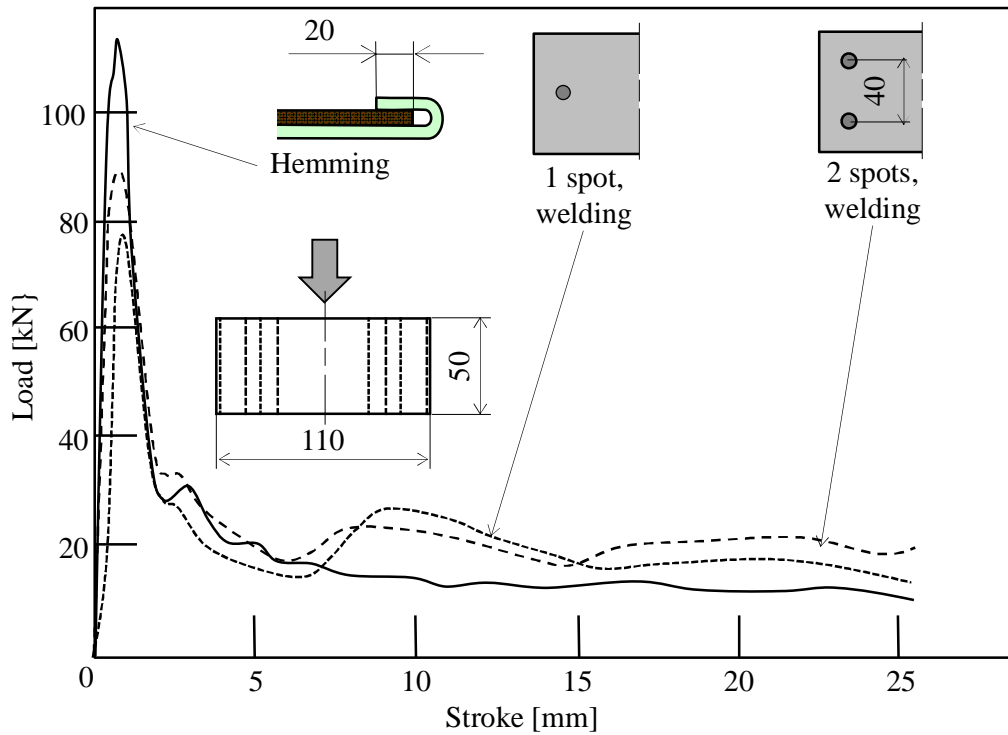


Fig. 5.8. Load-stroke curve for axial direction, 1, 2 spots welding, hemming and JSC590YN.

The relationship between the absorbed energy and stroke for the hollow section having joints by 1 and 2 spots welding and hemming for JSC590YN is shown in Fig. 5.9. As the stroke increased, the absorbed energy increased. The absorbed energy for the hollow section having hemmed joints is larger than those for the hollow section having 1 and 2 spots welding.

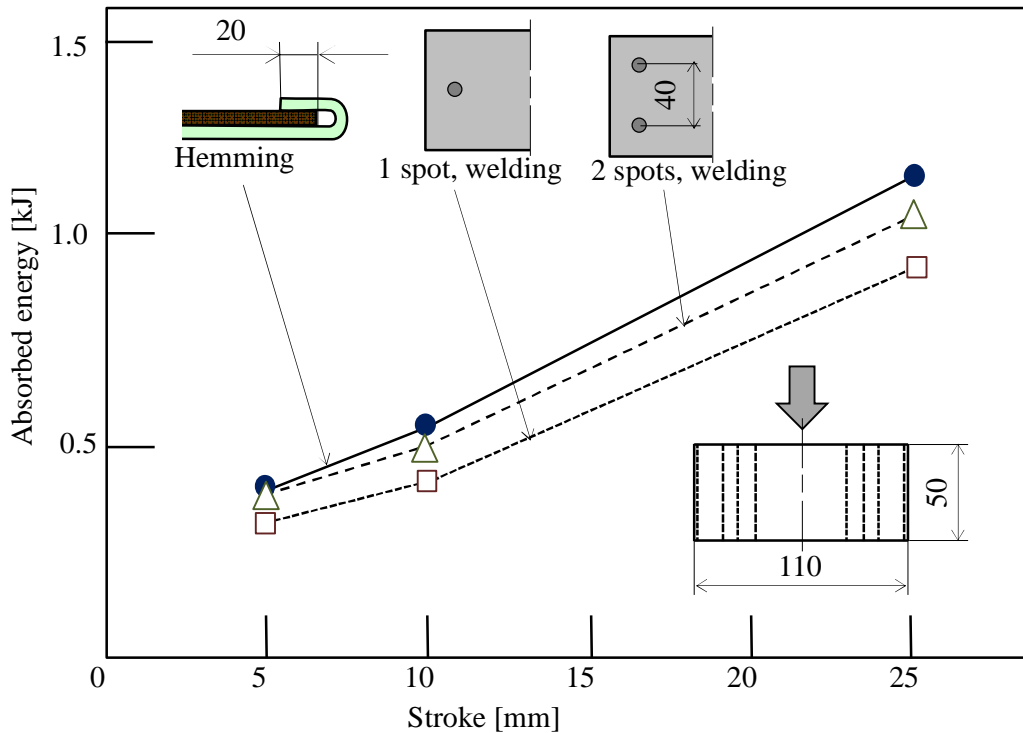


Fig. 5.9. Relationship between absorbed energy and stroke for 1 and 2 spots welding, hemming and JSC590YN.

5.3.2. Optimization of flange length in hemming

To optimize the flange length of the hemming, l , the crash test was performed. Fig. 5.10. shows the relationship between weight ratio and the flange length of hemming and between absorbed energy and the flange length of hemming for different strokes, s and JSC980YN. The weight ratio is increased linearly as the flange length of the hemming, l increased. In addition, for the flange length of the hemming, $l = 15$ and 20 mm of the absorbed energy are almost the same for all crash stroke, thus $l=15$ mm is considered an optimized flange length of hemming.

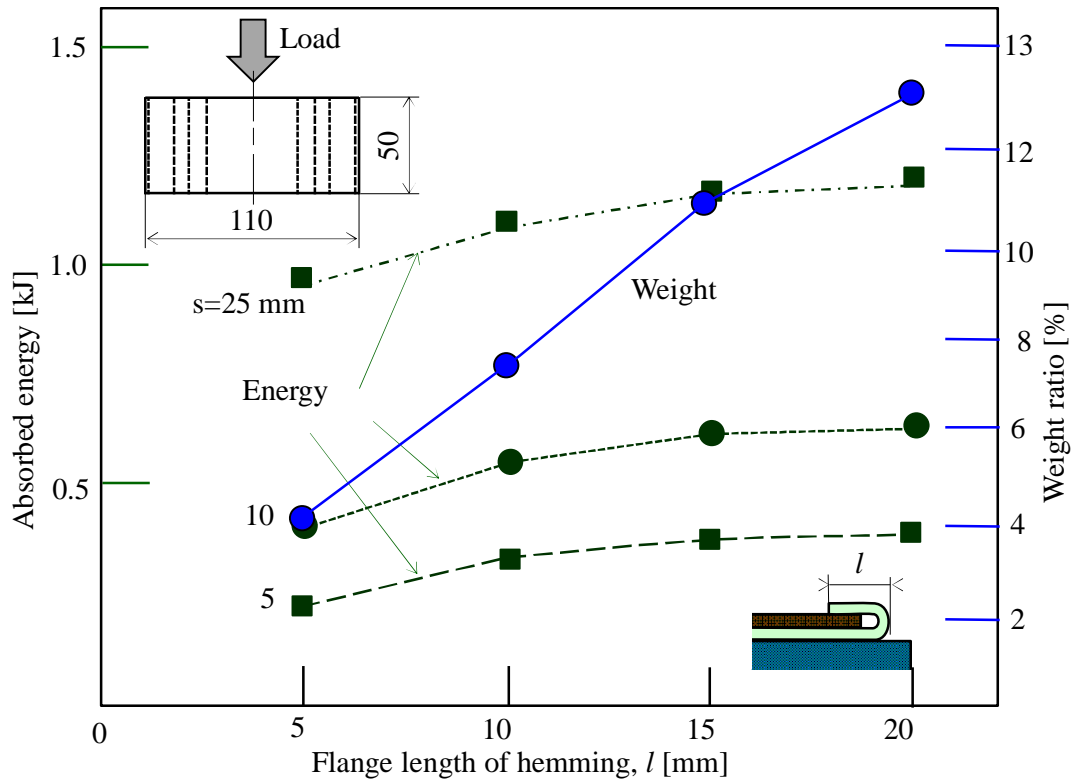


Fig. 5.10. Relationship of absorbed energy and weight ratio and flange length of hemming for different strokes and JSC980YN.

5.3.3 Crash test for long high strength steel hollow sections

Long hollow sections having hemmed and welded joints after crash test for JSC590YN, JSC780YN, JSC980YN and $H=300$ mm are shown in Fig. 5.11. In order to increase the strength of the joint of the hem, an adhesive is added between outer sheet and the inner sheets before it were hemmed together. After the crash, the inner sheet and the outer sheet of the hollow sections having joints for the JSC590YN, JSC780YN are deformed however the joint still attached to each other. Whereas, for JSC980YN hollow sections having hemmed joint is separated and the outer sheet resist deforming. Only

small deformation occurred to the outer hemmed sheet since hemmed structures had reinforced the hollow section become stronger. For the hollow sections having welded joint, the sheets is detached and the crack is occurred. In addition, some of the welds are also separated.



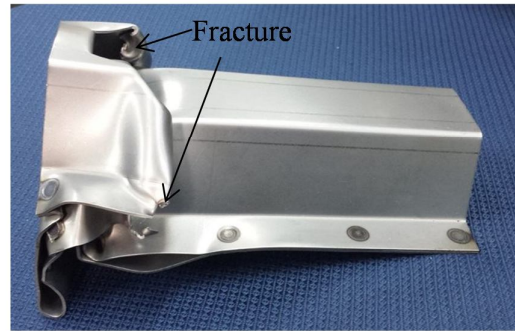
(a) Hemmed, JSC590YN



(b) Hemmed, JSC780YN



(c) Hemmed, JSC980YN



(d) Welded, JSC980YN

Fig. 5.11. Long hollow sections having hemmed and welded joints after crash test.

The relationship between the absorbed energy and stroke for the hollow section having joints by spots welding and hemming for JSC590YN for $H=300$ mm is shown in Fig. 5.12. Since the maximum load for the hollow section having the hemmed joints is

larger than those for the hollow section having spots welding, 12%, the hollow section having hemmed joint is considered as safer than those joined by spot weld.

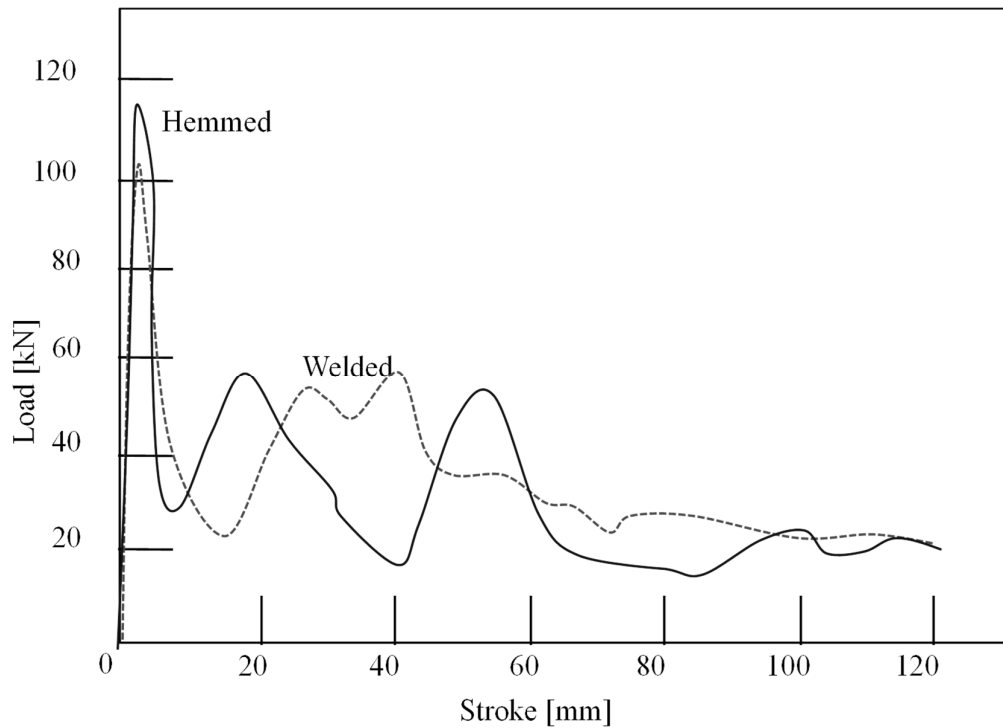


Fig. 5.12. Load-stroke curve for JSC980YN and $H=300$ mm.

The comparison of maximum crash load between the hollow sections having spot welded and hemmed joints is shown in Fig 5.13. The maximum crash load for JSC590YN, JSC780YN and JSC980YN are better than hollow section having joined using spot weld by 24%, 11% and 10%, respectively.

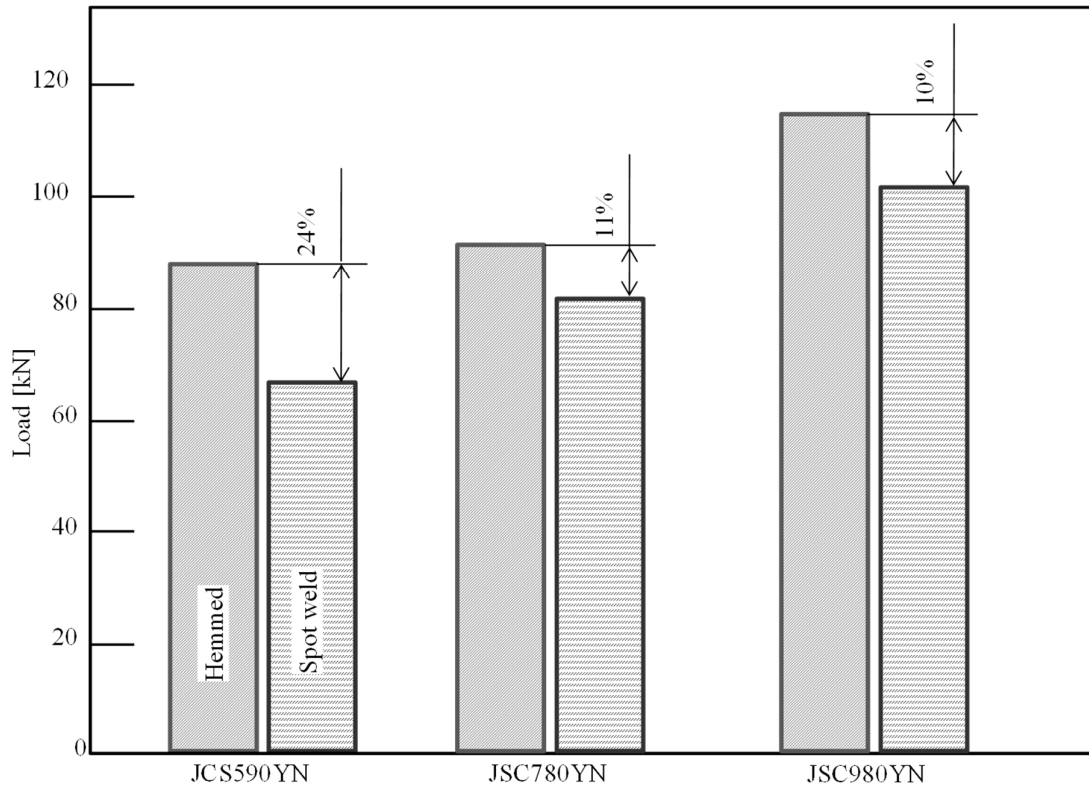


Fig. 5.13. Comparison of maximum crash load between hollow sections having spot welded and hemmed joints.

5.4. Conclusions

An experimental study of the hollow section in axial direction of high strength steel sheets with different strength was performed. The hollow section having hemmed and spot weld joint were crash at high speed using press machine in order to obtain the deformation behaviour of the sections. The experimental was divided into two according to size of the hollow section, which are, the experiment of short (50 mm) and long (300 mm) hollow section. All experiments were using the similar crash speed. The result showed the hollow section having hemmed joins is effective for absorbing the

energy during the crash test compared to the resistance spot welding for both the short and long hollow sections. Since the maximum load during the crash test and the absorbed energy for the hollow section having hemmed joints is larger than welded joints, the safety of the passenger inside the cabin is increased.

Chapter 6

Improvement of formability of titanium alloy sheet using hot bending by resistance heating

6.1. Introduction

The usage of titanium alloy sheets for airplane parts increases due to the high strength at high temperatures, low density and high corrosion resistance, etc. Since the cold formability of the titanium alloy sheets is low, the sheets are generally formed at elevated temperatures. Warm and hot forming processes are useful for improving the formability of workpieces having low ductility at room temperature. Vollertsen and Lange investigated on enhancement of the formability of aluminium by local heat treatment [60]. Groche et al. studied the deep drawing of aluminium sheets at elevated temperatures [22]. In the conventional hot stamping using a furnace, the productivity is very low [43] such as the heating time of tools is about 2 h, and the heating time of the sheets in the furnace and the forming time are about several minutes, respectively. Whereas, with the application of the resistance heating method the heating time is very fast, the production cost decreases due to the elimination of the additional heat treatment and the equipment becomes simple.

The rapid resistance heating was effective in the hot stamping, only a time of 2 s to a heating time of 900 °C. The resistance heating is generally employed for the preheating of forging billets. Mori et al. have largely heightened the formability of low formability

material such as ultra-high strength steel sheets by resistance heating [24]. In another process, rapid resistance heating is employed to control the temperature of the tube during forming [61]. Mori et al. have employed resistance heating for spline forming of an ultra-high strength gear drum to raise the temperature of a side wall of a cup. Maeno et al. applied in resistance heating in a gas forming of the the ultra-high strength steel hollow part [62]. Mori et al. have applied the resistance heating to the tailor die-quenching in hot stamping for producing ultra-high strength steel formed parts having a strength distribution [42]. In addition, Mori et al. [44] have developed a punching process of ultra-high strength steel sheets using local resistance heating of a shearing zone. Yanagimoto et al. have used the resistance heating in continuous hot forming system of the titanium alloy sheet [63]. Although Ozturk et al. [31] applied the resistance heating to the hot stamping of titanium alloy sheets, forming results were hardly shown.

In the present study, a hot bending process of a titanium alloy sheet using resistance heating was performed to increase the formability and to reduce the forming load. The springback and hardness of the hot bent sheet were also measured.

6.2. Procedure of hot bending of titanium alloy sheet

6.2.1 Experimental procedure

An alpha-beta titanium alloy Ti-6Al-4V sheet (Al: 6.0%, V: 4.0%, Fe: 0.4%, O: 0.2%, C: 0.08%, N: 0.05%, H: 0.015%) having 1.2 mm in thickness was bent at elevated temperatures. The mechanical properties of the titanium sheet were measured in the

uniaxial tensile test at different heating temperatures. A 50kN screw driven type universal testing instrument was used in the tensile test.

The variations of the tensile strength and elongation of the titanium alloy sheet with the heating temperature obtained by the tensile test are given in Fig. 6.1. As the heating temperature increases, the tensile strength decreases and the elongation increases, particularly above 560 °C.

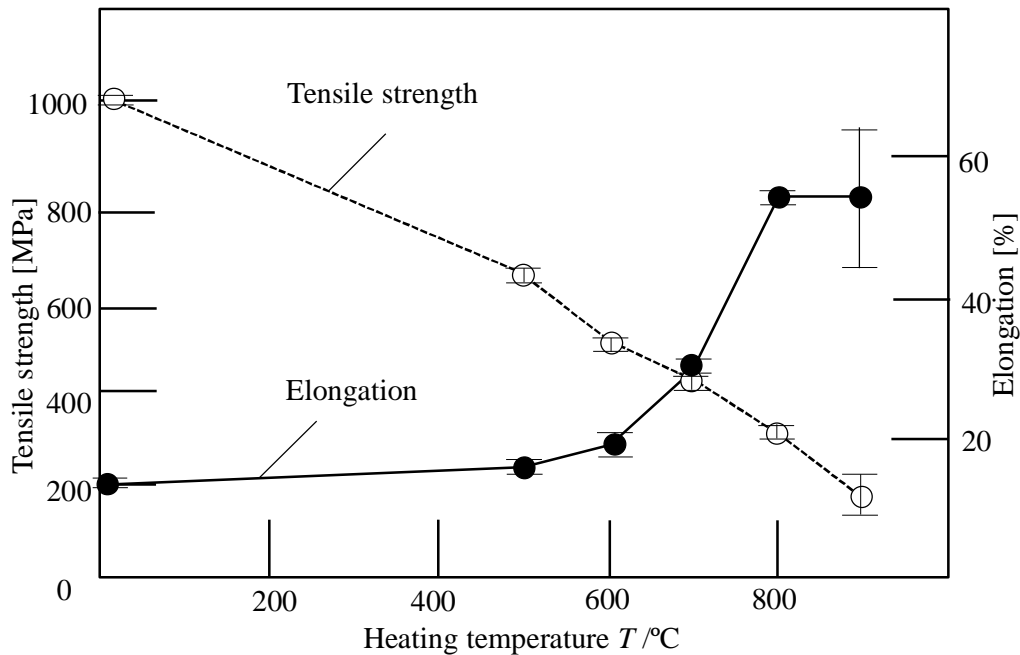


Fig. 6.1. Variations of tensile strength and elongation of titanium alloy sheet with heating temperature obtained by tensile test.

The hot hat-shaped bending of the titanium alloy sheet using the resistance heating is shown in Fig. 6.2. The length and width of the sheet were 130 and 20 mm, respectively, and only the regions of 5 mm from both edges of the sheet were in contact with the

electrodes, i.e. insufficient heating. During the resistance heating, the sheet is not in contact to the die, punch and blankholders in order to prevent the heating of these tools.

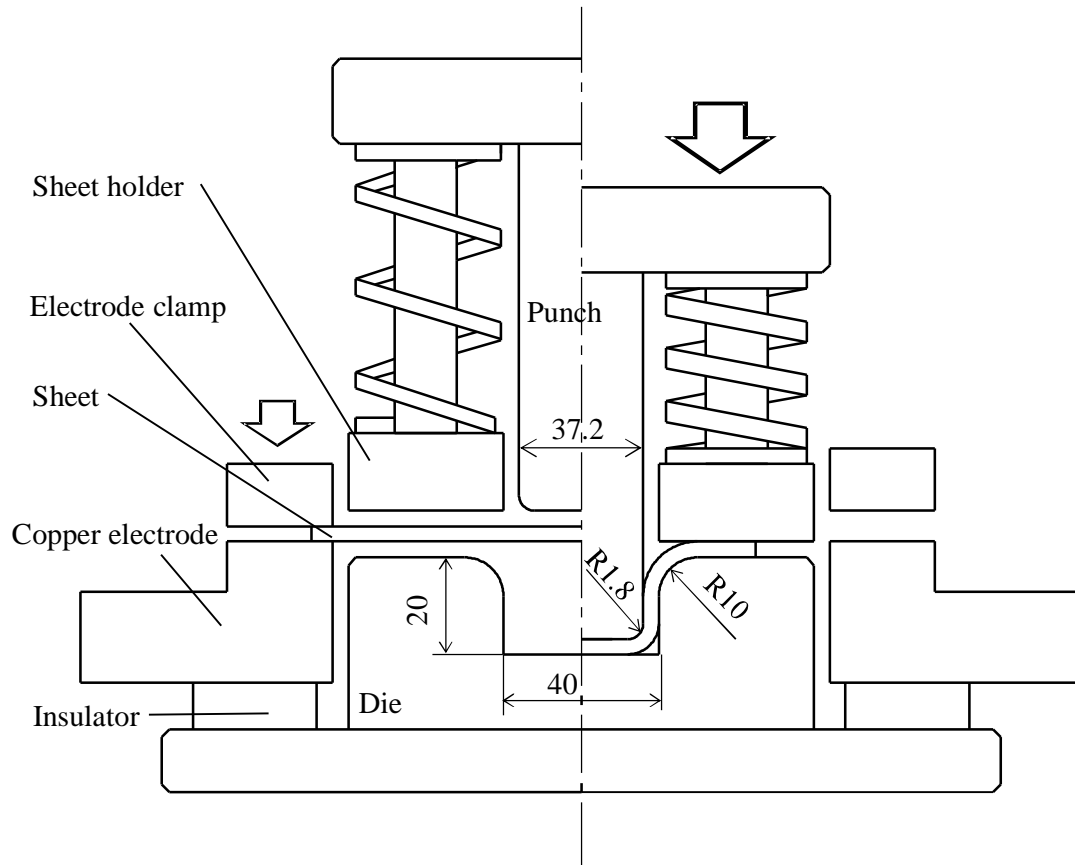


Fig 6.2. Hot hat-shaped bending using resistance heating of titanium alloy sheet.

A CNC servo press with a maximum load capacity of 800 kN is synchronized to a DC power supply with capacitors for the resistance heating, and the time interval between the end of heating and the beginning of the bending is only 0.2 s. The experimental conditions are given in Table 6.1.

Table 6. 1. Experimental conditions for hot bending.

Sheet holder pressure [MPa]	0.6				
Electrode clamping pressure [MPa]	4				
Holding time at bottom dead center t [s]	0, 3, 6				
Bending speed [mm/s]	150				
Current density [A/mm^2]	12.5				
Heating temperature T [$^{\circ}C$]	370	550	690	790	880
Heating time t_h [s]	2.8	4.9	6.1	7.3	8.0

6.2.2 Heating behaviour of sheet

The variation of the electrical resistivity of the titanium alloy sheet with the heating temperature is shown in Fig. 6.3. The variation of the electrical resistivity for the titanium alloy sheet is relatively small in comparison with the steel sheet. It is not easy to uniformly heat the sheet for the constant resistivity. The increase in resistance caused by the rise in temperature in local portions leads to the decrease in current, and thus the increase in temperature in these portions becomes small. The increase in resistivity has the function of uniform heating, and thus it is not easy to heat the titanium alloy sheet.

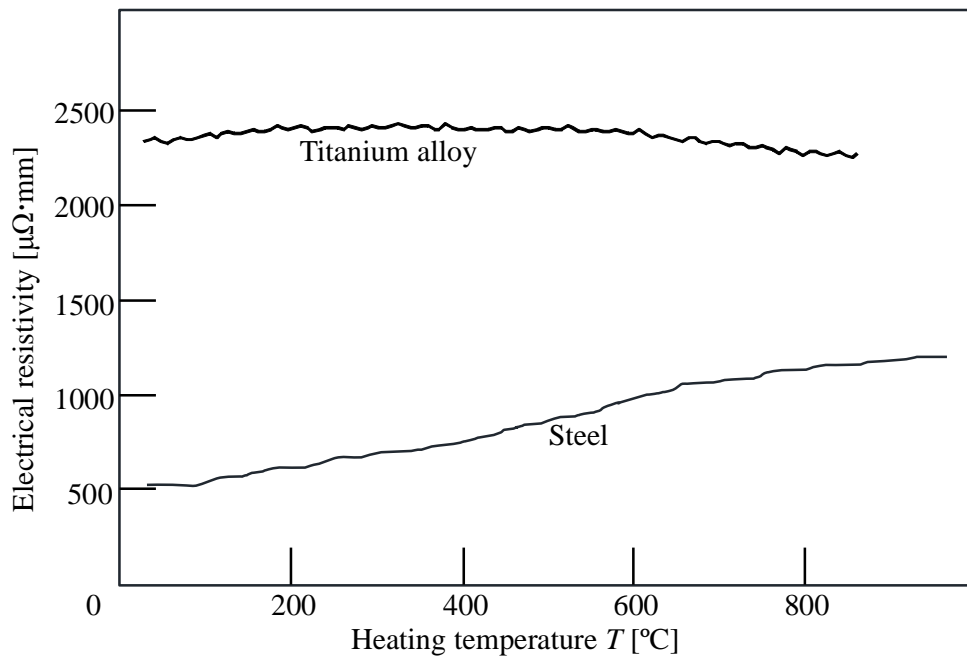


Fig. 6.3. Variations of electrical resistivity with heating temperature of titanium alloy sheet and pure titanium.

The distribution of heating temperature in the longitudinal direction of the titanium alloy sheet by the resistance heating is shown in Fig. 6.4. The heating temperature in the forming area is almost uniform, whereas both edges of the sheet are not sufficiently heated by the contact with the electrodes.

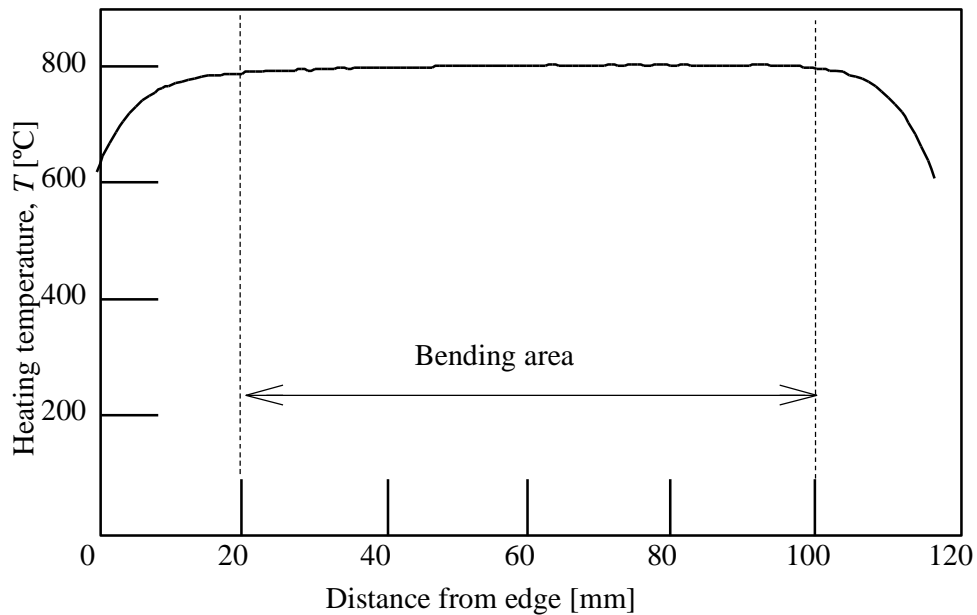


Fig. 6.4. Temperature distribution for resistance heating in longitudinal distance of titanium alloy sheet.

6.3 Results of hot bending of titanium alloy sheet using resistance heating

6.3.1 Bent sheets

The hat-shaped bent sheet for the resistance heating at $T = 880$ °C is compared with that for the furnace heating in Fig. 6.5. Although the springback and oxidation of the bent sheet for the furnace heating are remarkably large, these are very small for the resistance heating.

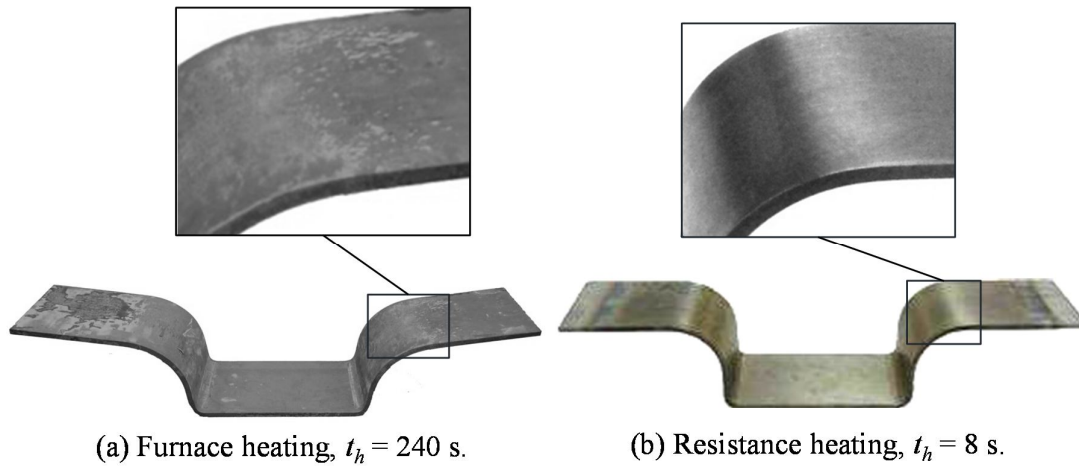
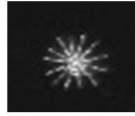


Fig. 6.5. Comparison between bent sheets for furnace heating and resistance heating for $T = 880$ °C and $t = 3$ s.

The non-destructive fluorescent penetrant test of the hat-shaped bent sheets was performed to check the occurrence of cracks. The reflective lighting of the bent titanium alloy sheet is shown in Fig. 6.6. Since the lighting was not observed for the bent sheets, no cracks occurred for the bent sheets.



(a) Example of reflective lighting for cracks



(b) $T=560\text{ }^{\circ}\text{C}$ $T=690\text{ }^{\circ}\text{C}$ $T=790\text{ }^{\circ}\text{C}$ $T=880\text{ }^{\circ}\text{C}$

Fig. 6.6. Bent sheets during non-destructive fluorescent penetrant test for $t = 3\text{ s}$.

6.3.2 Bending load and springback

The relationship between the bending load and heating temperature is given in Fig. 6.7. Although the titanium sheet fractured at room temperature due to low ductility, the sheet was successfully formed at elevated temperatures above for $T=370\text{ }^{\circ}\text{C}$. As the heating temperature increases, the bending load decreases. The bending load for $T=880\text{ }^{\circ}\text{C}$ is reduce from 6.5 kN at room temperature to 1.8 kN.

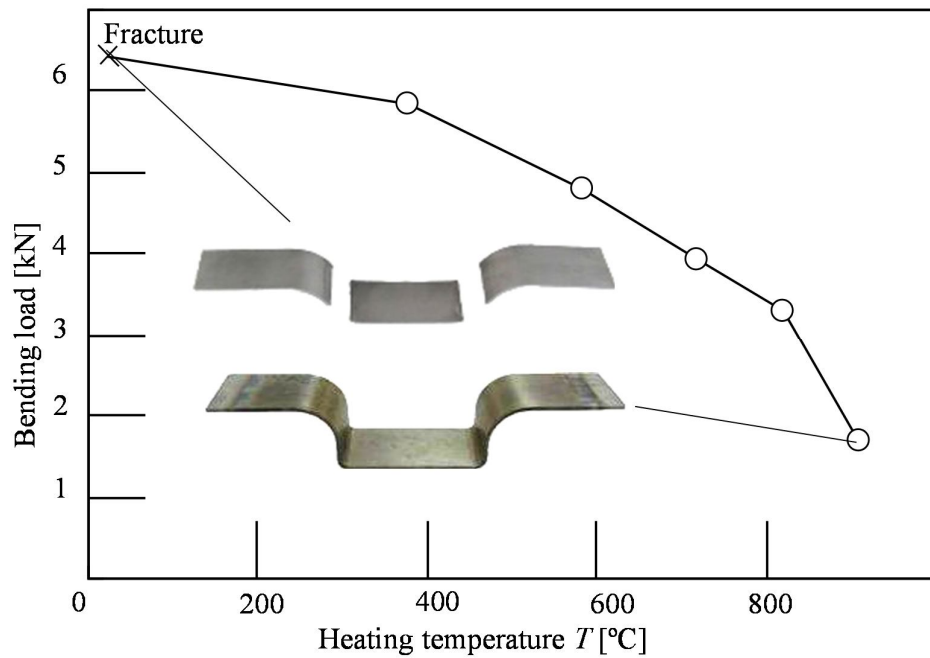


Fig. 6.7. Relationship between bending load and heating temperature for $t=3$ s.

The relationships between the springback angle and heating temperature and between the corner radius and heating temperature in the hat-shaped bending for $t = 3$ s are illustrated in Fig. 6.8. As the heating temperature increases, the springback angle and the corner radius decrease. It is found that the hot bending is effective in preventing the springback of the titanium alloy sheet.

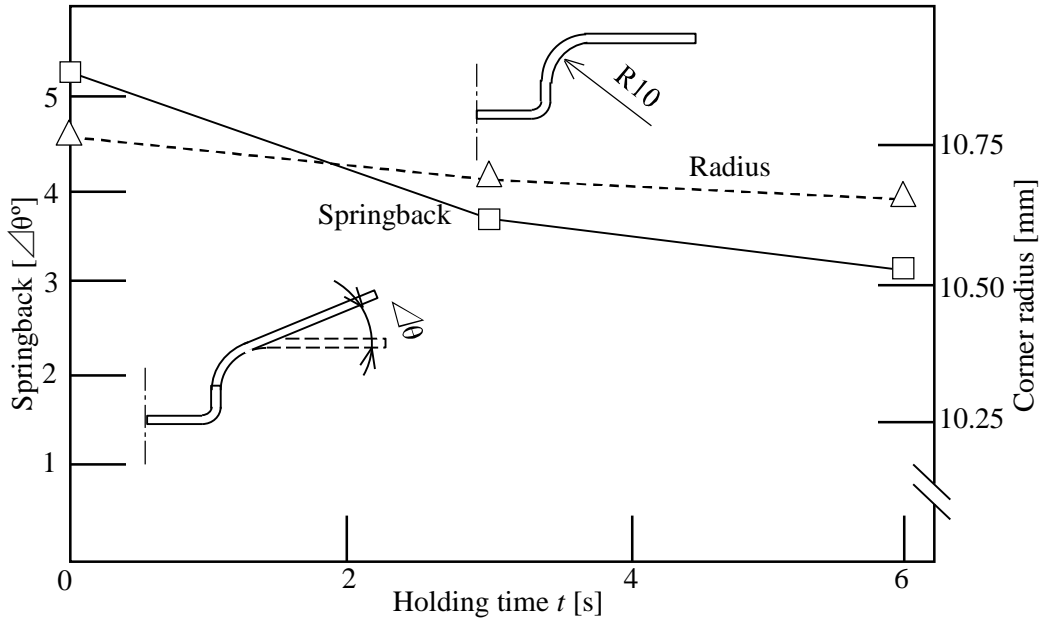


Fig. 6.8. Relationships between springback angle and heating temperature and between corner radius and heating temperature for $t = 3$ s.

The relationships between the springback angle and holding time and the corner radius and holding time at the bottom dead centre for $T=880^\circ\text{C}$ is illustrated in Fig. 6.9. As the holding time increases, the springback angle and the corner radius decrease.

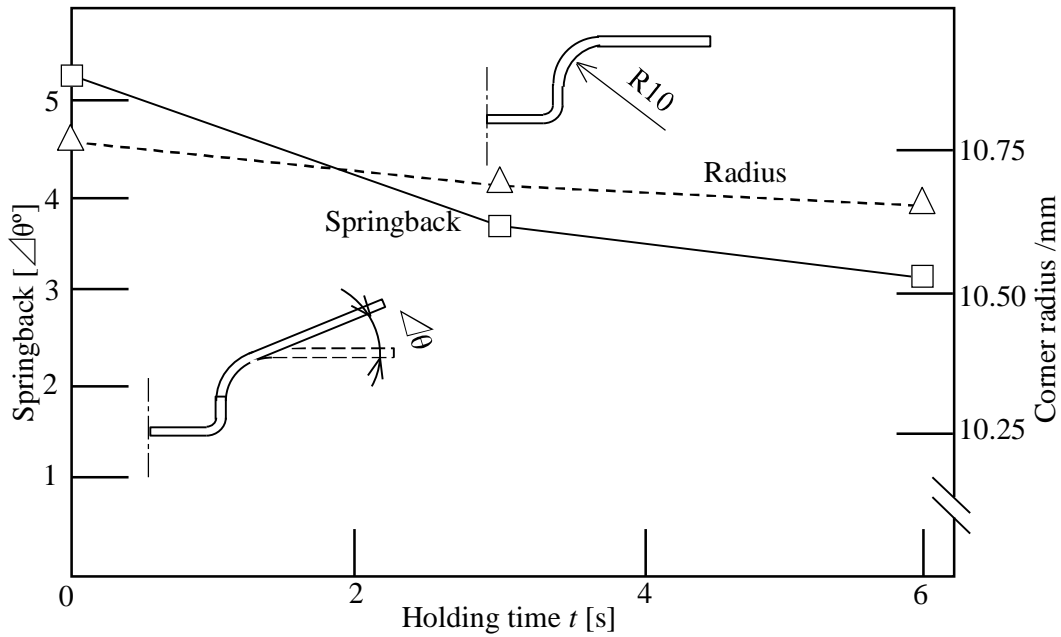


Fig. 6.9. Relationships between springback angle and holding time and between corner radius and holding time at bottom dead centre for $T = 880$ °C.

6.3.3 Microstructure and hardness of bent sheet

The microstructures of the bent sheet for the different heating temperatures are shown in Fig. 6.10. Although needle-shaped martensite having a low strength appears for $T=1050$ °C, the microstructure for $T=880$ °C is similar to that for the as-received sheet.

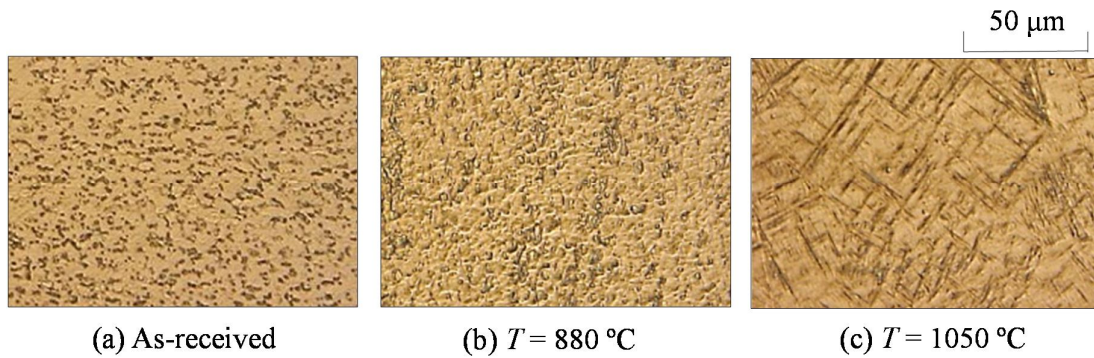


Fig. 6.10. Microstructures of bent sheet for different heating temperatures.

The distributions of the Vickers hardness in the longitudinal direction for the different heating temperatures are shown in Fig. 6.11. The hardness values for $T=550$ and $785\text{ }^{\circ}\text{C}$ are similar to that for the as-received sheet. When the heating temperature is increased to $880\text{ }^{\circ}\text{C}$, the hardness increases to 370 HV20. Therefore, the optimum heating temperature is $T=880\text{ }^{\circ}\text{C}$ due to the small springback, high hardness and no appearance of needle-shaped martensite.

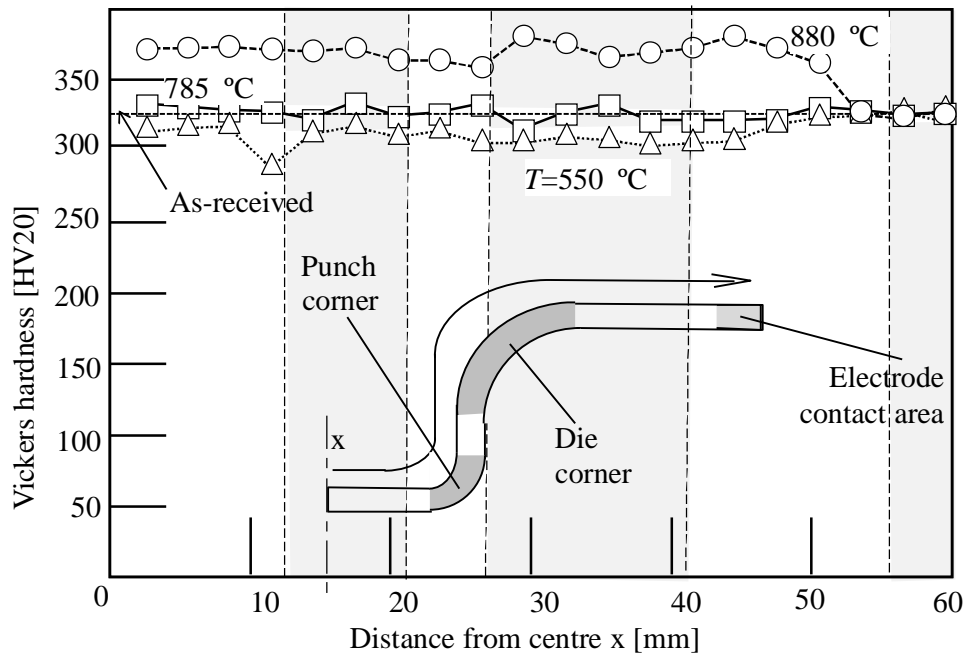


Fig. 6.11. Distribution of the Vickers hardness in the longitudinal direction for different heating temperatures.

6.4. Resistance heating of curve sheet

It is desirable in industry to bend curved sheets. For the curved sheets, the distributions of current density in the electrification direction becomes non-uniform as shown in Fig. 6.12(a), and thus the distribution of temperature becomes non-uniform. To obtain the uniform distribution of temperature, the electrodes are inclined as shown in Fig. 6.12(b).

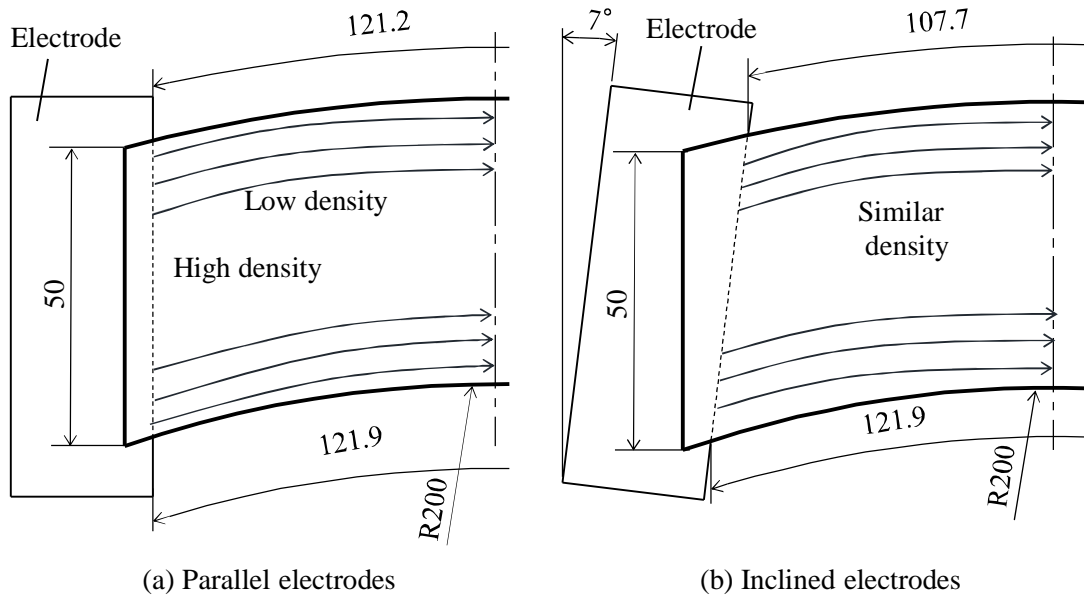


Fig. 6.12. Distributions of current density in electrification direction of curved sheet for parallel and inclined electrodes.

To calculate the distributions of heating temperature of the curved sheet for the parallel and inclined electrodes, the coupled thermal-electric analysis of the resistance heating was performed using the commercial FEM software ANSYS. In the calculation, the homogeneous contact between the sheet and the electrode was assumed. For the parallel electrodes, the distribution of temperature is not uniform as shown in Fig. 6.13(a), whereas the distribution of temperature in the bending area for the inclined electrodes is almost uniform, 825 ± 20 °C as illustrated in Fig. 6.13(b).

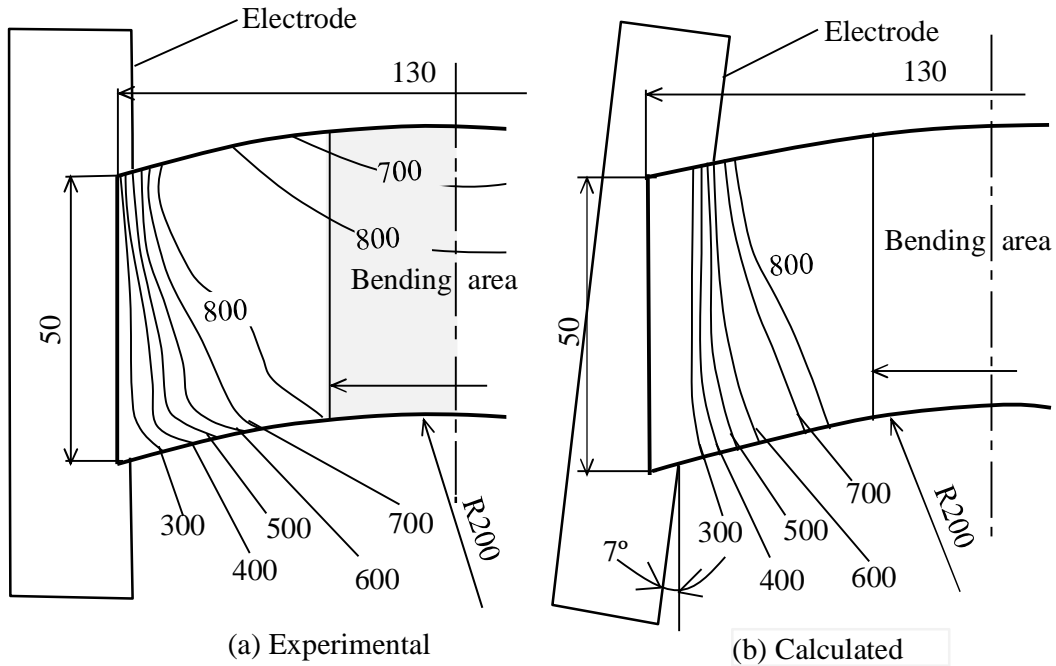


Fig. 6.13. Distribution of temperature in curved sheet having thickness of 1.6 mm for 750 A.

6.5. Conclusions

The hot hat-shaped bending of the Ti-6Al-4V titanium sheet using the resistance heating was carried out. The productivity of the bending of the titanium alloy sheet was improved by the resistance heating, because the heating process of the dies was eliminated and the heating time of the sheet was reduced. The hot bending using the resistance heating was also effective in preventing the springback and oxidation of the titanium alloy sheet. The sheet was successfully formed at the elevated temperatures

above 370 °C and the bending load for heating temperature 880 °C was reduce from 6.5 kN at room temperature to 1.8 kN. In the heating of the curved titanium alloy sheet, the distribution of temperature became more uniform, $825\text{ °C} \pm 20\text{ °C}$ for the inclined electrodes by 7°.

Chapter 7

Concluding remarks

7.1. Summary

7.1.1. In-situ measurement of deformation behaviour of sheet and tools during stamping using borescopes

The borescopes consisting of a small camera and a flexible cable have wide applicability to forming processes as an imaging sensor. Although it is not easy to observe deforming behaviour of the sheet surrounded with tools during stamping operations, the installation of the borescopes inside tools enables the in-situ measurement. It is strongly desirable in forming industry to visualise the deformation behaviour of inside tools. More useful information for designing forming processes can be obtained by investigating installation approaches of the borescopes inside tools. In addition, the borescopes are advantageous to monitoring malfunction of forming machines and tools as well as failures of products during forming operations. Although stamping of the high strength steel sheets were dealt with in this study, other materials such as stainless steel and aluminium and other processes such as forging and rolling can be applied.

Forming processes may be intellectualised by online control using borescopes. The in-situ measurement approach for three-dimensional deformation of sheet and tools during stamping using borescopes was developed. The borescope, consisting of a small CCD camera with a flexible cable, was connected to personal computer and placed

inside a small space between the tool cavities to measure the deforming behaviour of the sheet. The deformation behaviour of the sheet and punch, the real springback and wrinkling in shrink flanging were measured. The deformed shape of the sheet measured by the borescope was in good agreement with that measured by the laser displacement sensor. In addition, three-dimensional deforming behaviour was measured by a stereoscopic method using two borescopes. It was found that the borescopes are effective in in-situ measurement of three-dimensional deformation behaviour of the sheet and tools.

7.1.2. Formability improvement in flanging of high strength steel sheets

Since decrease in weight of automobiles is effective in improving the fuel consumption, the use of the ultra-high strength steel sheets for automobile body-in-white parts is increasing. In addition, the safety of the automobile is also increased. However the improvement of formability as well as the control of springback is strongly required. Although the increase in ductility of the ultra-high strength steel sheets is tried in steel making industry, the control of stress states during forming is an alternative approach.

The formability can be increased by reducing tensile stress during the forming process by controlling a stress state around sheared edges undergoing plastic deformation such as the present approach is considerably effective. A gradually contacting punch for improving flangeability of ultra-high strength steel sheets having small ductility was developed. In the gradually contacting punch, tensile and compressive stress around the corner edge of the sheet in stretch and shrink flanging are decreased by gradually pressing the edge of the sheet with the inclined bottom of the

punch. For the shrink flanging, compressive strain at the corner of the flange for high strength sheet was reduced, the flange height limit without wrinkling is improved and the maximum forming load for shrink flanging using gradual contact punch was tremendously decreased compared to the flat punch. In the stretch flanging, the formability of the high strength sheet increased by the gradual contact punch. However, the punch stroke increased thus increasing the production time and cost. In order to reduce the punch stroke, the 2-stage method using punch with recessed is used in stretch flanging. It was found that the 2-stage method using punch with recessed are effective in preventing the occurrence of cracking in stretch flanging. For the stretch flanging, the maximum height of the flange using the 2-stage method by a recessed and a flat punch is improved as compared with the flanging using 1-stage method by the flat punch and the occurrence of the delayed fracture in the stretch flanging is eliminated by flanging using the 2-stage method.

7.1.3. Joining of ultra-high strength steel sheets by hemming and improvement of joint strengths

In order to reduce the fatalities of the occupant of the vehicles, it is strongly desirable for the vehicle manufacturers to improve the safety of the cars. Extensive researches are carried out in optimizing the design of vehicle body structure in order to improve the crashworthiness and make the vehicles become stronger. To improve the crashworthiness of the vehicles without increasing the weight the vehicles, two approaches are applied for the improvement, the use of stronger materials and the optimization of structure of body members. The hollow sections or tubes with different shape are mainly used as a member frontal rail. This structure acts as energy absorber

during accident and is permanently deformed in order to absorb the kinetic energy during the crash in axial direction. This hollow sections typically joined by resistance spot welding have insufficient energy absorption because joint are not continuous. Although laser welding is a better approach to overcome this problem, high heating temperatures reduce the quality, accuracy and reliability of joined parts. In order to overcome this problem, the hollow section is joined using the hemming method. In particular, hemming is considered a joining technique more than plastic deformation process. The objective of this joining operation is to realize a connection between two or more sheets by bending the edge of the outer sheet on to the inner sheet. Both edges of hollow sections are joined by hemming to produce continuous joint without external heat supply. Since the hollow section having hemmed joints is overlapped, the strength is increased as compared to the resistance spot welding joints.

An experimental study by crashing the hollow section of high strength steel sheets with different strength in axial direction was performed. The hollow section having hemmed and spot weld joint were crashed at high speed using press machine in order to obtain the deformation behaviour of the sections. The result showed the maximum load during the crash test of the hollow section having hemmed joints is larger than welded joints, thus the safety of the occupants inside the vehicle is increased. In addition, the hollow section having hemmed joints is effective for absorbing the energy during the crash test compared to the resistance spot welding. Therefore, hemming is effective for increasing energy absorption during the crash test.

7.1.4. Improvement of formability of titanium alloy sheet using hot bending by resistance heating

The titanium alloy sheets are known for its properties of high strength at high temperatures, low density and high corrosion resistance. Due to these properties the titanium alloy sheet is widely used for airplane parts. However, a ductility of the titanium alloy sheet is very low thus difficult to be formed at room temperature. The sheets are generally formed at elevated temperatures. Warm and hot forming processes are useful for improving the formability of workpiece having low ductility at room temperature. The hot hat-shaped bending of the Ti-6Al-4V titanium sheet using the resistance heating was carried out. The productivity of the bending of the titanium alloy sheet was improved by the resistance heating, because the heating process of the dies was eliminated and the heating time of the sheet was reduced. The hot bending using the resistance heating was also effective in preventing the springback and oxidation of the titanium alloy sheet. The sheet was successfully formed at the elevated temperatures and the bending load was reduced.

7.2. Future perspectives

The reduction of CO₂ emissions by the new legislations worldwide increases the interest of the automotive industry for reducing the weight of the vehicles. This concern brings new interest in the use of high strength steel sheet for automotive body materials. A thinner sheet is possible to be used since the strength of the sheet is higher. Besides reducing the weight of the vehicles, the safety of the vehicles also increases. Since the high strength steel sheets have low ductility, forming of the sheet is a problem. Many researchers tried to measure the deformation behaviour of the sheets during the forming

of the high strength steel sheet by using various types of sensors. However, most of the sensors only provide local and 2-dimensional data. CCD cameras are also used to measure the deformation behaviour of the sheet during stamping by some researchers. Since the size of the CCD cameras is big, installation inside the dies becomes impossible. Borescope is a small CCD camera attached with flexible cable widely used in the medical field is attractive to be apply as a sensor for the stamping process.

In order to fully apply the borescopes as sensors to practical stamping operations, some treatments are required. Since lubricants are commonly used in stamping operations, the borescope is covered with a transparent protector from the lubricants and pictorial data may be corrected for a flood of lubricants. The use of the present borescope is limited below a temperature of 80°C and a heat protector is required for higher temperatures.



Fig. 7.1. Borescope with capability of transmitting data through WIFI.

When a space surrounded with tools is not enough to install the borescope, tools are machined for the installation and the installation of the borescope especially having cable become difficult. Fig. 7.1. show the borescope with a capability of transmitting the data through WIFI. With the used of the wireless borescope having capability of transmitting the data through WIFI, the problems of machining and locating the cable from tool to the computer are solved.

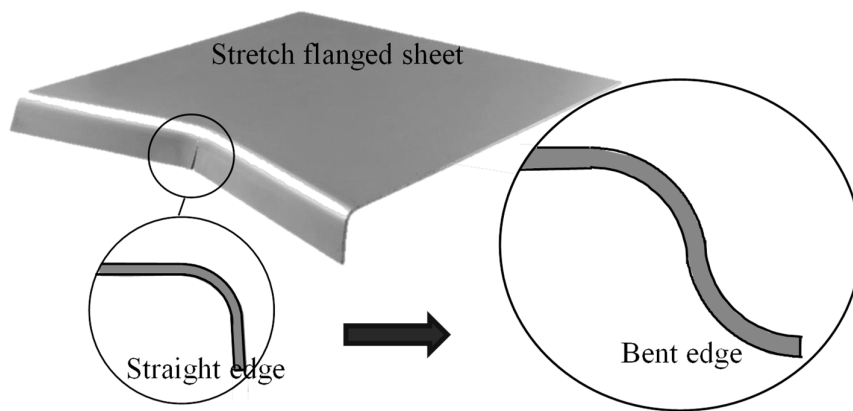


Fig. 7.2. Stretch flanging with reinforce sheet edge.

The weight reduction of the vehicles is an alternative to reduce the CO₂ emission in the development of new vehicles. However, reducing weight of the vehicles is always conflicting with an improvement of safety of the vehicles. Therefore, to improve the safety and reduce the weight of the vehicles at the same time, are the challenges to the car manufacture. The application of the high strength sheets is steel sheets for automobile body-in-white parts is increasing. However the improvement of formability is strongly required. In order to prevent the occurrence of the crack during the stretch flanging and wrinkling during shrink flanging, the edge of the sheet is bent. Fig. 7.2.

show the stretch flanging with bent edge. The method of 1-shot flanging with reinforce sheet edge is shown in Fig. 7.2.

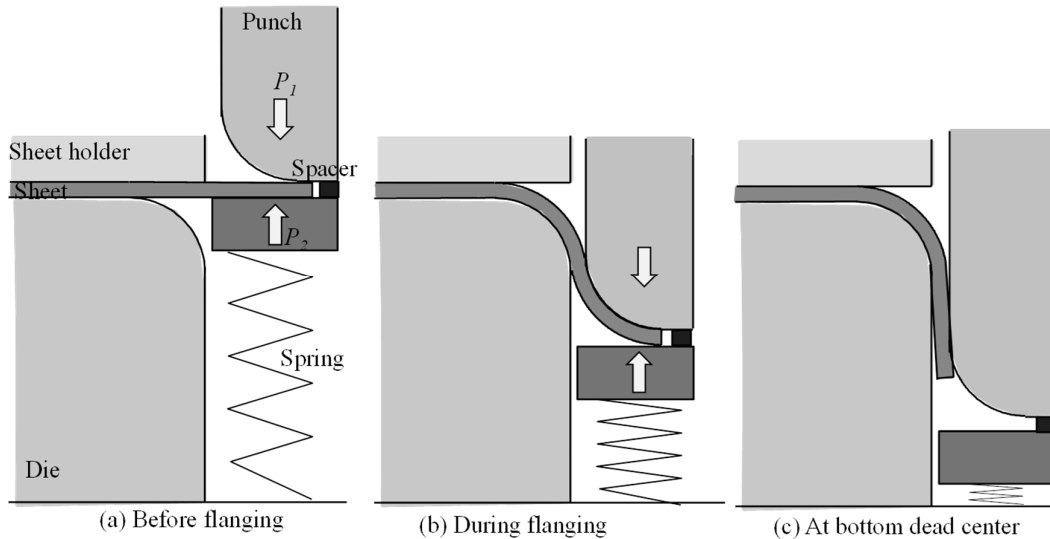


Fig. 7.2. Mechanism of 1-shot flanging with reinforce sheet edge.

Beside the used of the high strength steel sheets, a new material having higher strength to weight ratio is required to achieve the target. Although material such as CFRP or titanium alloy sheet is one of the solutions for this problem, the high cost and small formability are crucial problems, thus the industry is still interested to use the steel sheets. The steels with higher strength are developed by the steel maker to fulfil the need of the automotive industry. However problems such as large springback, small formability, short tool life, etc. are the disadvantages to the application of the high strength steel sheet. The best solution with a lower cost is tried, to increase in the ductility of the ultra-high strength steel sheets in steel making industry. Besides that, the control of stress states during forming by optimizing the mechanism is an alternative approach. Hot forming technologies in stamping of the high strength steel sheets is also

an attractive solution in producing the parts made of low formability without the problems at the assembly phase.

Although titanium alloy sheets are attractive materials for airplane components due to its lightness in weight, high strength and corrosion resistance, the high cost and small formability are crucial problems. Since the formability of the titanium alloy sheet, at the room temperature is limited, the application of warm and hot forming is a solution. However, the heating using the furnace needs longer time and produces the part with the oxidised scale. As an alternative, resistance heating method is used to heat the sheets. Although the hot forming using the resistance heating method is faster and produces better part without oxidised scale, the size is limited to small part only. For the bigger parts, the uniform heating is difficult to obtain.

References

- [1] M. Merklein, J.M. Allwood, B.-A. Behrens, A. Brosius, H. Hagenah, K. Kuzman, K. Mori, A.E. Tekkaya, A. Weckenmann, Bulk forming of sheet metal, *CIRP Annals - Manufacturing Technology*, 61 (2012), 725–745.
- [2] K. Mori, K. Akita, Y. Abe, Springback behaviour in bending of ultra-high-strength steel sheets using CNC servo press, *International Journal of Machine Tools & Manufacture*, 47 (2) (2007), 321-325.
- [3] T. Yoneyama, Y. Tozawa, Direct measurement of stress and heat between work and tool in metal forming, *CIRP Annals - Manufacturing Technology*, 39 (1) (1990), 219–222.
- [4] X. Roizard, J.M. Pothier, J.Y. Hihn, G. Monteil, Experimental device for tribological measurement aspects in deep drawing process, *Journal of Materials Processing Technology*, 209 (3) (2009), 1220–1230.
- [5] R. Lupoi, F.H. Osman, Under surface pressure sensing technique for the evaluation of contact stresses, *Journal of Materials Processing Technology*, 164–165 (2005), 1537-1543.
- [6] J. Jeswiet, C. Nyahumwa, A sensor for measuring metal deformation interface forces, *Journal of Materials Processing Technology*, 39 (3-4) (1993), 251–268.
- [7] K. Siegert, E. Dannenmann, S. Wagner, A. Galaiko, Closed-loop control system for blank holder forces in deep drawing, *CIRP Annals - Manufacturing Technology*, 44 (1) (1995), 251–254.
- [8] M. Yang, K. Manabe, K. Hayashi, M. Miyazaki, N. Aikawa, Data fusion of distributed AE sensors for the detection of friction sources during press forming.

-
- Journal of Materials Processing Technology, 139 (1–3) (2003), 368–372.
- [9] H. Kim, T. Altan, Q. Yan, Evaluation of stamping lubricants in forming advanced high strength steels (AHSS) using deep drawing and ironing tests. *Journal of Materials Processing Technology*, 209 (8) (2009), 4122–4133.
- [10] A. Azushima, Direct observation of contact behaviour to interpret the pressure dependence of the coefficient of friction in sheet metal forming, *CIRP Annals - Manufacturing Technology*, 44 (1) (1995), 209–212.
- [11] J. Bech, N. Bay, M. Eriksen, A study of mechanisms of liquid lubrication in metal forming, *CIRP Annals - Manufacturing Technology*, 47 (1) (1998), 221–226.
- [12] A. Jäger, D. Risch, A.E. Tekkaya, Thermo-mechanical processing of aluminum profiles by integrated electromagnetic compression subsequent to hot extrusion, *Journal of Materials Processing Technology*, 211 (5) (2011), 936–943.
- [13] J.T. Hofman, B. Pathiraj, J-van. Dijk, D.F-de. Lange, J. Meijer, A camera based feedback control strategy for the laser cladding process, *Journal of Materials Processing Technology*, 212 (11) (2012), 2455–2462.
- [14] T. Kuwabara, F. Sugawara, Multiaxial tube expansion test method for measurement of sheet metal deformation behavior under biaxial tension for a large strain range, *International Journal of Plasticity*, 45 (2013), 103–118
- [15] M. Kaupper, M. Merklein, Bendability of advanced high strength steels—A new evaluation procedure, *CIRP Annals - Manufacturing Technology*, 62 (1) (2013), 247–250.
- [16] K. Fujiyama, S. Nagai, Y. Akikuni, T. Fujiwara, K. Furuya, S. Matsumoto, K. Takagi, T. Kawabata, Risk-based inspection and maintenance systems for steam

- turbines, *International Journal of Pressure Vessels and Piping*, 81 (10-11) (2004), 825–835.
- [17] J. Jurkovic, M. Korosec, J. Kopac, New approach in tool wear measuring technique using CCD vision system, *International Journal of Machine Tools & Manufacture*, 45 (9) (2005), 1023–1030.
- [18] M. Barletta, V. Tagliaferri, Development of an abrasive jet machining system assisted by two fluidized beds for internal polishing of circular tubes. *International Journal of Machine Tools and Manufacture*, 46 (3–4) (2006), 271–283.
- [19] D. Carle, G. Blount, The suitability of aluminium as an alternative material for car bodies, *Materials & Design*, 20 (5) (1999), 267-272.
- [20] A. Tharumarajah, P. Koltun, Is there an environmental advantage of using magnesium components for light-weighting cars?, *Journal of Cleaner Production*, 15 (11-12) (2007), 1007-1013.
- [21] B.L. Mordike, T. Elbert, Magnesium: Properties – applications – potential, *Materials Science and Engineering*, A302 (1) (2001), 37-45.
- [22] P. Groche, R. Huber, J. Dorr, D. Schmoeckel, Hydromechanical deep-drawing of aluminium-alloys at elevated temperatures, *Annals of the CIRP*, 51 (1) (2002), 215-218.
- [23] K. Siegert, S. Jager, M. Vulcan, Pneumatic bulging of magnesium AZ31 sheet metals at elevated temperatures, *Annals of the CIRP*, 52 (1) (2003), 241-244.
- [24] K. Mori, S. Maki and Y. Tanaka, Warm and hot stamping of ultra-high tensile strength steel sheets using resistance heating, *Annals of the CIRP*, 54 (1) (2005), 209-212.

-
- [25] K. Mori, T. Kato, Y. Abe, Y. Ravshanbek, Plastic joining of ultra-high strength steel and aluminium alloy sheets by self-piercing rivet, *Annals of the CIRP*, 55 (1) (2006), 283-286.
- [26] Y. Abe, K. Mori, K. Norita, Gradually contacting punch for improving stretch flangeability of ultra-high strength steel sheets, *CIRP Annals - Manufacturing Technology*, 62 (1) (2013), 263–266.
- [27] K. Mori, Y. Abe, Y. Suzui, Improvement of stretch flangeability of ultra-high strength steel sheet by smoothing of sheared edge, *Journal of Material Processing Technology*, 210 (4) (2010), 653–659.
- [28] M. Miyanishi, Manufacturing of light weight cars, *Steel Research International*, 81 (9) (2010), Supplement Metal Forming 2010, 1-8.
- [29] N. A. K. Bashah, N. Muhamad, B. M. Deros, A. Zakaria, S. Ashari, A. Mobin, M. S. M. A. Lazat, Multi-regression modeling for springback effect on automotive body in white stamped parts, *Materials and Design*, 46 (2013), 175–190.
- [30] H. Lim, M.G. Lee, J.H. Sung, J.H. Kim, R.H. Wagoner, Time-dependent springback of advanced high strength steels, *International Journal of Plasticity*, 29 (2012), 42–59.
- [31] S. Toros, A. Polat, F. Ozturk, Formability and springback characterization of TRIP800 advanced high strength steel, *Materials and Design*, 41 (2012), 298–305.
- [32] K. Kubota, T. Ohba, S. Morito, Frictional properties of new developed cold work tool steel for high tensile strength steel forming die, *Wear*, 271 (2011), 2884–2889.
- [33] K. Mori, Y. Abe, Y. Kidoma, P. Kadarno, Slight clearance punching of ultra-high

- strength steel sheets using punch having small round edge, *International Journal of Machine Tools and Manufacture*, 65 (2013), 41-46.
- [34] Y. Abe, Y. Murata, K. Mori, Z. Hamedon, Joining by hemming of high strength steel sheet, *Proceeding of 2013 Japanese Spring Conference for the Technology of Plasticity*, (2013), 269-270.
- [35] K. Mori, N. Bay, L. Fratini, F. Micari, E.A Tekkaya, Joining by plastic deformation, *CIRP Annals - Manufacturing Technology*, 62 (2) (2013), 673-694.
- [36] K. Mori, S. Saito, S. Maki, Warm and hot punching of ultra-high strength steel sheet. *CIRP Annals - Manufacturing Technology*, 57 (1) (2008), 321-324.
- [37] K. Mori, T. Maeno, Y. Maruo, Punching of small hole of die-quenched steel sheets using local resistance heating of shearing zone, *Annals of CIRP*, 61 (1) (2012), 255- 258.
- [38] K. Mori and D. Ito, Prevention of oxidation in hot stamping of quenched steel sheet by oxidation preventive oil, *CIRP Annals*, 58 (1) (2009), 267-270.
- [39] <http://bookguidebywingback.air-nifty.com/military/2005/08/>.
- [40] Z. Hamedon, K. Mori, T. Maeno, Y. Yamashita, Hot stamping of titanium alloy sheet using resistance heating, *Vestnik of Nosov Magnitogorsk State Technical University*, 5 (45) (2013), 12-15.
- [41] K. Mori, S. Maki, Y. Tanaka, Warm and hot stamping of ultra-high tensile strength steel sheets using resistance heating, *CIRP Annals - Manufacturing Technology*, 54-1 (2005), 209-212.
- [42] K. Mori, Y. Okuda, Tailor die quenching in hot stamping for producing ultra-high strength steel formed parts having strength distribution, *Annals of the CIRP -*

- Manufacturing Technology, 59-1 (2010), 291–294.
- [43] K. Mori, T. Maeno, Y. Fukui, Spline forming of ultra-high strength gear drum using resistance heating of side wall of cup, *CIRP Annals - Manufacturing Technology*, 60-1, (2011), 299-302.
- [44] K. Mori, T. Maeno, S. Fuzisaka, Punching of ultra-high strength steel sheets using local resistance heating of shearing zone, *Journal of Materials Processing Technology*, 212-2 (2012), 534- 540.
- [45] F. Ozturk, R.E. Ece, N. Polat, A. Koksall, Assessment of electrical resistance heating for hot formability of Ti-6Al-4V alloy sheet, *Key Engineering Materials*, 473 (2011), 130-136.
- [46] Z. Hamedon, K. Mori, Y. Abe, In-situ measurement of three-dimensional deformation behaviour of sheet and tools during stamping using borescope, *Journal of Materials Processing Technology*, 214 (4) (2014), 945-950.
- [47] Z. Hamedon, K. Mori, Y. Abe, S. Nishino, In-situ measurement of deformation shape and die deflection during stamping in small space tool cavity using borescope, *Proceeding of 63rd Japan Joint Conference for Technology of Plasticity*, (2012), 369-370.
- [48] M. Kleiner, M. Geiger, A. Klaus, Manufacturing of lightweight components by metal forming, *CIRP Annals - Manufacturing Technology*, 52 (2) (2003) 521-542.
- [49] X. Wang, J. Cao, On the prediction of side-wall wrinkling in sheet metal forming processes, *International Journal of Mechanical Science*, 42 (2000), 2369-2394.
- [50] C. Qi, S. Yang, F. Dong, Crushing analysis and multiobjective crashworthiness optimization of tapered square tubes under oblique impact loading, *Thin-Walled*

-
- Structures, 59 (2012), 103–119.
- [51] S. Ramakrishna, H. Hamada, Energy absorption characteristics of crashworthy structural composite materials, *Key Engineering Materials*, 141–143 (1998), 585–620.
- [52] F. Tarlochan, F. Samer, A.M.S. Hamouda, S. Ramesh, K. Khalid, Enhancement of crashworthiness due to axial and oblique impact forces, *Thin-Walled Structures*, 71 (2013), 7–17.
- [53] A.G. Olabi, E. Morris, M.S.J. Hashmi, Metallic tube type energy absorbers: a synopsis, *Thin Walled Structures*, 45 (2007), 707–726.
- [54] T.Y. Reddy, R.J. Wall, Axial compression of foam filled thin walled circular tubes, *International Journal of Impact Engineering*, 7 (2) (1988), 151–166.
- [55] M. Seitzberger, F.G. Rammerstorfer, R. Gradingner, H.P. Degischer, M. Blaimachein, C. Walch, Experimental studies on the quasi static axial crushing of steel columns filled with aluminum foam, *International Journal of Solids and Structures*, 37 (30) (2000), 4125–4147.
- [56] A.K. Toksoy, M. Guden, The strengthening effect of polystyrene foam filling in aluminum thin walled cylindrical tubes, *Thin-Walled Structures*, 43 (2) (2005), 333–350.
- [57] P. Chatterjee, V. M. Athawale, S. Chakraborty, Materials selection using complex proportional assessment and evaluation of mixed data methods, *Materials and Design*, 32 (2011), 851–860.
- [58] B. Dehghan-Manshadi, H. Mahmudi, A. Abedian, R. Mahmudi, A novel method for materials selection in mechanical design: Combination of non-linear

- normalization and a modified digital logic method, *Materials and Design*, 28 (2007), 8–15.
- [59] P. Jimbert, I. Eguia, I. Perez, M.A. Gutierrez, I. Hurtado, Analysis and comparative study of factors affecting quality in the hemming of 6016T4AA performed by means of electromagnetic forming and process characterization, *Journal of Materials Processing Technology*, 211 (5) (2011), 916–924.
- [60] F. Vollertsen, K. Lange, Enhancement of drawability by local heat treatment, *CIRP Annals - Manufacturing Technology*, 47 (1) (1998), 181–184.
- [61] T. Maeno, K. Mori, C. Unou, Optimisation of condition in hot gas bulging of aluminium alloy tube using resistance heating set into dies, *Key Engineering Material*, 473 (2011), 69–74.
- [62] T. Maeno, K. Mori, K. Adachi, Gas forming of ultra-high strength steel hollow part using air filled into sealed tube and resistance heating, *Journal of Materials Processing Technology*, 214 (1) (2014), 97–105.
- [63] J. Yanagimoto, R. Izumi, Continuous electric resistance heating - Hot forming system for high-alloy metals with poor workability. *Journal of Materials Processing Technology*, 209 (1) (2009), 3060–3068.

List of publications

1. **Z. Hamedon**, K. Mori, T. Maeno, Y. Yamashita, Hot stamping of titanium alloy sheet using resistance heating, *Vestnik of Nosov Magnitogorsk State Technical University*, 45 (2013), 12-15.
2. **Zamzuri Hamedon**, Ken-ichiro Mori, Yohei Abe, In-situ measurement of three-dimensional deformation behaviour of sheet and tools during stamping using borescope, *Journal of Materials Processing Technology*, 214 (4) (2014), 945-950.
3. 安部 洋平, 渡部 沙春, **Zamzuri Hamedon**, 森 謙一郎, 超高張力鋼板の縮みフランジ変形における逐次接触パンチによるしわの抑制, *Journal of Japan Society for Technology of Plasticity* (in press, April 2014).

List of conferences

International

1. Tomoyoshi Maeno, Ken-ichiro Mori, **Zamzuri Hamedon**. Hot bending of titanium alloy sheet using resistance heating. *The 14th International Conference on Metal Forming*, AGH University of Science and Technology, Krakow, Poland, 16-19 September 2012.

Local

1. Tomoyoshi Maeno, Ken-ichiro Mori, Shohei Nakamoto, Yuya Yamashita, **Zamzuri Hamedon**. Hot bending of titanium alloy sheet using resistance heating. *The 2011 Japanese Spring Conference for the Technology of Plasticity*, Waseda University, Tokyo, Japan, 27-29 May 2011.
2. **Zamzuri Hamedon**, Yohei Abe, Saharu Watanabe, Ken-ichiro Mori. Optimization of shape of punch having gradual contact for prevention of wrinkling in shrinks flanging of ultra-high strength steel sheets. *The 62nd Japanese Joint Conference for the Technology of Plasticity*, Nikko Hotel, Toyohashi, Japan, 27-29 October 2011.
3. **Zamzuri Hamedon**, Ken-ichiro Mori, Yohei Abe, Saharu Watanabe. In-situ measurement of deforming shapes during bending of high strength steel sheet using borescope. *The 2012 Japanese Spring Conference for the Technology of Plasticity*, Komatsu Way Comprehensive Learning Centre, Komatsu, Japan, 7-9 June 2012.

4. **Zamzuri Hamedon**, Ken-ichiro Mori, Yohei Abe, Shoma Nishino. In-situ measurement of deforming shapes and die deflection during stamping in small space toll cavity using borescope. *The 63rd Japanese Joint Conference for the Technology of Plasticity*, Kitakyushu International Conference Center, Kitakyushu, Japan, 4-6 November 2012.
5. **Zamzuri Hamedon**, Ken-ichiro Mori, Yohei Abe, In-situ measurement of 3-dimensional deformation during flanging of sheet metal using 2 borescopes. *The 2013 Japanese Spring Conference for the Technology of Plasticity*, Daido University, Nagoya, Japan, 7-9 June 2013.
6. **Zamzuri Hamedon**, Ken-ichiro Mori, Yohei Abe, Yuji Murata. Crashing behaviour of high strength steel hollow section having hemmed joints. *The 64th Japanese Joint Conference for the Technology of Plasticity*, Osaka University, Suita Campus, Osaka, Japan, 1-3 November 2013.

Acknowledgements

It would not have been possible to write this doctoral thesis without the help and support of the kind people around me, to only some of whom it is possible to give particular mention here.

First of all, my highest gratitude belong to my supervisor Professor Ken-Ichiro Mori, Toyohashi University of Technology for his help, support and patience, not to mention his advice and unsurpassed knowledge in metal forming technology.

I would like to express my appreciation Professor Takayuki Shibata for serving me as the committee member in my final defense. Thank you very much for valuable discussions, comments and suggestions for my thesis.

I would also like to express special gratitude to Associate Professor Dr. Yohei Abe and Dr. Tomoyoshi Maeno for the good advice, support and friendship, have been invaluable on both an academic and a personal level.

I would like to express my appreciations to Mr. Saharu Watanabe, Mr. Yuya Yamashita, Mr. Yuji Murata, Mr. Shohei Nakamoto and Mr. Shoma Nishino who helped me during the experiments and discussions. I would also like to thank to Mr. Purwo Kadarno and other lab members from 2010 until 2014 for their kindness, friendship and support.

I would like to acknowledge the financial and technical support of the University Malaysia Pahang, Ministry of Education of Malaysia and its staff, particularly in the award of a Postgraduate Research Studentship that provided the necessary financial support for this study. I also thank the Department of Mechanical

Engineering and International Student Division of Toyohashi University of Technology for their support and assistance since the start of my postgraduate work in 2010.

I would like to thank my wife Fatin Laily and my children Aiman, Haikal, Zulaikha and Athirah for their support and great patience at all times. My parents, brother, sister also in-law has given me their unequivocal support throughout, as always, for which my mere expression of thanks likewise does not suffice. Special thanks to my late brother Zuhadi who encourage me to never stop studying.

I thank my Malaysian friends in Toyohashi and others for their support and encouragement throughout. Last, but by no means least, I would also like to thank my colleagues and friends in the Faculty of Manufacturing Engineering of UMP, GMI and also Kuantagħ`89 .

For any errors or inadequacies that may remain in this work, of course, the responsibility is entirely my own.

Zamzuri Hamedon

Toyohashi

April 2014

Resume



Zamzuri Hamedon was born on January 8th, 1972, in Temerloh, a small city of state of Pahang, Malaysia. He grew up in a village call Bukit Tajau and studied an elementary school at Sekolah Kebangsaan LKTP Bukit Tajau from 1979 to 1984. In 1985, he entered MARA Junior Science College, a boarding school in Kuantan for next 5 years. In Sept 1989 he passed the Sijil Pelajaran Malaysia examination to finish his high school and continued his studies at MARA community College for two years.

In July 1993 he entered the German Malaysian Institute and obtained a Diploma of Production Technology in Sept 1996. Soon after that, he begin to work as CAD/CAM programmer at AquaCut Sdn. Bhd for 2 years in Shah Alam and then as production supervisor Angkasa Jasa Sdn. Bhd in Balakong, Selangor until year of 2000. In 2000, he pursue his studied for bachelor of engineering at University Technology of Tun Hussien Onn until July 2002. In Sept 2002 he begin his career as technical training officer at German Malaysia Institute for 5 years. During this period, in 2005 -2007 he pursued his master degree in Manufacturing System Engineering at University Kebangsaan Malaysia. In 2008, he came to University Malaysia Pahang to serve as junior lecturer. October 2010, he entered the Doctor of Engineering program at Toyohashi University of Technology. He expected to graduate by March 2014.